NASA CONTRACTOR REPORT

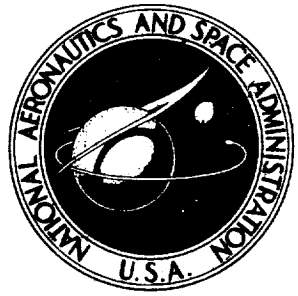

NASA CR-2443

NASA CR-2443

DEVELOPMENT OF A FOWLER FLAP SYSTEM FOR A HIGH PERFORMANCE GENERAL AVIATION AIRFOIL

by W. H. Wentz, Jr., and H. C. Seetharam

Prepared by
WICHITA STATE UNIVERSITY
Wichita, Kansas
for the
CENTER FOR RESEARCH, INC.
UNIVERSITY OF KANSAS
Lawrence, Kansas
for Langley Research Center

NATIONAL AERONAUTICS AND SPACE ADMINISTRATION • WASHINGTON, D. C. • DECEMBER 1974

1. Report No.	2. Government Accession No.	3. Recipient's Catalog No.
CR-2443		

4. Title and Subtitle	5. Report Date
DEVELOPMENT OF A FOWLER FLAP SYSTEM FOR A HIGH PERFORMANCE GENERAL AVIATION AIRFOIL	December 1974
	6. Performing Organization Code
7. Author(s)	8. Performing Organization Report No.
W. H. WENTZ, JR., AND H. C. SEETHARAM	
9. Performing Organization Name and Address	10. Work Unit No.
WICHITA STATE UNIVERSITY WICHITA, KANSAS	760-60-01-09
	11. Contract or Grant No.
	NGR 17-002-072
12. Sponsoring Agency Name and Address	13. Type of Report and Period Covered
NATIONAL AERONAUTICS AND SPACE ADMINISTRATION WASHINGTON, D. C. 20546	14. Sponsoring Agency Code
	760-60-01-09

15. Supplementary Notes

PREPARED BY WICHITA STATE UNIVERSITY FOR UNIVERSITY OF KANSAS

TOPICAL REPORT

16. Abstract

THIS PAPER REPORTS ON A TWO-DIMENSIONAL WIND-TUNNEL EVALUATION OF TWO FOWLER FLAP CONFIGURATIONS ON THE NEW GA(W)-1 AIRFOIL. ONE CONFIGURATION USED A COMPUTER-DESIGNED 29-PERCENT CHORD FOWLER FLAP. THE SECOND CONFIGURATION WAS MODIFIED TO HAVE INCREASED FOWLER ACTION WITH A 30-PERCENT CHORD FLAP. FORCE, PRESSURE, AND FLOW-VISUALIZATION DATA WERE OBTAINED AT REYNOLDS NUMBERS OF 2.2×10^6 TO 2.9×10^6. OPTIMUM SLOT GEOMETRY AND PERFORMANCE WERE FOUND TO BE CLOSE TO COMPUTER PREDICTIONS. A $C_{L\ MAX}$ OF 3.8 WAS ACHIEVED. OPTIMUM FLAP DEFLECTION, SLOT GAP, AND FLAP OVERLAP ARE PRESENTED AS FUNCTIONS OF C_L. TESTS WERE MADE WITH THE LOWER SURFACE CUSP FILLED IN TO SHOW THE PERFORMANCE PENALTIES THAT RESULT. SOME DATA ON THE EFFECTS OF ADDING VORTEX GENERATORS AND HINGED-PLATE SPOILERS WERE OBTAINED.

17. Key Words (Suggested by Author(s))	18. Distribution Statement
TWO-DIMENSIONAL FORCE MEASUREMENTS COMPUTER DESIGNED AIRFOIL AND FLAP OPTIMIZED SLOT GEOMETRY PRESSURE DISTRIBUTION, FLOW VISUALIZATION	UNCLASSIFIED - UNLIMITED STAR CATEGORY: 01

19. Security Classif. (of this report)	20. Security Classif. (of this page)	21. No. of Pages	22. Price*
UNCLASSIFIED	UNCLASSIFIED	113	$4.50

*For sale by the National Technical Information Service, Springfield, Virginia 22151

SUMMARY

Wind tunnel tests have been carried out for computer designed 29% and 30% chord Fowler flap systems on an advanced technology general aviation airfoil at Reynolds numbers from 2.2×10^6 to 2.9×10^6. Force, pressure and flow visualization data were obtained. Optimum slot geometry and performance are found to be close to computer predictions. A c_{lmax} of 3.8 was achieved with the 30% single-slotted Fowler flap. Optimum flap deflection, slot gap and flap overlap are presented as functions of c_l, to assist the vehicle designer in obtaining the airfoil configuration for best takeoff, climb, cruise, and landing performance.

Modifying the airfoil section by straightening the trailing edge cusp results in substantial performance penalties at c_l values above 0.8. Adding vortex generators results in increases in c_{lmax} of 0.2 with flaps either up or down. Drag values are increased with vortex generators at low c_l values, but decreased at high c_l values. Tests demonstrate that spoilers are generally highly effective on the new airfoil. For certain negative angle of attack conditions, however, loss of spoiler effectiveness was observed with some configurations.

Recommendations are made to develop additional general aviation airfoils based upon the new technology, to conduct detailed tests of spoiler effectiveness, and to carry out measurements of the separated boundary layer in order to provide a basis for improvements to the theoretical computer programs.

INTRODUCTION

Background

New airfoils are being developed for general aviation aircraft as one component of an Advanced Technology Light Twin (ATLIT) flight demonstration program under the auspices of NASA Langley Research Center. Program management is provided by the University of Kansas, hardware design by Robertson Aircraft, and flapped airfoil development by Wichita State University. The particular aircraft selected for flight demonstration of advanced technology is the Piper Seneca, a current "light twin" model. Principal modifications include fitting the aircraft with new wing panels and engine nacelles.

Other aspects of the overall ATLIT program are given in References 1, 2, 3, and 4. Although the present airfoil development is to satisfy a general aviation requirement, the airfoils will have potential application to any aircraft designed for cruising below critical Mach number.

New airfoil section design techniques have evolved from extensive wind tunnel, flight test and computational experience, related to transonic and V/STOL technology research programs conducted by NASA within the past few years. In the present program, high Reynolds number (cruising conditions) wind tunnel tests of the new general aviation airfoil were carried out at NASA Langley Research Center to evaluate cruising performance, while lower Reynolds number flap development tests were carried out at WSU.

The GA(W)-1 Airfoil

This airfoil was designed by Dr. R. T. Whitcomb and associates of NASA Langley Research Center. The design was based upon technology acquired during the development of supercritical airfoils for transonic flight. The airfoil evolved from a 17% thick supercritical airfoil developed and flown on a T2-C test aircraft (Ref. 5). The GA(W)-1 section was designed utilizing a theoretical potential flow and boundary layer analysis computing routine developed by the Lockheed Corporation (Ref. 6). Salient features of the new airfoil are: fairly large (17%) thickness to chord ratio, substantial camber near the trailing edge, a reflexed lower surface contour and a blunt trailing edge (Fig. 1). The airfoil was designed for an essentially fully turbulent boundary layer to permit design performance to be achieved with conventional fabrication techniques. Design c_l is 0.4, but the design was tailored to provide for a wide c_l range without flow separation. The trailing edge region is cusped in a manner reminiscent of Joukowski (Ref. 7), Wortmann (Ref. 8) and supercritical airfoils. The parallel trailing edge surfaces which result from cusping are designed to reduce the adverse pressure gradient in this region and therefore delay flow separation. A slight trailing edge bluntness allows for easier manufacture of the cusped region.

Flaps

A 29% chord Fowler flap was designed for the airfoil by Mr. Harry Morgan and associates of the NASA Langley Research Staff, utilizing the multi-element Lockheed computing program

to optimize flap slot geometry to avoid separation. The flap forms the aft 4% of the airfoil upper surface, so that the main or forward airfoil section chord is 96% of the total flap-nested airfoil chord. Tabulated flap geometry and flap locations are given in Figures 2 and 3.

CR-2443

A 30% chord Fowler flap was designed for the airfoil by Robertson Aircraft. This flap is contoured so that the main airfoil extends to 100% chord. The resulting configuration has a total flap plus airfoil chord of 130% compared to 125% for the 29% c flap model. Coordinates for this flap are given in Figure 4.

SYMBOLS

The force and moment data have been referred to the 25% C location of the flap nested airfoil chord. Dimensional quantities are given in both International (SI) Units and U.S. Customary Units. Measurements were made in U.S. Customary Units. Conversion factors between SI Units and U.S. Customary Units may be found in Reference 9. The symbols used in the present report are defined as follows:

c	wing reference chord.
c_l	airfoil section lift coefficient, section lift/(dynamic pressure x chord).
C_L	airplane lift coefficient, lift/(dynamic pressure x area).
c_d	airfoil section drag coefficient, section drag/(dynamic pressure x chord).
c_m	airfoil section pitching moment coefficient with respect to the 25% C location, section moment/dynamic pressure x $(\text{chord})^2$.
c_n	normal force coefficient, normal force/(dynamic pressure x airfoil chord).
(l/d)	lift to drag ratio.
RN	Reynolds number based upon wing reference chord.
X	chordwise coordinate.
Y	coordinate normal to local surface.
Z	coordinate normal to airfoil chord plane.
X'	flap track coordinate, inclined 17° to airfoil chord.
Z'	flap track coordinate, orthogonal to X'.
α	angle of attack.
δ	rotation of surface from nested position, and boundary layer thickness.

Subscripts:

f	flap
s	spoiler

EXPERIMENTAL INVESTIGATIONS

Wind Tunnel Models and Instrumentation

Two airfoil-flap configurations were tested: the GA(W)-1 airfoil fitted with a 29% Fowler flap and the same airfoil modified to accommodate a 30% Fowler flap. The airfoil was fabricated from mahogany laminated over a 2.54 cm x 34.92 cm (1" x 13.75") aluminum spar. The model was scaled to have a 61.0 cm (24") chord with the flap nested, and a 91.4 cm (36") span. All tests were conducted in the WSU 213 cm x 305 cm (7' x 10') Low Speed tunnel, fitted with inserts which provide a 213 cm x 91.4 cm (7' x 3') two-dimensional test section (Fig. 5). Models were fitted with 107 cm dia (42" dia) aluminum end plate disks. The disks were mounted flush in holes in the sidewalls, with a 0.64 cm (.25") circumferential gap to prevent fouling. This clearance gap was sealed with a soft foam rubber wiper seal, adjusted to give negligible interference.

The airfoil was fitted with 0.81 mm (.032") I.D. stainless steel surface static pressure taps along the centerline section. An aluminum plate was bonded into the airfoil to provide a stiff trailing edge. This fabrication technique resulted in a 1.5 mm (.062") step in the upper surface contour at the 96% chord station on the 29% c model. The flaps were fabricated from solid aluminum plate machined to contour. The 29% c flap was fitted with centerline static pressure taps.

The 30% c flap model was fabricated by modifying the original airfoil aft section and fabricating a new flap. Because of time limitations, no pressure taps were provided in the 30% c flap or modified airfoil aft section.

The flaps were attached to the end plate disks by means of double sliding tracks designed to provide for adjustment in two orthogonal directions. These flap tracks were inclined 17° upward from the wing chord trailing edge to coincide with a set of flap pivot locations based upon NASA Langley computer studies. Flap deflections are rotations from the nested position about a pivot point which moves with the flap. The

flap positioning mechanism is illustrated in Figure 6. Thus a flap setting is completely described by specifying three coordinates: (a) X position of the pivot location, (b) Z position of the pivot location, and (c) flap deflection (rotation) about the pivot point. This same flap track was utilized for setting the 30% c flap. The entire track and pivot mechanisms are external to the wind tunnel test section.

The variety of flap settings tested necessitated fairly large flap mounting cutouts in the end plate disks. These cutouts were covered with 0.81 mm (.032") aluminum plates. Several sets of cover plates were required to accommodate the full range of flap settings.

Force data were obtained from the tunnel main balance system. In addition, a wake rake was utilized to obtain flap nested drag data. End plate drag tares were determined from the flap nested tests. Surface pressure distributions were obtained for the 29% c flap configuration, but not for the 30% c flap configuration. Pressures were obtained using a system of pressure selector switches and pressure transducers which permits acquisition of 96 channels through 4 transducers. Flow visualization photos were obtained utilizing yarn tufts.

Initial tests were carried out with the flap nested, model clean and with several sizes of grit applied to fix transition. Because the intent of the program was to develop practical construction airfoils, all subsequent tests were carried out with transition fixed at the 5% chord location on both upper and lower surfaces, utilizing 2.5 mm (0.10") wide strips of #80 carborundum grit.

A rather complete calibration of the tunnel two-dimensional test section was carried out prior to testing. This calibration included: velocity distribution, turbulence factor, longitudinal static pressure gradient and flow angularity. Detailed calibration results are given in Reference 10.

Data Reduction

The force data from the tests were reduced employing a calculating routine developed for the IBM 1130 computer at the University, applying the usual wind tunnel boundary corrections. Surface pressure and wake rake pressure data were reduced utilizing a computing routine on the University IBM 360-44 computer. The pressure data computational routine carries out integrations to calculate flap and airfoil normal force and axial force coefficients and overall lift and pitching moment coefficients as well as pressure coefficient

distributions. Detailed analysis methods and computer program listings are given in Reference 11.

Airfoil Design Conditions

Since airfoil drag and maximum lift coefficient are dependent upon Reynolds number, any interpretation of wind tunnel results must be carried out in light of pertinent full scale flight Reynolds numbers. For airplanes which have a large ratio of maximum to minimum speed, a large altitude envelope, and high wing taper ratios, the range of flight Reynolds number is large.

Design point conditions for the ATLIT airplane illustrate the range of Reynolds numbers to be considered (Table 1). These values are derived from the data presented in Reference 1. Minimum and maximum Reynolds numbers are quoted for each flight condition based upon unflapped tip and root chord lengths. These figures are root chord = 155 cm (61") and tip chord = 79 cm (31") for the ATLIT design.

Table 1. - ATLIT Design Conditions

Flight Condition	Altitude	Speed	C_L	Reynolds Number
Cruise	6000 ft	194 mph	0.4	3.8 to 7.6 x 10^6
Climb	Sea Level	107 mph	1.0	2.5 to 5.0 x 10^6
Flaps Up, $C_{L_{max}}$	Sea Level	83 mph	1.4	2.0 to 4.0 x 10^6
Takeoff Flaps, $C_{L_{max}}$	Sea Level	62 mph	2.5	1.5 to 3.0 x 10^6
Landing Flaps, $C_{L_{max}}$	Sea Level	57 mph	3.0	1.4 to 2.8 x 10^6

As seen in the table, the design Reynolds numbers for the ATLIT airplane range from 1.5 x 10^6 to 5.0 x 10^6 for takeoff, climb and landing; and from 4.0 x 10^6 to 8.0 x 10^6 for cruising. Tunnel power, balance limitations and model geometry limited the Reynolds numbers of the WSU test to a range between 2.2 x 10^6 and 2.9 x 10^6. This is a reasonable range for development of the flap system. Tests at Reynolds numbers above 3.0 x 10^6 to evaluate flap nested high speed cruising performance were carried out by NASA in the low turbulence pressure tunnel at the Langley Research Center (Ref.3).

Force Measurements and Comparisons With Theory

29% c Flap Model. - Results of the lift and pitching moment measurements for the 29% flap model with computer

designed flap slot geometry for various flap settings are shown in Figures 7 and 8, along with theoretical computer predicted results. Agreement between experiment and theory is quite good except for the flap nested and 40° flap deflection cases. The discrepancy between theory and experiment for the flap nested case is disturbing, in that the progressive loss of lift prior to stall indicates premature boundary layer thickening, possibly with separation. It is to be expected that such a trend would result in high drag. Flow visualization studies confirm this separation, but NASA tests reveal that separation is greatly delayed at higher Reynolds numbers (Ref. 3). Comparison of the results of the present tests with airfoils of similar thickness at comparable Reynolds numbers (Ref. 12) reveals that non-linearity of the lift curve is the rule rather than the exception. Reducing Reynolds number from 6×10^6 to 3×10^6 leads up to substantial non-linearity for c_l values greater than 0.4 for virtually all airfoils having thickness to chord ratios of 15% or more. Since the ATLIT airplane ordinarily cruises at Reynolds numbers in the range of 4×10^6 to 8×10^6, this boundary layer thickening phenomenon at lower Reynolds numbers is not viewed as a serious shortcoming.

Comparisons of theoretical and experimental pitching moment data reveal the same trends observed with the lift data, i.e. excellent agreement except for the flap nested and 40° flap cases. The airfoil with flap nested has a substantial zero lift pitching moment, as would be anticipated for a configuration with rather large camber near the trailing edge.

Experimental drag data for the computer developed flap settings are given in Figure 9. No comparisons between theoretical and experimental drag data are provided, since the computing routine in its present form does not have the capability of drag prediction. (See Ref. 6 for a discussion of this limitation.)

Results of force tests to determine slot geometry for highest $c_{l_{max}}$ with 35° and 40° flap deflections are shown in Figures 10, 11, and 12. These data show substantial improvements in $c_{l_{max}}$ compared to the computer developed slot geometry. The changes in slot gap are quite small, however, Maximum lift coefficients for 35° and 40° flap deflections are essentially equal for this configuration.

Data for flap deflections of 50° and 60° are included in these same figures. These runs with the higher deflections

were made to provide information as to the feasibility of generating additional drag with flaps for approach path control. For these settings, the flap was simply rotated about the wind tunnel flap fixture pivot point, without changing the track settings from the optimum 40° flap positions. Consequently, the performance presented for 50° and 60° settings cannot be considered as optimum. A more detailed discussion of optimization is given in a later section of this report.

Examination of the lift, drag and moment data shows that deflecting the flap from 35° to 40° results in very little change, while rotating the flap from 40° to 50° results in a large drag change with essentially no change in lift or moment. Rotation of the flap from 50° to 60° results in a severe loss of $c_{l_{max}}$ as well as a large drag increase. Thus flap rotation between 35° and 50° might be utilized to change drag without changing lift for airplane path control.

30% c Flap Model. - Results of the force tests of this model are shown in Figures 13, 14, and 15 for flap deflections of 0° to 40°. The data for 35° and 40° flap deflections represent gap and overlap settings optimized for highest $c_{l_{max}}$. The gap and overlap for the 20° through 30° flap deflections were selected as intermediate values to give a constant gap of 2.5%, and nearly linear overlap adjustment.

Data for flap deflections of 50° to 60° are shown in Figures 16, 17, and 18, along with the 35° and 40° settings for comparison. As before, the 50° and 60° data were obtained by simple rotation from the 40° flap pivot position. Again, the gaps are not necessarily optimum for these cases. Trends are very similar to those observed for the 29% flap. Rotations above 40° result in a modest change in $c_{l_{max}}$ and pitching moment, with large changes in drag.

Optimization of Flap Settings - Objectives

Considerable test time in the present program was devoted to optimization of flap settings. Determination of any "optimum" must be related to airplane flight conditions. For a typical light twin, the desired flap system performance characteristics may be identified as follows:

Takeoff. - The requirement for takeoff is to attain a satisfactory $c_{l_{max}}$ at an angle of attack within the landing gear capability of the configuration, i.e. an angle of attack that can be achieved by rotation about the main gear without aft fuselage contact with the runway.

Climb. - For twin-engine aircraft, single engine rate of climb is ordinarily a crucial performance parameter. It is desirable to have the maximum airplane lift-drag ratio occur at climb lift coefficient or higher in order to avoid the difficulties associated with flight operations in the "region of reversed command" or "back side of the power curve". While the maximum airplane lift-drag ratio must, of course, be evaluated including fuselage and nacelle drag as well as the three-dimensional wing induced drag, it is imperative that the airfoil section have the minimum possible drag at the climb lift coefficient.

Another consideration for total airplane climb performance is the adverse influence of angle of attack on fuselage and nacelle drag. To minimize fuselage and nacelle drag it is desirable to operate at near zero fuselage incidence. Thus the desired airfoil characteristics for climb performance may be summarized as follows:

a) attainment of the lowest possible section c_d value (or highest possible l/d value) at best climb c_l.

b) attainment of best climb c_l at an angle near the cruising angle (zero degrees in the present case).

Landing. - Low approach speeds are required for short landings. This requirement dictates high maximum lift coefficient. Fairly high drag levels are permissible in this flight regime.

Summary of Objectives. - The desired performance goals outlined above may be summarized into two optimization objectives as follows:

(1) attainment of a high value for $c_{l_{max}}$.

(2) attainment of maximum l/d for a given c_l.

Optimization of Flap Settings - Results

Maximum Lift Coefficient. - Results of the optimization tests for $c_{l_{max}}$ are presented in Figure 19 for the 30% c model. These data show the locus of slot gap and flap-airfoil overlap for constant values of $c_{l_{max}}$, for flap deflections of 35° and 40°. These figures show a $c_{l_{max}}$ value of 3.8 for 40° flap deflection with 2.7 % gap and a negative 0.7 % overlap. (Flap

nose aft of wing trailing edge.) The attainment of a $c_{l_{max}}$ value of 3.8 is considered to be a significant achievement for a single-slotted Fowler flap at these low Reynolds numbers without leading edge devices and without blowing or suction boundary layer control. While it is recognized that optimum slot geometry is influenced to some degree by flap and airfoil contours, some generalization of these data should be possible. In fact, the optimum slot gap and overlap contours presented here are quite similar to those presented in Reference 13 based upon tests of a Clark Y airfoil conducted in 1932, even though the maximum c_l values from the present tests are substantially higher.

Maximum (l/d) for a Given c_l. - The optimums for $(l/d)_{max}$ were determined from consolidated plots of c_d versus c_l for all flap settings. (Figs. 9, 12, 15, and 18). The envelopes of these curves represent the desired optimums. Cross-plots of these envelopes are presented in Figures 20 and 21. Flap deflection, gap and overlap required to achieve optimum performance are also presented.

Runs were made for several overlap and gap positions with flap deflections of 5° and 10°, in an attempt to identify a configuration which would substantially reduce drag in the climb condition ($c_l = 1.0$) to a level below the flap nested value. This search was unsuccessful in that no deflected flap setting could be found which reduced the drag at climb c_l. These tests did provide, however, a slot configuration which results in minimum drag for the 10° flap deflection. Furthermore, total airplane considerations, such as fuselage and nacelle drag and the sensitivity of these items to angle of attack may lead to a situation in which some modest flap deflection such as 5° or 10° will provide minimum total airplane drag at the climb condition. Thus the optimum airplane configuration during climb may be with some flap deflection, even though the optimum isolated airfoil configuration would be with flap nested. It should be noted that detailed optimizations of slot gap were carried out only for 10°, 35°, and 40° flap deflections. Therefore, slightly better performance might be found for the intermediate flap deflections if additional slot gap and overlap variations were studied. However, the data presented here represent achievable performance for the settings specified, and are probably near the "absolute" optimum in every case.

It can be argued that the gaps for highest $c_{l_{max}}$ with 35° and 40° flap deflections are not necessarily the gap settings for maximum (l/d). Examination of the consolidated c_d vs. c_l plots reveals that the c_l range for which any flap

deflection produces minimum drag is fairly narrow. Furthermore, the 35° and 40° flap settings provide minimum c_d only for c_l values very close to $c_{l_{max}}$ Thus any change in slot geometry which reduces $c_{l_{max}}$ will almost certainly result in higher c_d values. These arguments are also consistent with the premise that the function of the slot is to reduce separation, and that reducing separation will reduce drag and increase $c_{l_{max}}$.

Comparative Performance of the 29% and 30% Flap Models

Comparison of Figures 20 and 21 illustrates that the two flap configurations are nearly identical in $(l/d)_{max}$ performance. The 30% c flap with slightly larger effective chord, provides a slightly higher $c_{l_{max}}$. The performance differences between the two configurations are so small that a choice between them should probably be dictated by non-aerodynamic factors such as strength, stiffness or ease of manufacturing. Close examination of the main airfoil trailing edge geometry indicates that the 30% c flap model with the finite trailing edge thickness main airfoil is probably the easier to manufacture.

Pressure Distributions

Flap Nested. - Pressure coefficient data for the GA(W)-1 airfoil, flap nested are shown in Figures 22 and 23, for 0° and 6° angles of attack. Computer generated theoretical data are also shown for these cases. Agreement between theory and experiment is excellent. The kink in the lower surface C_p data at the 70% chord location is a result of the lower surface notch on the model in the flap nested configuration. This notch was not represented on the computer program. The 0° angle of attack case illustrates the pressure distribution at design cruise lift coefficient, characterized by a flat region over the forward portion and a concave region of pressure rise over the aft portion of the airfoil.

The C_p distributions at higher angles (Fig. 24) show substantial flat regions over the aft portion indicating the effects of upper surface separation. Separation locations are marked, based upon flow visualization studies. No theoretical curves are available for these cases, since the computing routine is not presently capable of predicting pressure distributions for cases with partial separation.

Computer integrations of the C_p data provide c_l and c_m values for comparison with the direct force measurements.

A comparison of this type is shown in Figure 25, and the agreement is seen to be quite good. Similar agreement exists for flap extended cases, although no direct comparisons of this type are shown.

Flap Extended. - Flap extended pressure distributions are given in Figures 26 through 43. Integrated normal force coefficient values for flap and main airfoil are tabulated for convenience. This series is for the 29% c flap, and the flap positions shown here are the "computer design settings". These settings were established in the preliminary development phase of the project based upon computer design studies. For angles of attack below separation, theoretical C_p values are also shown for comparison. In general, the computer program provides an excellent modeling of the flow. The pressure distributions over the forward portion of the airfoil and over the entire flap consistently show only minute differences between experiment and theory. Significant differences are present on both upper and lower surfaces near the trailing edge of the main airfoil. Evidently some improvement in modeling of the slot flow and its influence on upper surface pressures is required. Nevertheless, the high order of agreement shown here between theory and experiment establishes the credibility of the computer program as an airfoil/flap design tool.

An unusual pressure distribution is shown by the data for 40° flap deflection and $\alpha = 10°$ in Figure 41. Pressures along the upper surface show a high degree of scatter for this case. The implication is that a "long" laminar separation bubble is present and that the reattachment point is not fixed, resulting in wide variations in the surface suction developed. At lower angles, the pressure distributions are quite stable. At 15° angle of attack (Fig. 42) the pressure distribution is again quite stable. In this case, an extensive "flat" C_p region appears from about 40% chord aft. This is indicative of a turbulent separation in this region. Similar patterns are found for higher angles of attack.

Most of the flap pressure distributions are of the characteristic "peaky" type, indicating that the flap flow remains attached, even in cases for which the main airfoil flow is separated.

The effects of Reynolds number change from 2.2×10^6 to 2.8×10^6 for a typical flaps down C_p distribution are shown in Figure 43. While this Reynolds number change is admittedly rather small, the data show a consistent increase in upper surface suction at the higher Reynolds number, which is compatible with a decrease in boundary layer thickness.

Boundary Layer Measurements

Although it was not the primary purpose of the present research to conduct boundary layer studies, a limited number of boundary layer measurements were made as a part of this program. A boundary layer rake was mounted on the airfoil upper surface at the 94% chord location. Resultant boundary layer profiles are shown in Figure 44, for angles of attack of 0°, 5°, and 10°, in the flap nested configuration. Although no provisions were made for measurement of the reversed flow magnitudes within the separated boundary layer, it was possible to establish the vertical extent of the separated region by determining the inner boundary of the non-reversed flow region. These data have been combined with flow visualization separation information in Figure 45. These sketches indicate the approximate limits of the reversed flow region of the boundary layer for several angles of attack.

Effects of Recontouring the Airfoil Section

Since the first appearance of the GA(W)-1 airfoil (Ref. 3), manufacturers have asked about the importance of the reflex curvature in the lower surface near the trailing edge. In order to provide some definitive performance information related to trailing edge geometry, a test was run with a re-contoured section. The basic GA(W)-1 airfoil was modified by forming a straight-line lower surface contour from the 60% chord location to the trailing edge. The temporary recontouring was accomplished by utilizing modeling clay.

Results of this test are shown in Figure 46. The results of the force tests show significant changes in angle of zero lift and in pitching moment. These effects are attributed to the uncambering effect of the recontouring, and would be expected from fundamental inviscid flow theory. Maximum lift coefficient is reduced, and section drag coefficient is increased substantially at lift coefficients greater than 0.8. These latter changes are the result of a combination of viscous and potential flow effects. The increased trailing edge angle would be expected to result in a more adverse pressure gradient near the trailing edge (See Ref. 7), and the more adverse pressure gradient will cause boundary layer thickening and premature separation.

The results of this test illustrate clearly that substantial performance penalties will result from a straight line contour modification of this airfoil.

Because the flap-nested tests indicated boundary layer thickening and flow separation at modest angles of attack (as described earlier), it was decided that tests with vortex generators should be conducted. Because of the authors' previous experience with delta wing vortex flows, it was believed that delta wings would probably be a more efficient planform for vortex generators than the more commonly used rectangular or trapezoidal forms.

Based upon tuft studies, a 60% chord location was selected for installing vortex generators. The vortex generators were designed in the following way:

1. A flat plate turbulent boundary layer thickness was calculated for a plate length corresponding to the 60% chord location, and this theoretical boundary layer thickness was utilized to size the span of the generators.

2. The generators were designed to be small delta wings set at an angle of attack which would provide strong vortex flow, but a substantial margin below the vortex bursting angle of attack.

3. The generator array was designed so that it could be easily fabricated from a single sheet of 0.4 mm (.016") aluminum.

The boundary layer thickness (for 99% of free-stream velocity) computation carried out as described in (1) above leads to:

$$\delta = 7.62 \text{ mm} = 0.3"$$

Selecting a centerline chord of 2.54 cm (1") in combination with the semi-span of 7.62 mm (0.3") results in an equivalent leading-edge sweepback of 73.3°. For the simple cut-and-fold fabrication technique as shown in the sketch the resulting angle of attack is (90° - 73.3°) or 16.7°.

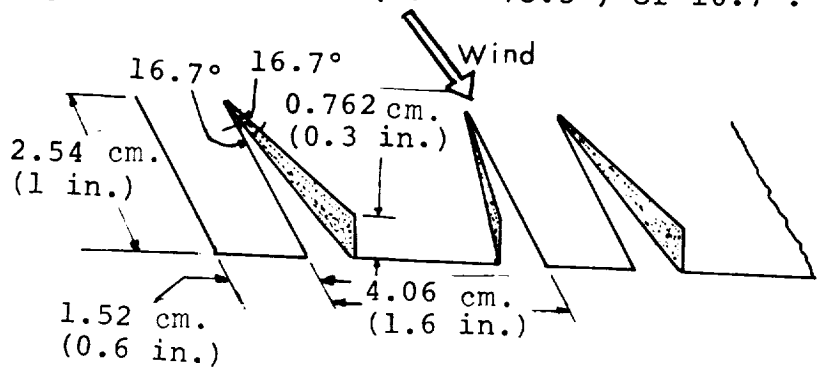

Vortex Generator Detail

The vortex bursting angle of attack corresponding to this sweepback is 36°, according to Reference 14. Thus the combination selected allows the vortex generators to operate with a comfortable margin below bursting conditions. While vortex bursting is known to be responsible for rapid turbulent mixing of the flow, it seems likely that the generators could operate more efficiently without bursting. The questions as to whether an optimum set of vortex generators should operate at pre- or post-bursting angle of attack, or whether the planform should be triangular can only be resolved by more extensive experimentation.

The vortex generators were arranged in alternating pairs to avoid inducing a net sidewash into the flow field. Spacing was staggered to give approximately equal spacing between rolled up vortices. The generators were installed with the trailing edges of the delta wings located at the 60% chord position on the upper surface of the GA(W)-1 airfoil.

Results of tests with and without vortex generators are shown in Figures 47 through 51 for flap nested and 40° flap deflection cases. These data exhibit clearly the powerful effects of vortex generators as boundary layer control devices. The flap nested c_l vs. α relationship is essentially linearized up to an angle of attack of 13°, at which point the separation point evidently moves in front of the vortex generators. At higher angles, the vortex generators have negligible influence on force characteristics. The pitching moment curve is also linearized, again indicating suppression of the boundary layer thickening tendency prior to stalling. The drag data show a substantial drag penalty (Δc_d = .0025) for the vortex generators at low angles of attack. At higher angles of attack, however, the delay of separation results in significant drag reductions.

For the flap down case, similar trends are noted, although the effects are not so large percentage-wise. Nevertheless, the flap down $c_{l_{max}}$ is increased from 3.8 to 4.0.

Vortex generators are, of course, a mixed blessing. The gains attained at high c_l are attained at the cost of additional drag at cruise. It should be noted that because of time limitations, no wind tunnel runs were made to optimize the generators. It may well be that smaller, relocated, or more widely spaced vortex generators could provide most of the gains obtained, with substantially smaller penalties. A comparison of the present vortex generators with design values recommended in the literature is given in Table 2.

Table 2. - Vortex Generator Design Data

Source	Span	Pitch	Distance Forward of Separation	Angle of Attack
United Aircraft (Ref. 15)	1.2δ	4 to 10 spans	10 to 30δ	16°
Pearcy (Ref. 16)	1.0δ	4 to 10 spans	Not Specified	20-25°
Present Design	1.0δ	7.3 spans	32δ	16.7°

This table illustrates that the present design is probably near optimum, although use of actual rather than flat plate boundary layer thickness as a design parameter might alter the resulting configuration. In any case, further experimentation would certainly be enlightening.

In a three-dimensional wing design situation, part-span use of vortex generators may provide an alternative to other parameters such as twist and thickness variations as a means for delaying stall near the wing tips.

Tests with Spoilers

One of the design concepts of the ATLIT program is to utilize spoilers for lateral control, thereby allowing the use of full-span flaps. A limited series of tests were conducted as a portion of the present program, to explore the effectiveness of spoilers on the GA(W)-1 airfoil section. Table 3 lists the spoiler configurations tested.

Table 3. - Spoiler Test Configurations

Flaps	Spoiler Chords	Hingelines	Deflections
0°, 40°	7.5%, 15%	60%, 70% c	20°, 40°, 60°

Spoilers were all of simple rectangular plate configuration, sealed at the hingelines. Spoiler tests were carried out at a Reynolds number of 2.2×10^6.

Results of these tests are shown in Figures 52 through 54. The data generally indicate the very powerful effects of spoilers as lateral control devices. Under certain conditions, however, spoiler effectiveness deteriorates rapidly. For example, the data for 7.5% spoiler chord, flaps down, 20° spoiler deflection show a region of loss of spoiler effectiveness at negative angles of attack. Under these conditions the

spoilers not only have negligible effect on lift, but also show little change in drag and pitching moment. The inference is that the flow reattaches beyond the spoiler trailing edge for these small spoiler deflections.

This trend holds true for both 60% and 70% hingeline locations. The effect does not appear for 15% chord spoilers, although it might occur for spoiler deflections smaller than 20°. This possibility should be explored carefully for any proposed design configuration.

Flow Visualization Studies

Flow visualization studies were carried out by attaching tufts to the upper surface of the model. In two-dimensional testing, questions always arise regarding the influence of the sidewall boundary layers on the airfoil stalling characteristics. To study such possible effects, the sidewalls were also fitted with tufts. No auxiliary blowing or suction was provided.

None of these photos (Figs. 55 to 58) indicate significant influence of the sidewall boundary layer on separation patterns. Initial tuft studies on the model with 29% c flap, at Reynolds numbers of 2.2×10^6 and 2.9×10^6 indicated no appreciable difference in the separation pattern due to Reynolds number change. Hence all subsequent visualization tests were carried out at a Reynolds number of 2.2×10^6. During the initial phase of tests, it was suspected that the separation pattern might be influenced by the thickness and the density distribution of the tufts on the model. In order to explore the possible adverse effects of tufts, a few oil flow studies were made. The results of the oil flow studies indicated no significant changes in separation location. However, the density of the tufts was reduced in the tests with 30% c flap in order to obtain clearer pictures and minimize mutual interference of tufts.

Tests with Flap Nested. - Tuft photos for the flap nested case are shown in Figure 55. A few words of explanation are in order concerning interpretation of the tuft behavior. At angles of attack up to about 6°, a careful study of the photos reveals that the flow is not reversed in the region of adverse pressure gradient, even though the tufts appear disturbed. The tufts appear blurred in the photos due to rapid flapping sideways within a band up to ±90° to the main flow direction. At 8° and higher angles of attack full separation is clearly observed, with complete reversal of the tufts. The separation originates at the airfoil trailing edge and progresses upstream with increasing angle of attack. It is interesting to note that

the tufts just upstream of the separation point exhibit the sideways flapping described above. Substantial boundary layer thickening is expected to occur just forward of separation. Thus the tuft flapping condition observed near the trailing edge at low angles of attack is interpreted as boundary layer thickening with incipient separation, rather than full separation.

Tuft photos at angles of attack through the stalling range (α = 12°, 14°, 16° & 18°) exhibit a striking feature of the airfoil: a very clean attached flow from the leading edge up to about 50% c even under the post-stalled conditions. This is consistent with patterns observed from pressure distributions (Fig. 24).

Tests With Flap Down. - Tests with a flap setting of 10° are shown for both 29% c and 30% c flap models in Figure 56. At an angle of attack of 2.5°, the 29% c model shows some evidence of incipient separation on the main airfoil. At angles of attack of 5° and 7.5° separation near the trailing edge on the main component of the 29% c model is clearly seen, whereas the 30% c flap model seems to remain attached up to an angle of attack of about 10°. At this angle, the separation is just beginning on the main airfoil. For both models the flap flow is reasonably steady even after main airfoil separation.

Photos for 35° flap deflection are shown in Figure 57. The 29% c flap configuration shows improvement in the flap flow from 0° to 7.5° angle of attack. At 7.5°, separation is observed on the aft region of the main foil. The 30%c flap model does not show separation until 10° angle of attack. Again, separation begins on the aft region of the main airfoil.

A comparative study of the flow over the 29% and 30% c models with 40° flap deflections is shown in Figure 58. In this case three configurations are shown: (1) the computer designed gap and overlap for the 29% c flap; (2) wind tunnel optimum gap and overlap for the 29% c flap; and (3) wind tunnel optimum gap and overlap for the 30% c flap. At zero angle of attack all three configurations show some separation on the flap. At an angle of attack of 5°, the flap flow for all the three configurations is beginning to become attached, evidently as a result of improved slot flow. At this angle, the 29% c flap model with the computer designed gap and overlap settings shows fully reversed flow forward to about 85% or 90% on the main airfoil, whereas the 29% c model with wind tunnel optimized gap setting exhibits only incipient separation in the same region.

The 30% c model has fully attached flow on the main component up to 7.5° angle of attack. At 10° angle of attack, separation appears near the trailing edge of the main foil of the 30% c flap model. Again the trends observed are in conformity with the force measurements which show higher maximum c_l values for the 30% flap configuration.

Tests With Vortex Generators. - Tuft studies with the vortex generator configuration described earlier for the flap nested case reveal the powerful effects of vortex generators as devices to delay flow separation (Fig. 59).

CONCLUDING REMARKS

1. Wind tunnel tests of a new low speed airfoil and flap have verified that high lift coefficient performance indicated by computerized theories which include viscous and slot flow effects can be achieved. Although drag is not yet predicted, the validity of the computing routines as airfoil design tools is confirmed.

2. Rather complete pressure distribution and flow visualization data have been obtained, along with limited boundary layer measurements. The computer predictions of pressures on the main airfoil and flap are quite satisfactory, except for the main airfoil in the vicinity of the flap, and for cases with partial flow separation.

3. The new airfoil has achieved a maximum lift coefficient of 3.8 with a 30% chord Fowler flap at a Reynolds number of 2.2×10^6 without leading edge devices or boundary layer suction or blowing. Optimum flap slot gap arrangements are close to computer predictions. Recontouring the airfoil trailing edge region resulted in a loss in $c_{l_{max}}$ of about 0.15, and in increased drag levels for high c_l values. Vortex generators added to the airfoil provided about 0.2 increase in $c_{l_{max}}$ flaps up or flaps down, with some drag penalty at the low lift coefficient conditions of cruise.

4. Tests have demonstrated that spoilers are very effective on the new airfoil, although loss of effectiveness was observed for certain combinations of high flap deflections, negative angles of attack and small spoiler deflections.

RECOMMENDATIONS

1. The technology utilized in the achievement of high performance from the GA(W)-1 airfoil should be exploited to develop a complete family of airfoils of differing camber and thickness. Development of the new airfoils should be computer based with wind tunnel tests of selected configurations.

2. Computer modeling of the main airfoil upper surface and lower surface pressures in the vicinity of the slot needs to be improved.

3. Detailed flow field and boundary layer measurements should be made for both the flap up and flap down configurations of the GA(W)-1 airfoil to provide a basis for extending the computational modeling to include separated flow phenomena.

4. Additional tests should be conducted to determine the effectiveness of spoilers on this airfoil at negative angles of attack, as well as the effectiveness of ailerons.

Aeronautical Engineering Department
Wichita State University
Wichita, Kansas 67208
October 1973

REFERENCES

1. Raisbeck, J.D.: Consideration of Application of Currently Available Transport-Category Aerodynamic Technology in the Optimization of General Aviation Propeller-Driven Twin Design. SAE Paper No. 720337, National Business Aircraft Meeting, March 1972.

2. Crane, Harold L.; McGhee, Robert J.; and Kohlman, David L.: Applications of Advanced Aerodynamic Technology to Light Aircraft. SAE Paper No. 730318, Business Aircraft Meeting, April 1973.

3. McGhee, Robert J.; and Beasley, William D.: Low-Speed Aerodynamic Characteristics of a 17-Percent-Thick Airfoil Section Designed for General Aviation Applications. NASA TN D-7428, 1973.

4. Wentz, W.H., Jr.: New Airfoil Sections For General Aviation Aircraft. SAE Paper 730876, 1973.

5. Palmer, W.E.: Thick Wing Flight Demonstrations. SAE Paper No. 720320, National Business Aircraft Meeting, March 1972.

6. Stevens, W.A.; Goradia, S.H.; and Braden; J.A.: Mathematical Model for Two-Dimensional Multi-Component Airfoils in Viscous Flow. NASA CR-1843, July 1971.

7. Karamcheti, K.: Principles of Ideal - Fluid Aerodynamics, John Wiley and Sons, 1966.

8. Wortmann, F.X.: On the Optimization of Airfoils with Flaps. Soaring Magazine, May 1970.

9. Mechtly, E.A.: The International System of Units - Physical Constants and Conversion Factors (Revised). NASA SP-7012, 1969.

10. Siew, R.: Calibration of a Two-Dimensional Insert for the WSU 7' x 10' Wind Tunnel. WSU AR73-2, 1973.

11. Rotramel, J.; and Breidenthal, R.: Computing Routines for Airfoil Section Wind Tunnel Data Reduction. WSU AR73-3, 1973.

12. Abbott, I.H.; and Van Doenhoff, A.E.: Theory of Wing Sections. Dover, 1959.

13. Weick, F.E.; and Platt, R.G.: Wind Tunnel Tests of the Fowler Variable - Area Wing. NACA TN 419, May 1932.

14. Wentz, W.H., Jr.; and Kohlman, D.L.: Vortex Breakdown on Slender Sharp-Edged Wings. AIAA J. of Aircraft, Vol. 8, No. 3, March 1971.

15. Taylor, H.D.: Summary Report on Vortex Generators. United Aircraft Corp. Research Dept. Rept. R-05280-9, 7 March 1950.

16. Pearcy, H.H.: Shock Induced Separation and Its Prevention by Design and Boundary Layer Control. (In Boundary Layer and Flow Control, Vol. 2, Ed. by G.V. Lachmann, 1961.)

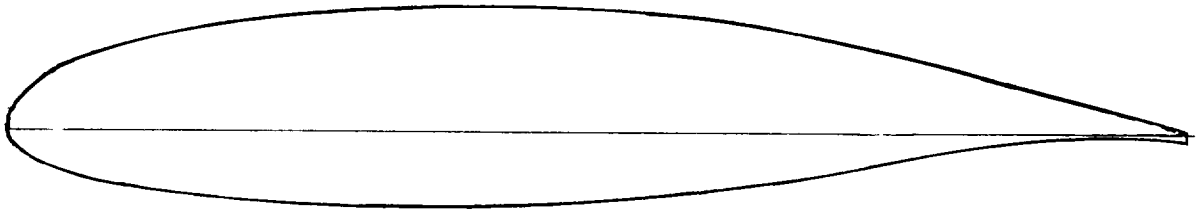

Upper Surface		Lower Surface	
X /c	Z /c	X /c	Z /c
0.00000	0.00000	0.00000	0.00000
.00200	.01300	.00200	-.00930
.00500	.02040	.00500	-.01380
.01250	.03070	.01250	-.02050
.02500	.04170	.02500	-.02690
.03750	.04965	.03750	-.03190
.05000	.05589	.05000	-.03580
.07500	.06551	.07500	-.04210
.10000	.07300	.10000	-.04700
.12500	.07900	.12500	-.05100
.15000	.08400	.15000	-.05430
.17500	.08840	.17500	-.05700
.20000	.09200	.20000	-.05930
.25000	.09770	.25000	-.06270
.30000	.10160	.30000	-.06450
.35000	.10400	.35000	-.06520
.40000	.10491	.40000	-.06490
.45000	.10445	.45000	-.06350
.50000	.10258	.50000	-.06100
.55000	.09910	.55000	-.05700
.57500	.09668	.57500	-.05400
.60000	.09371	.60000	-.05080
.62500	.09006	.62500	-.04690
.65000	.08599	.65000	-.04280
.67500	.08136	.67500	-.03840
.70000	.07634	.70000	-.03400
.72500	.07092	.72500	-.02940
.75000	.06513	.75000	-.02490
.77500	.05907	.77500	-.02040
.80000	.05286	.80000	-.01600
.82500	.04646	.82500	-.01200
.85000	.03988	.85000	-.00860
.87500	.03315	.87500	-.00580
.90000	.02639	.90000	-.00360
.92500	.01961	.92500	-.00250
.95000	.01287	.95000	-.00260
.97500	.00609	.97500	-.00400
1.00000	-.00070	1.00000	-.00800

Figure 1 - GA(W)-1 Airfoil Coordinates

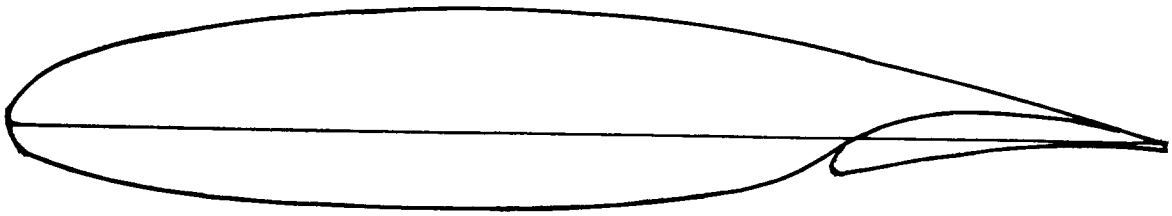

29%C Fowler Flap Coordinates

Upper Surface		Lower Surface	
X_f/c	Z_f/c	X_f/c	Z_f/c
0.00000	-.02350	0.00000	-.02350
.00030	-.02000	.00100	-.02700
.00200	-.01790	.00200	-.02880
.00400	-.01550	.00400	-.03000
.00800	-.01130	.00800	-.03100
.01200	-.00780	.01200	-.03040
.01800	-.00330	.02000	-.02880
.02300	.00000	.03000	-.02700
.02800	.00230	.05000	-.02350
.03800	.00700	.07000	-.01980
.04800	.01100	.09000	-.01600
.05800	.01410	.11000	-.01300
.06800	.01680	.13000	-.01000
.07800	.01900	.15000	-.00770
.08800	.02070	.17000	-.00580
.09800	.02180	.19000	-.00360
.10800	.02230	.21000	-.00270
.11800	.02280	.23000	-.00280
.12800	.02300	.25000	-.00350
.13800	.02340	.27000	-.00500
.14800	.02280	.29000	-.00800
.15800	.02230		
.16800	.02190		
.19000	.01980		
.21000	.01680		
.23000	.01380		
.25000	.00980		
.27000	.00590		
.29000	-.00070		

Nose Radius = .0075c

Nose Radius Location ($X_f/c, Z_f/c$) = (.0075,-.0235)

Figure 2 - 29% c Fowler Flap Configuration

29%C Flap Pivot Point Locations - Computer Design Settings

δ_f	X/c	Z/c
0° (Nested)	.730	-.040
10°	.880	-.061
15°	.900	-.055
20°	.920	-.049
25°	.930	-.046
30°	.940	-.043
40°	.950	-.040

(See Figure 6 for flap positioning mechanism)

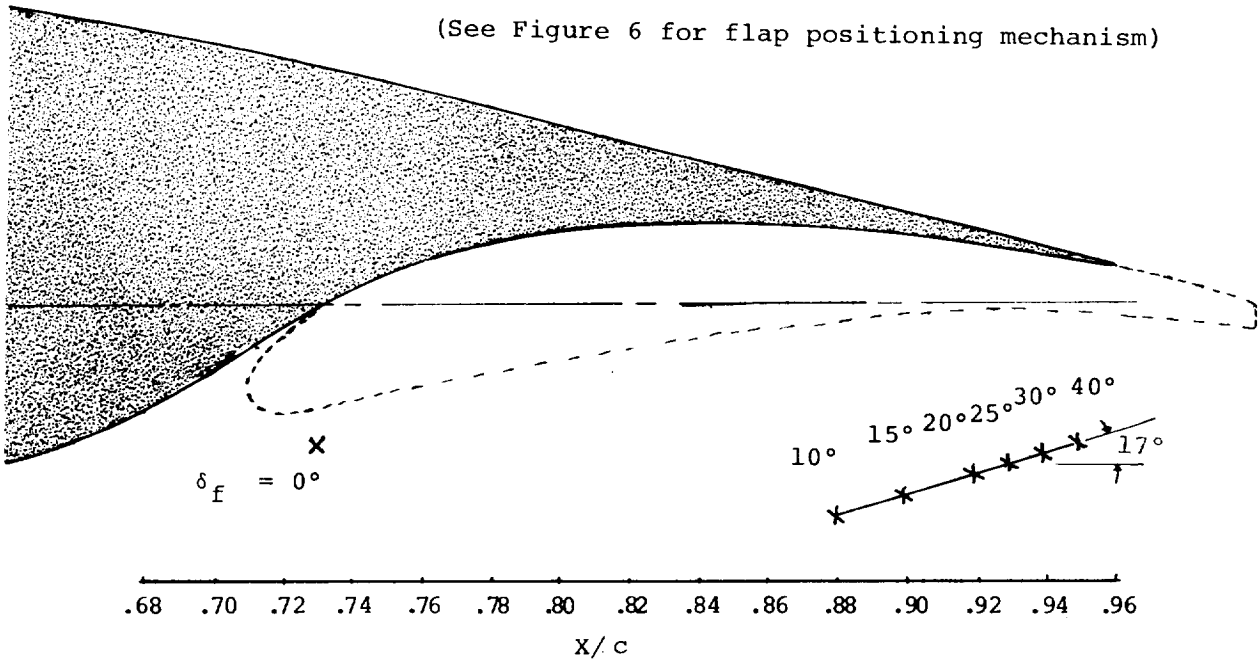

Figure 3 - Flap Pivot Point Locations

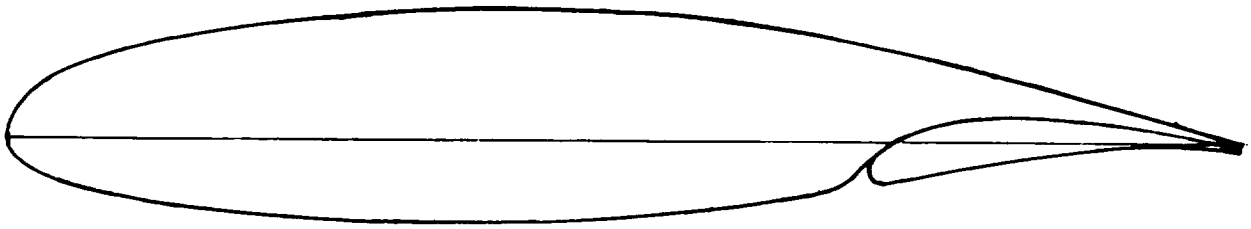

30%c Fowler Flap Coordinates

Upper Surface		Lower Surface	
X_f/c	Z_f/c	X_f/c	Z_f/c
.000	-.01920	.000	-.01920
.025	.00250	.025	-.02940
.050	.01100	.050	-.02490
.075	.01630	.075	-.02040
.100	.01900	.100	-.01600
.125	.01950	.125	-.01200
.150	.01820	.150	-.00860
.175	.01670	.175	-.00580
.200	.01330	.200	-.00360
.225	.00950	.225	-.00250
.250	.00530	.250	-.00260
.275	.00100	.275	-.00400
.300	-.00435	.300	-.00800

L.E. Radius = 0.0122c

Figure 4 - 30% c Fowler Flap Configuration

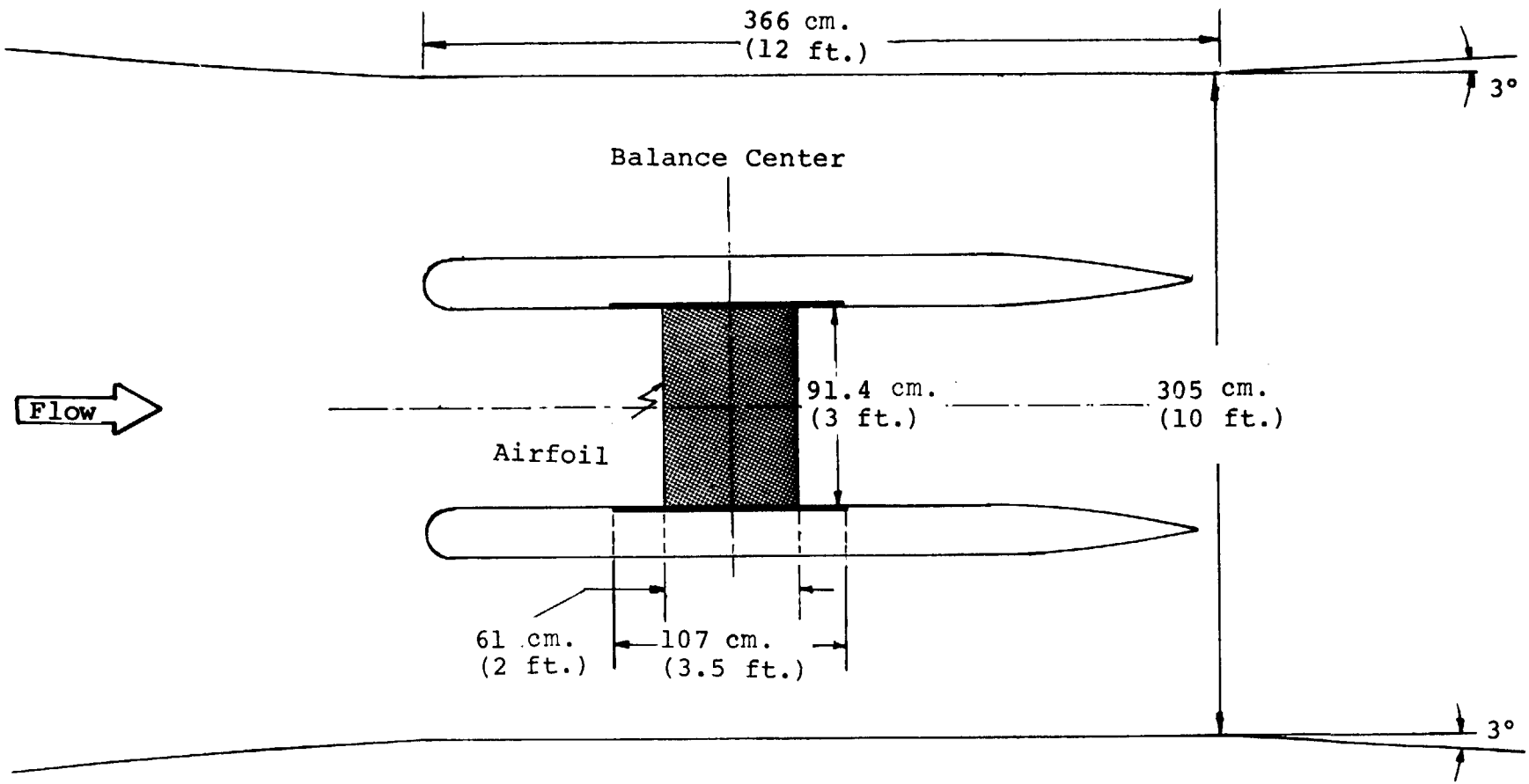

Figure 5 - W.S.U. Low Speed Tunnel With Two Dimensional Insert

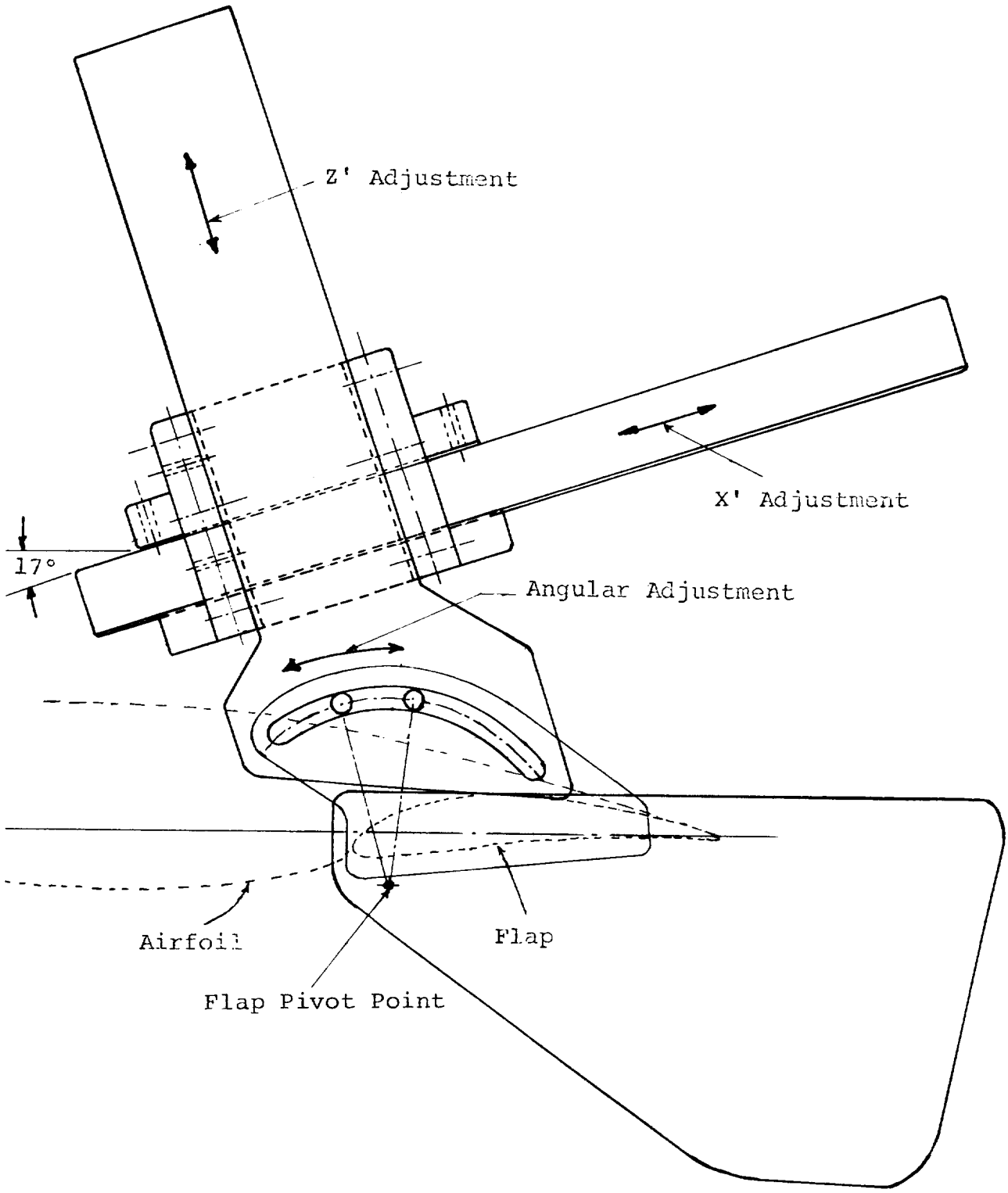

Figure 6 - Flap Positioning Mechanism

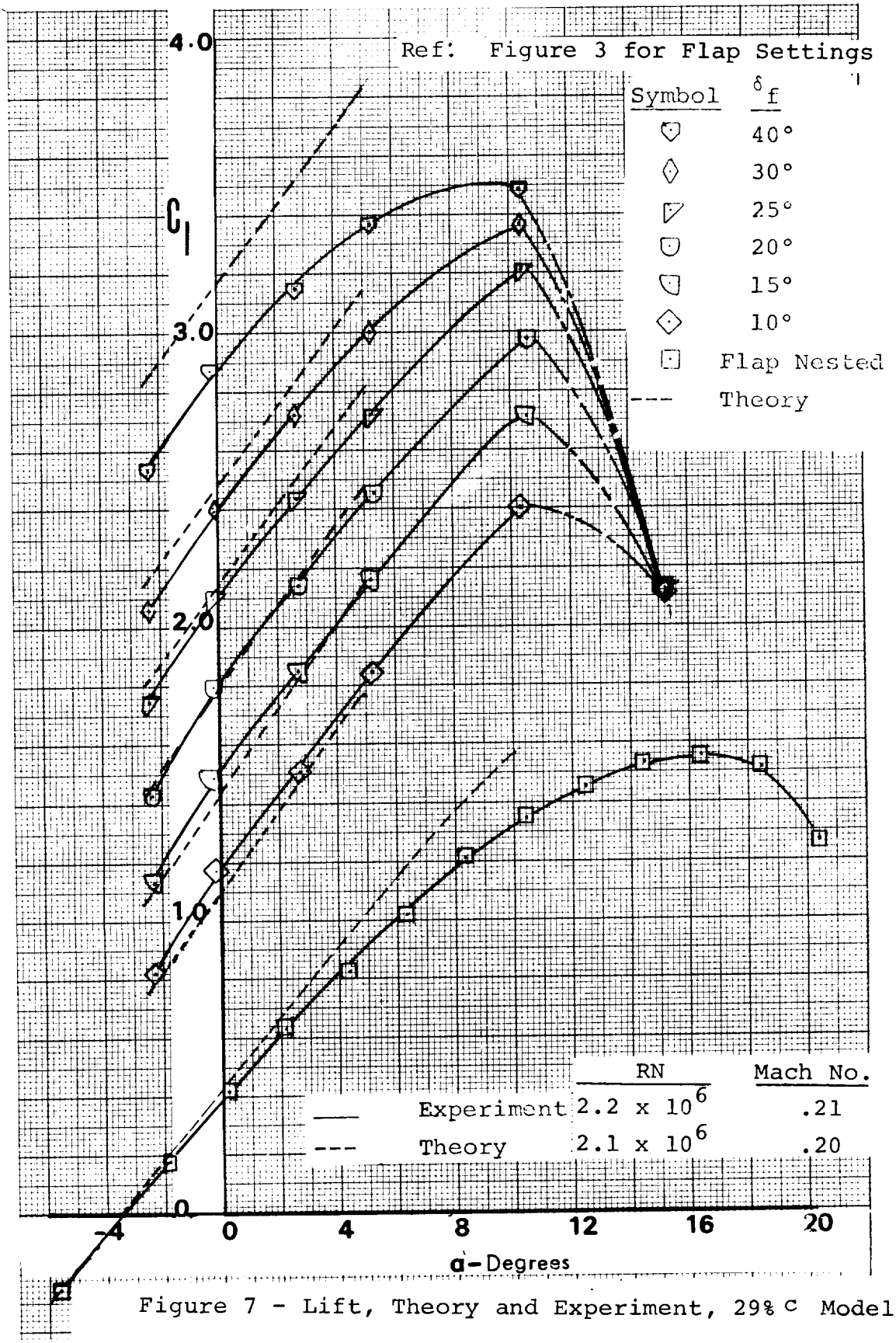

Figure 7 - Lift, Theory and Experiment, 29% c Model

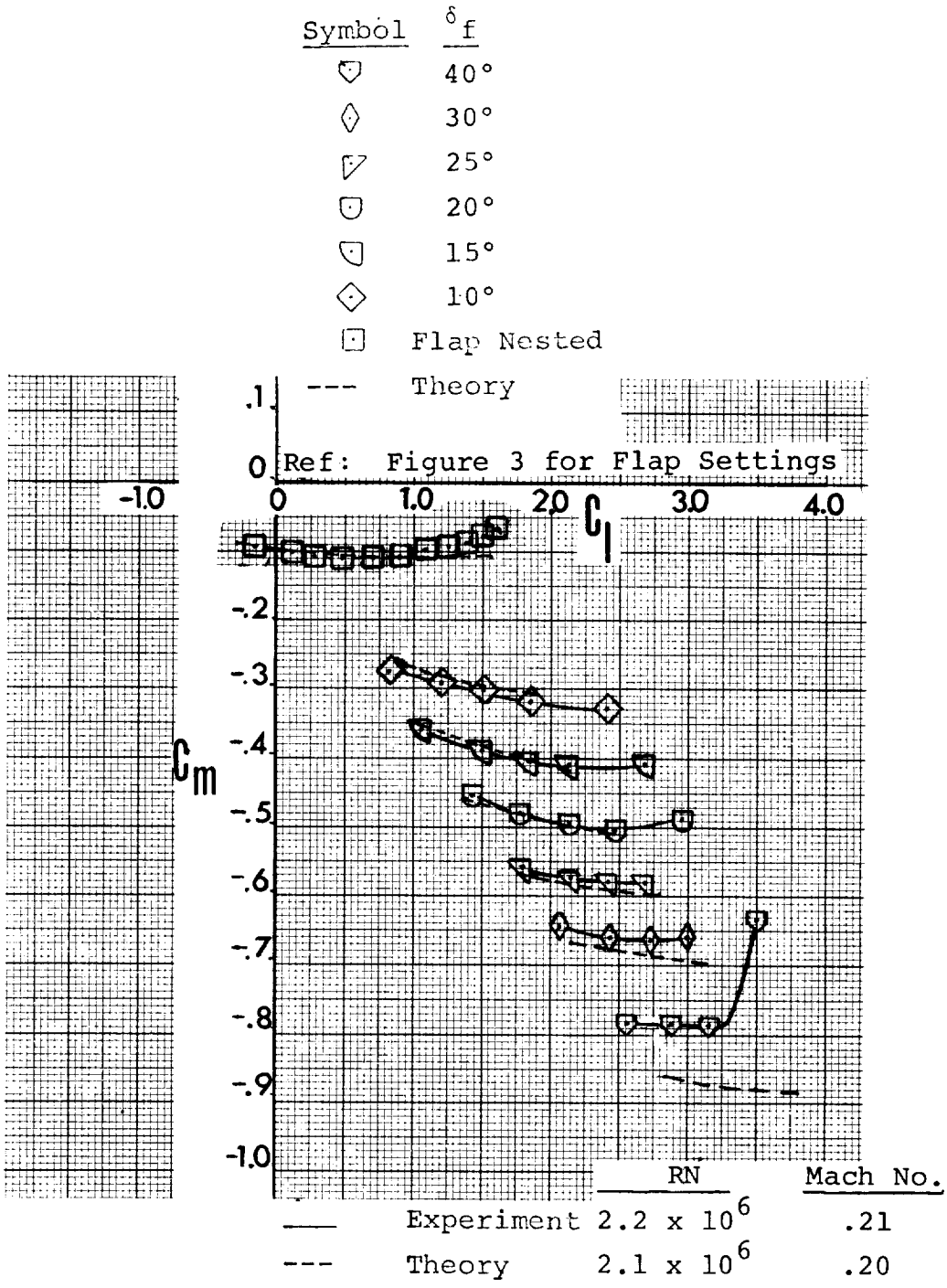

Figure 8 - Pitching Moments, Theory and Experiment, 29% c Model

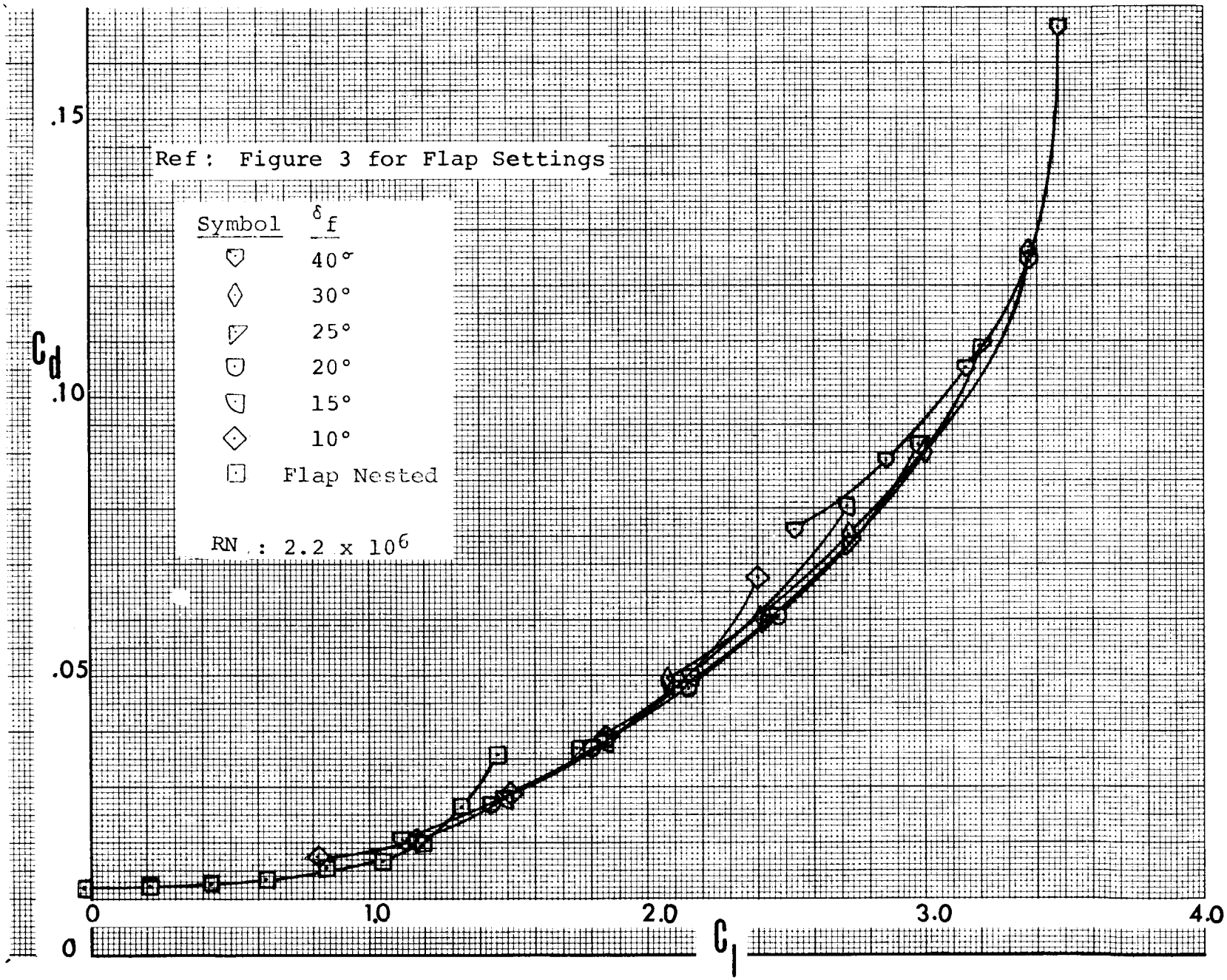

Figure 9 - Experimental Drag, 29% c Model

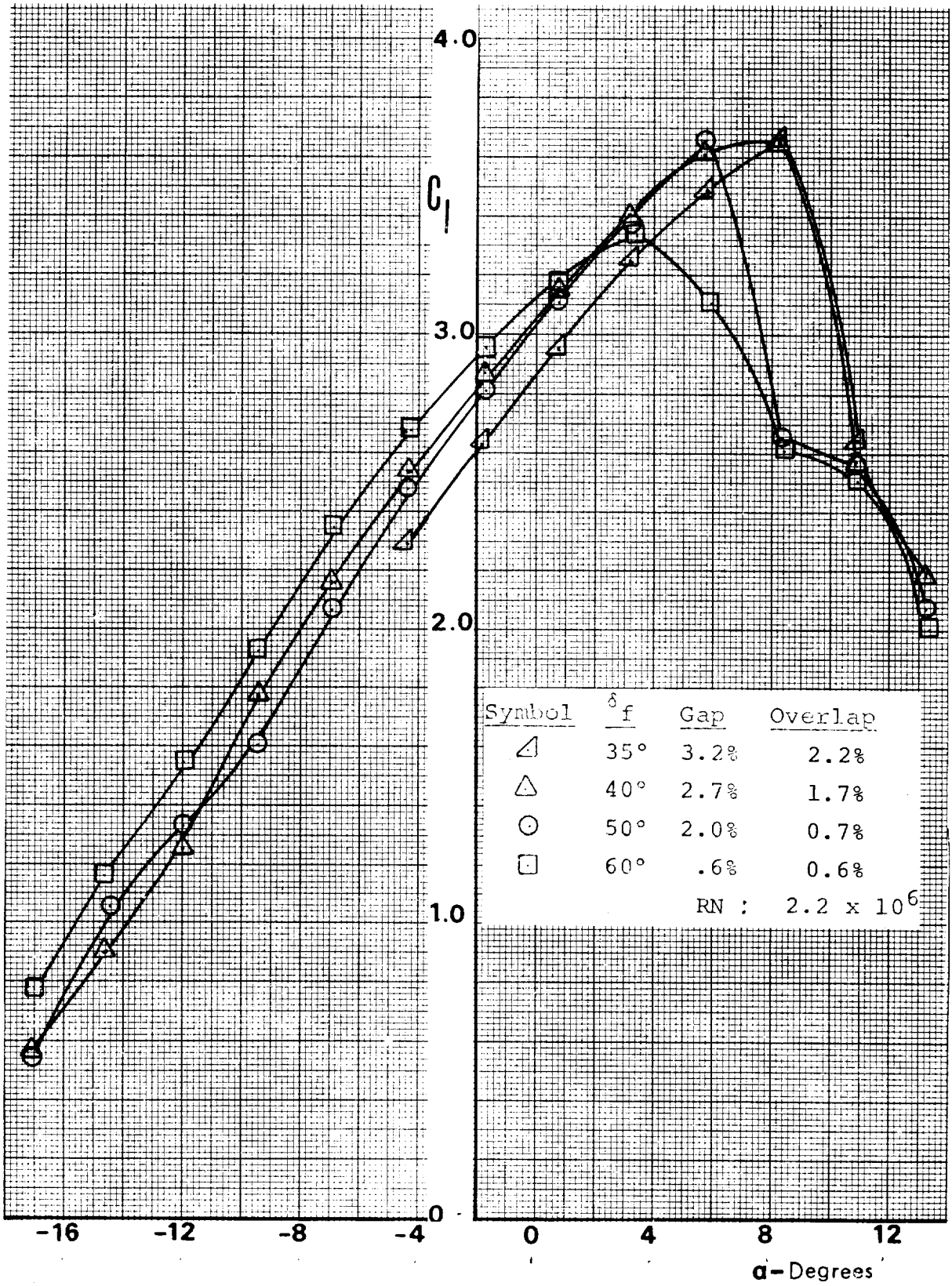

Figure 10 - Lift, High Flap Deflections, 29% c Model

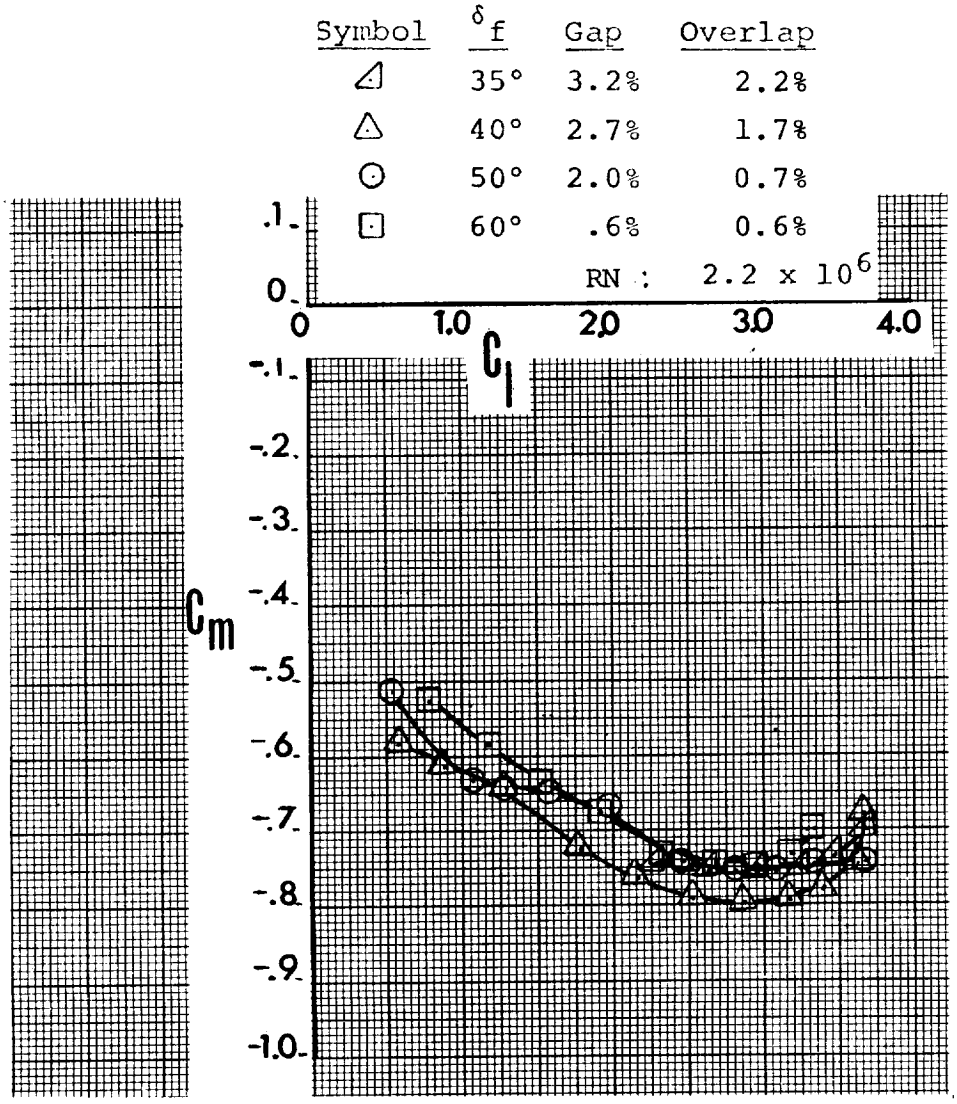

Figure 11 - Pitching Moments, High Flap Deflections, 29% c Model

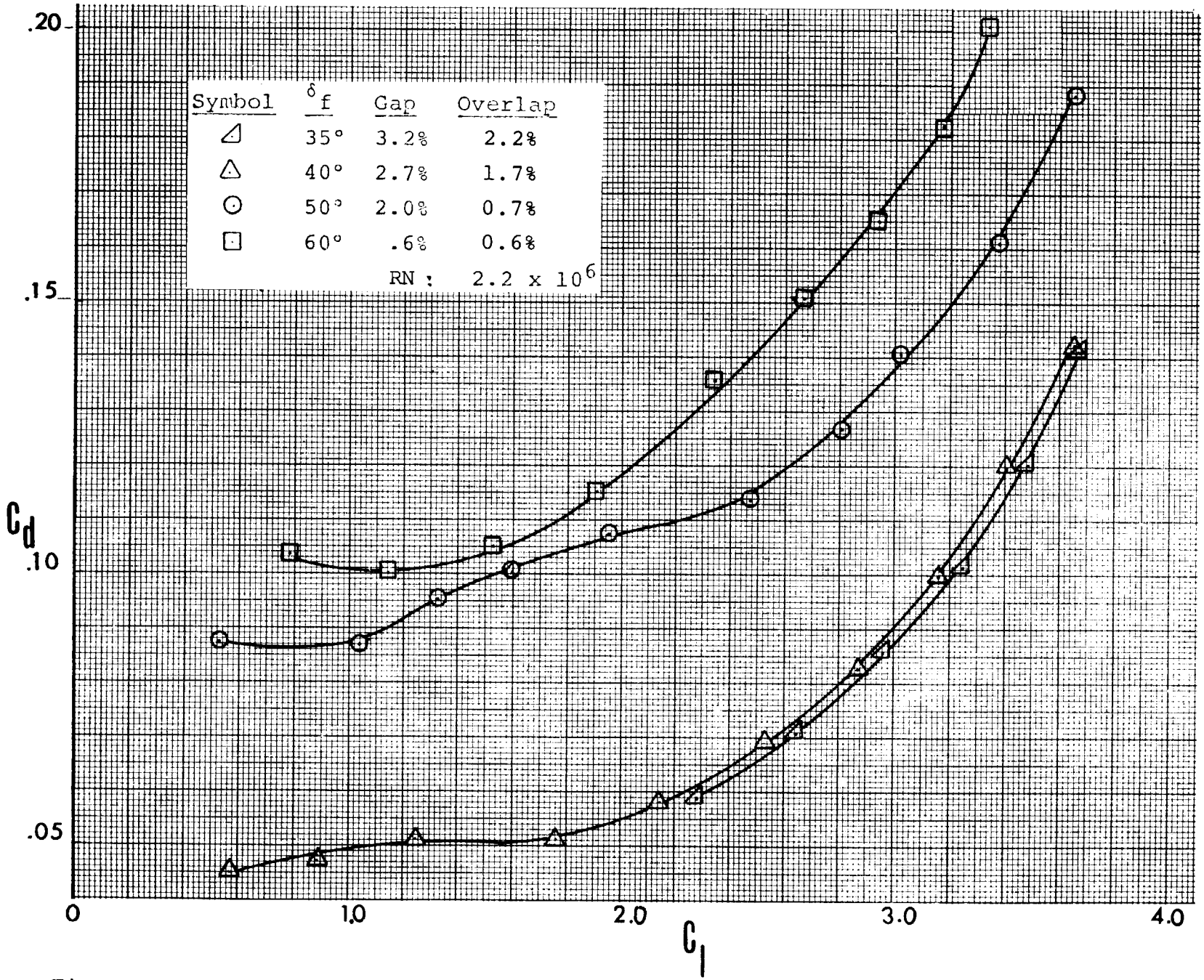

Figure 12 - Drag, High Flap Deflections, 29% c Model

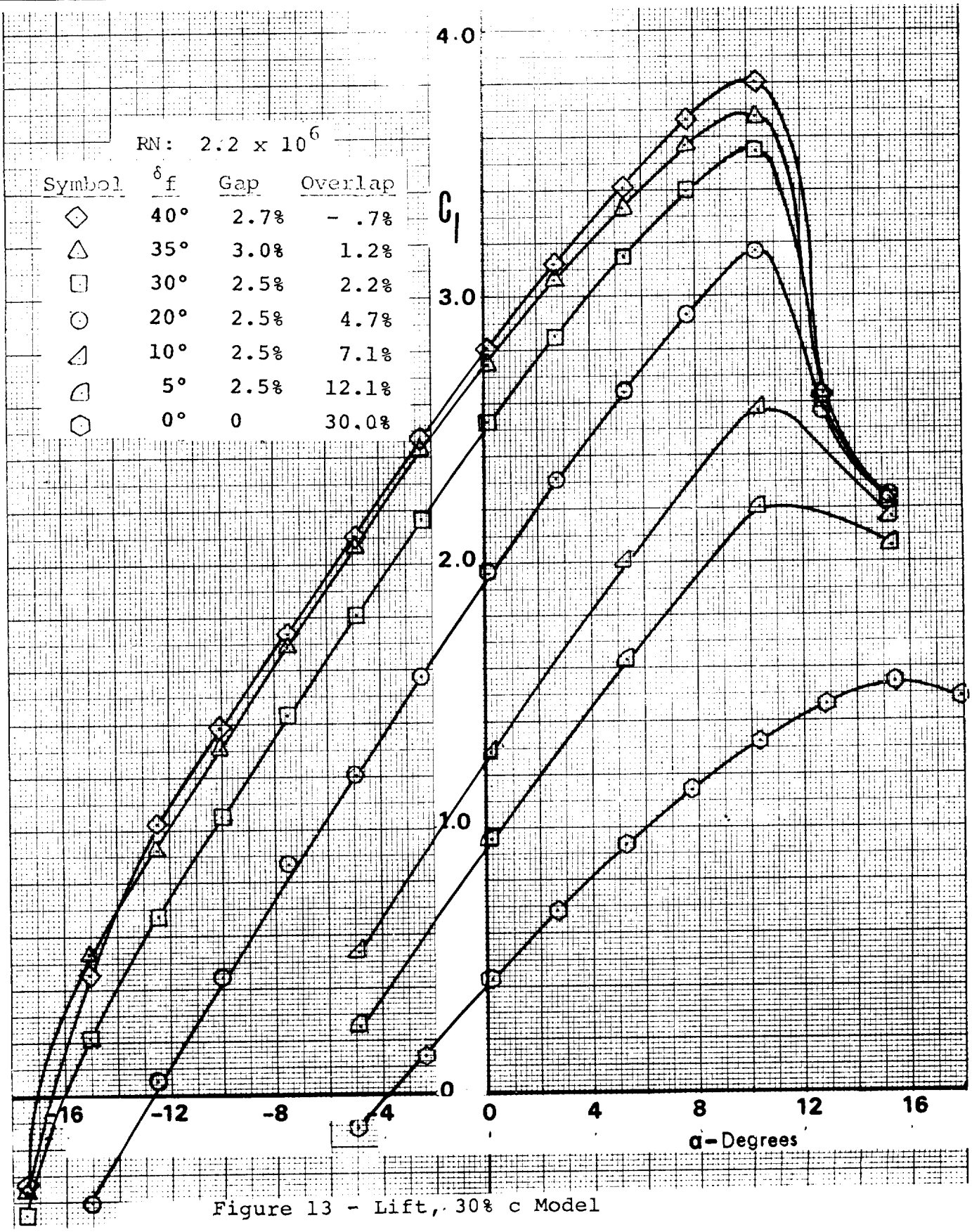

Figure 13 - Lift, 30% c Model

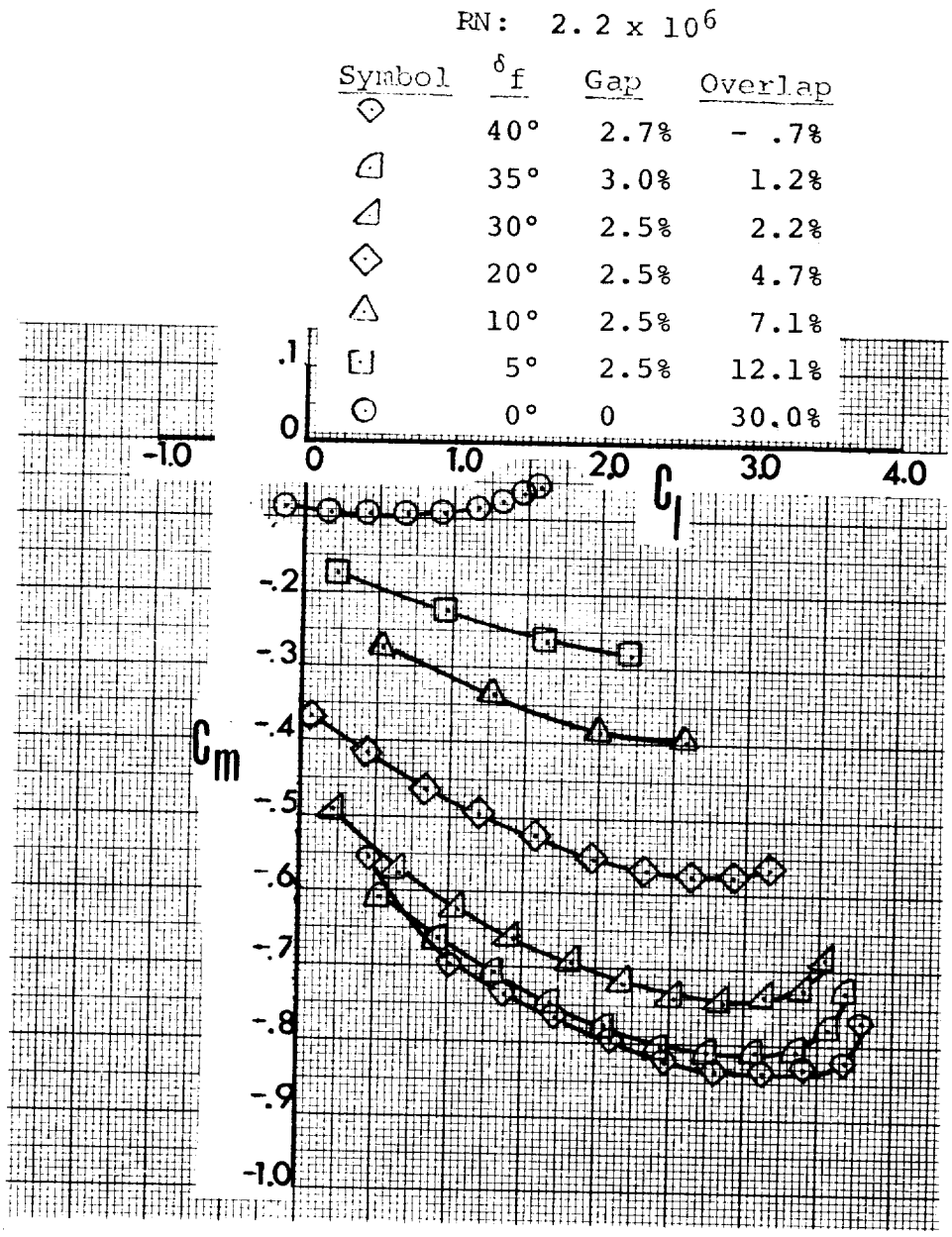

Figure 14 - Pitching Moments, 30% c Model

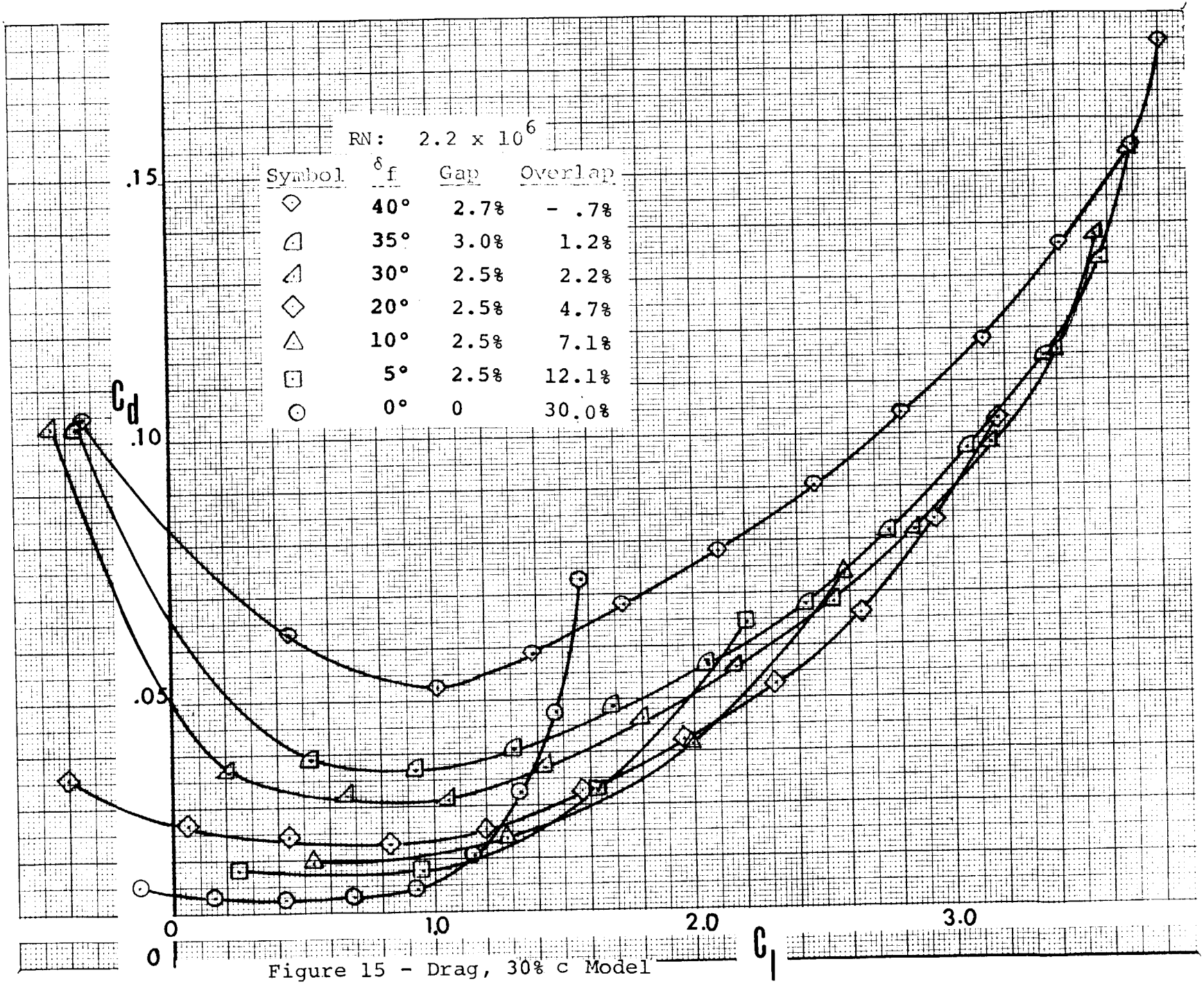

Figure 15 - Drag, 30% c Model

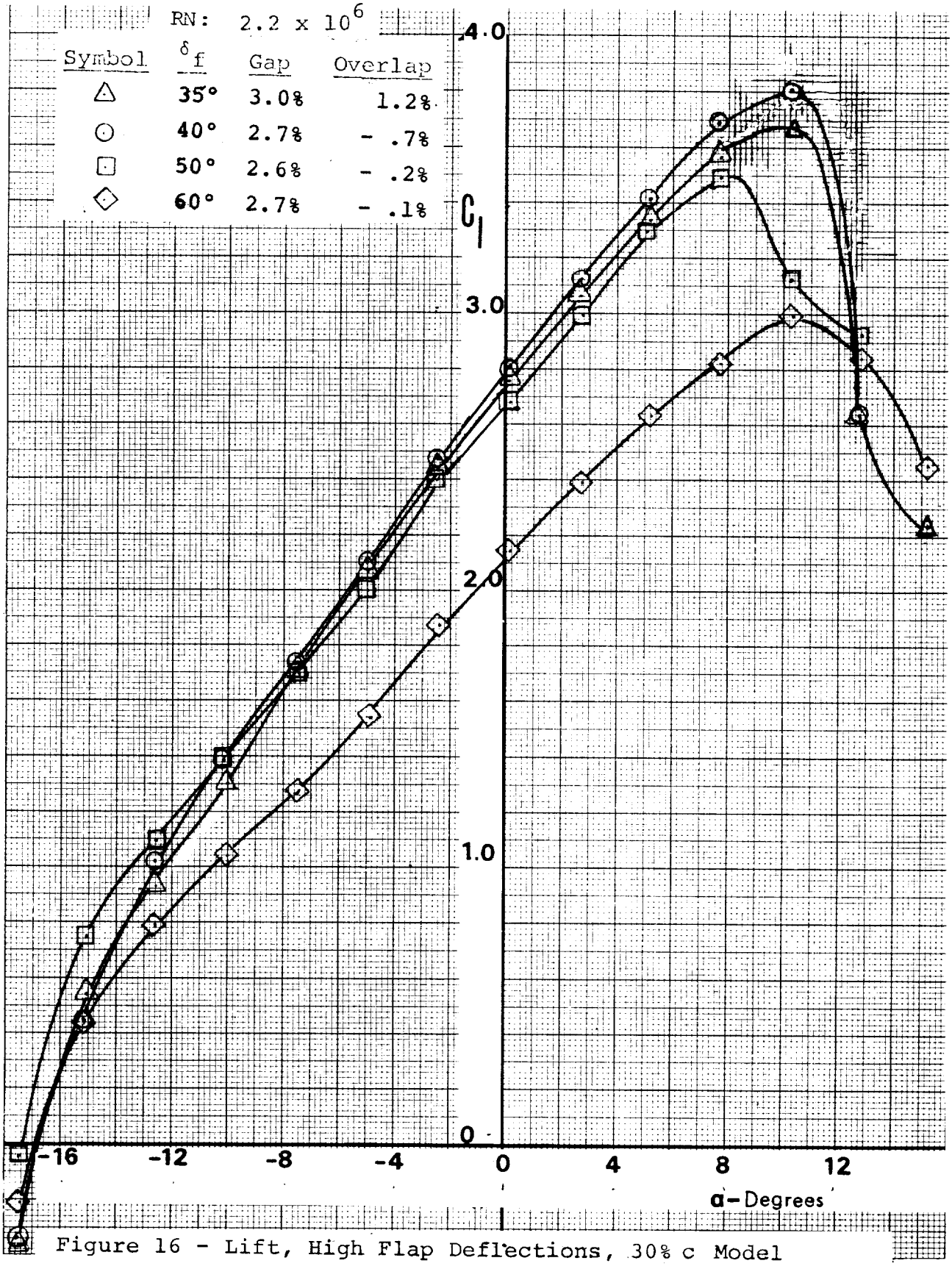

Figure 16 - Lift, High Flap Deflections, 30% c Model

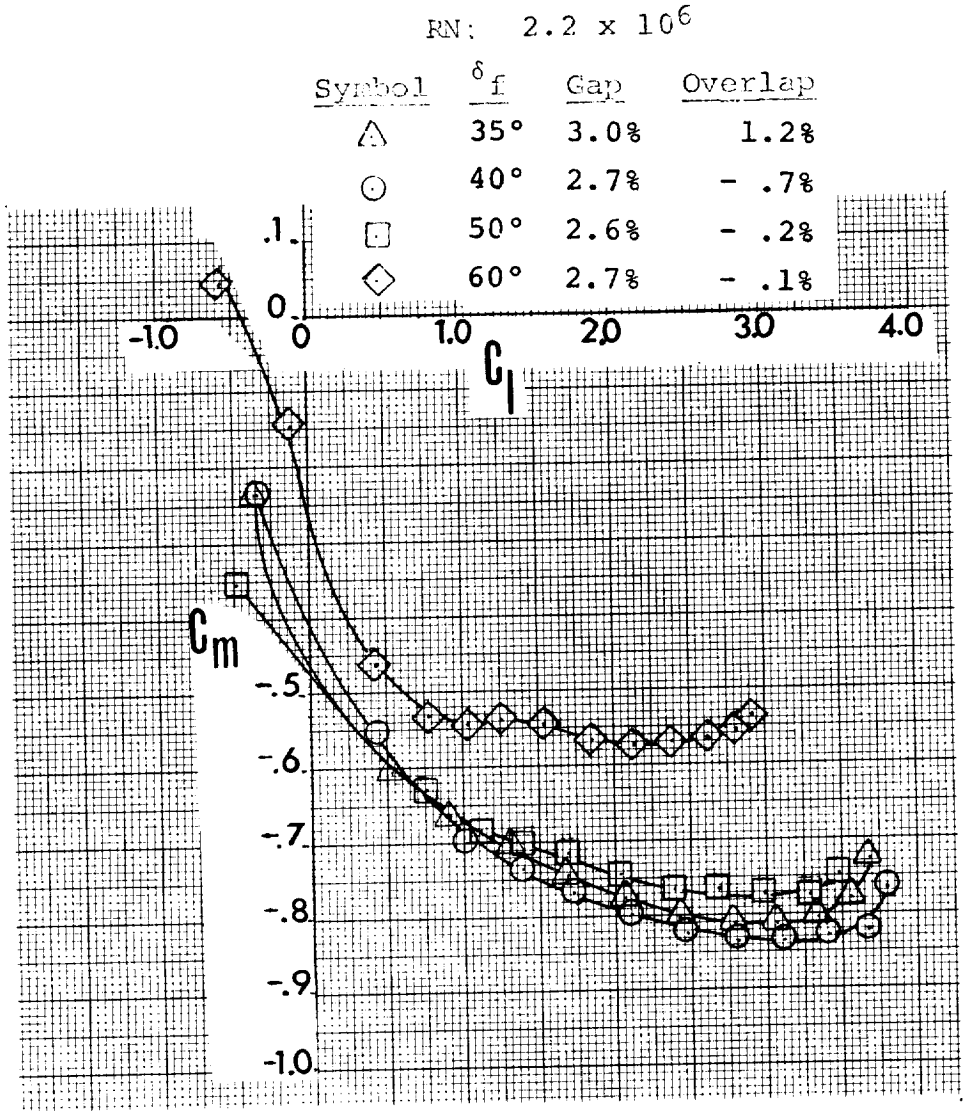

Figure 17 - Pitching Moments, High Flap Deflections 30% C Model

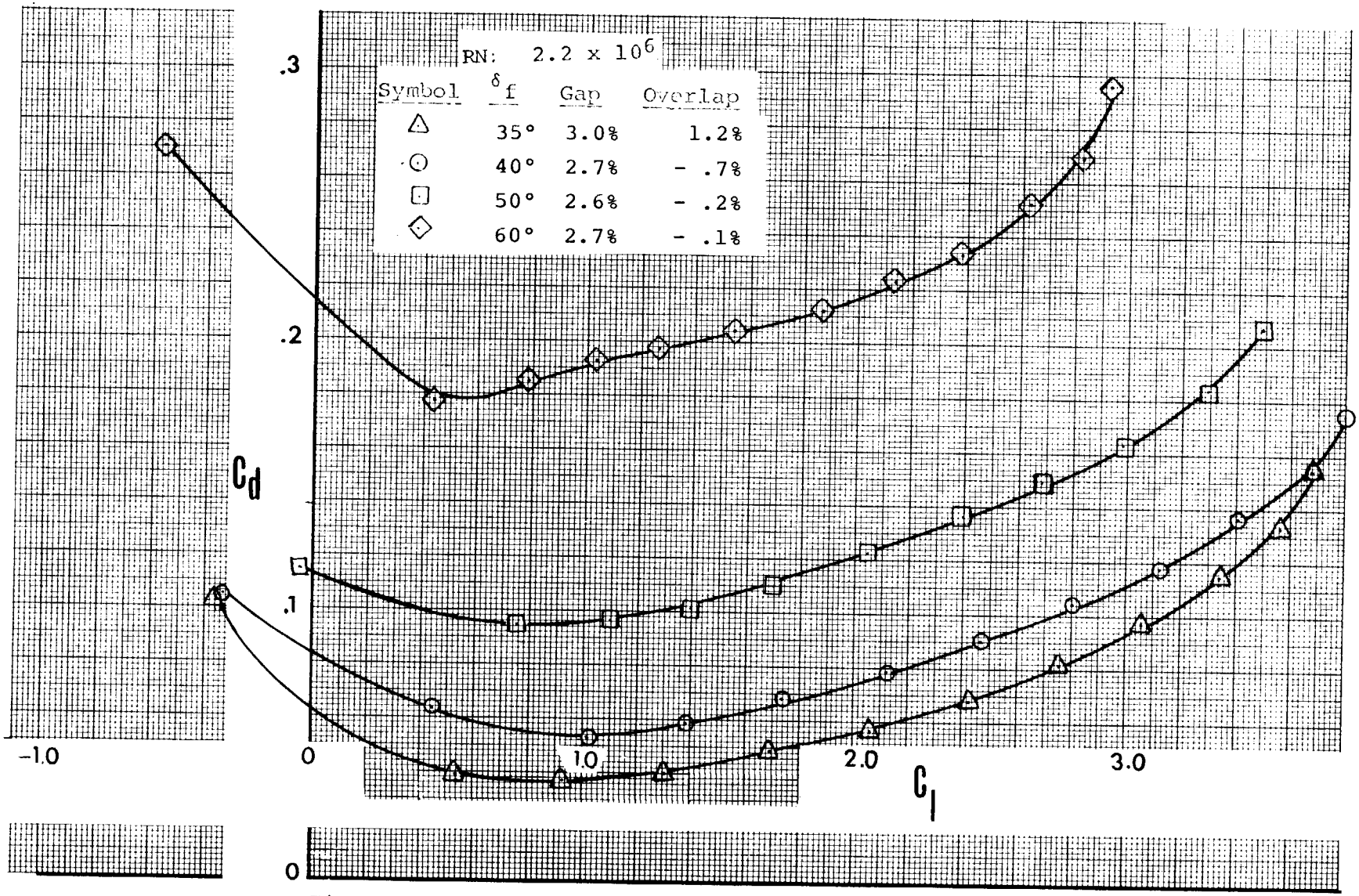

Figure 18 - Drag, High Flap Deflections, 30% c Model

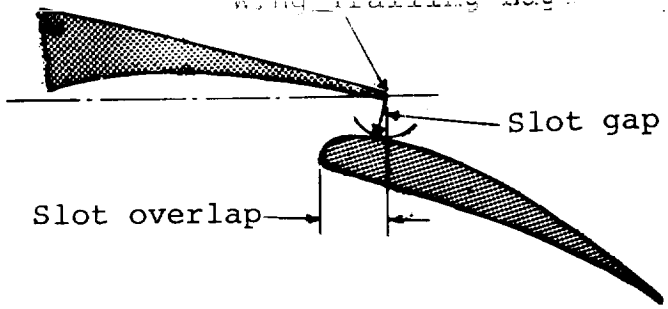

Definitions of gap and overlap.

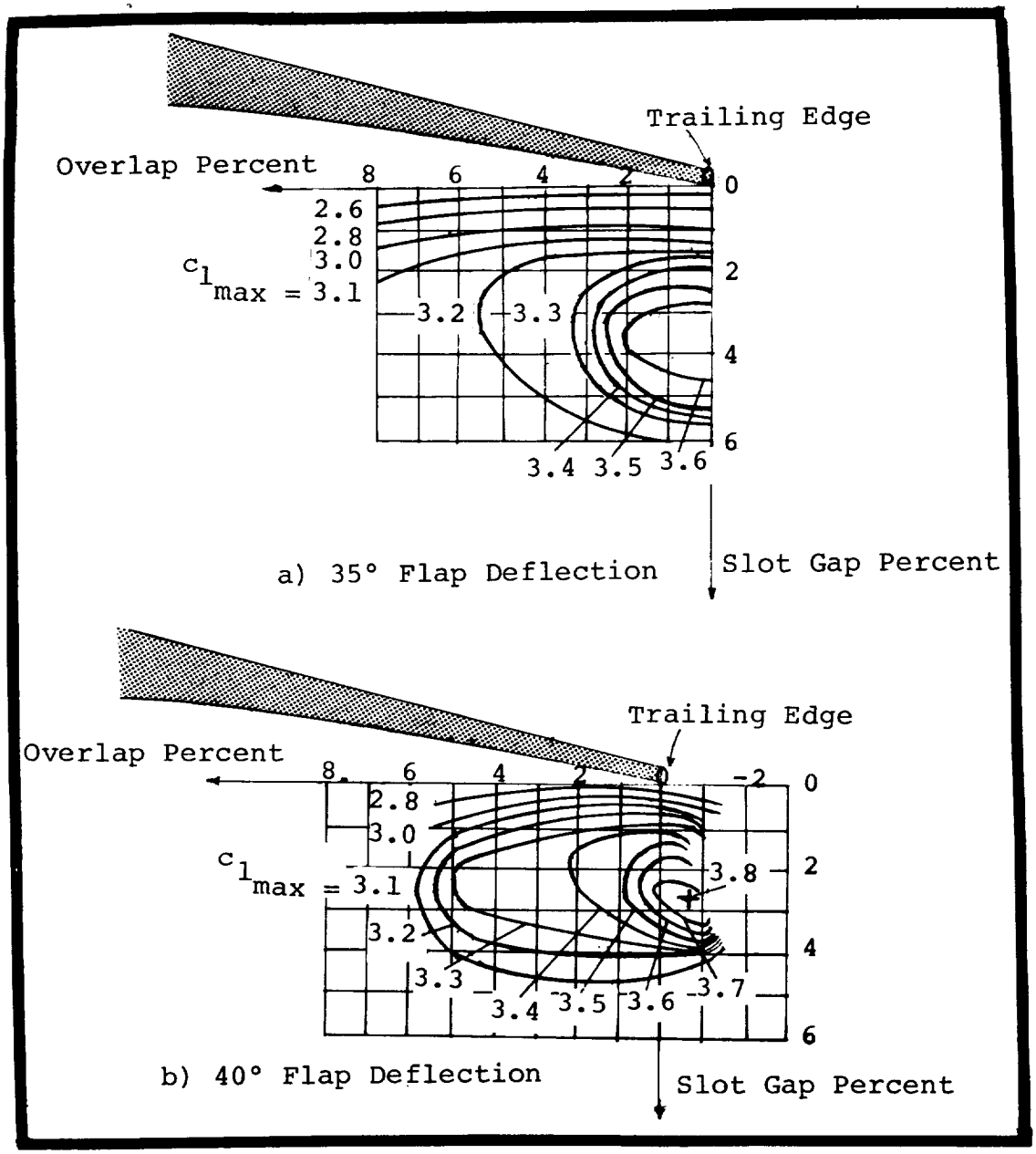

Figure 19 - Optimization of Slot Geometry for Maximum c_l, 30% c Model

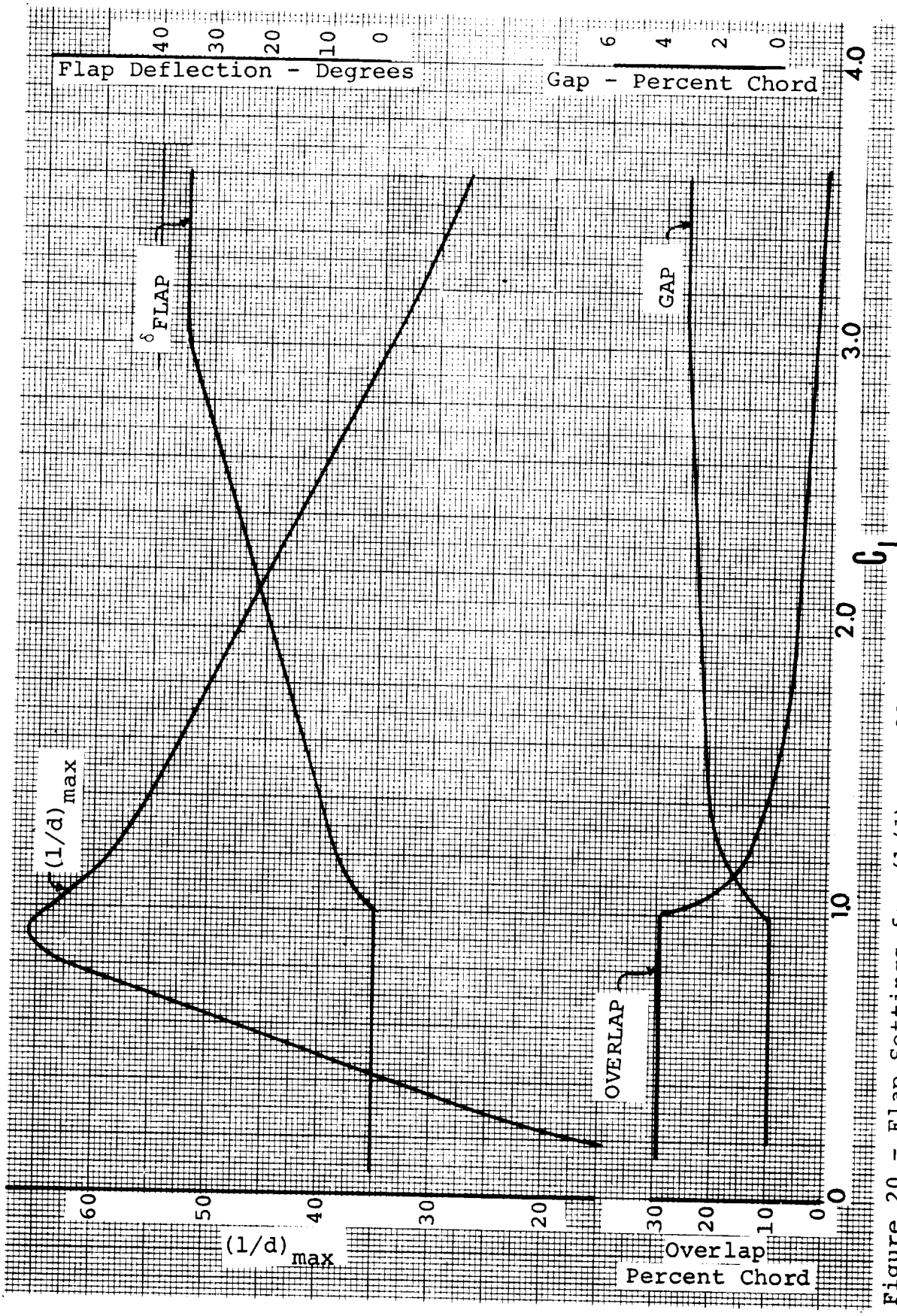

Figure 20 - Flap Settings for $(1/d)_{max}$, 29% c Model

Figure 21 - Flap Settings for $(l/d)_{max}$, 30% c Model

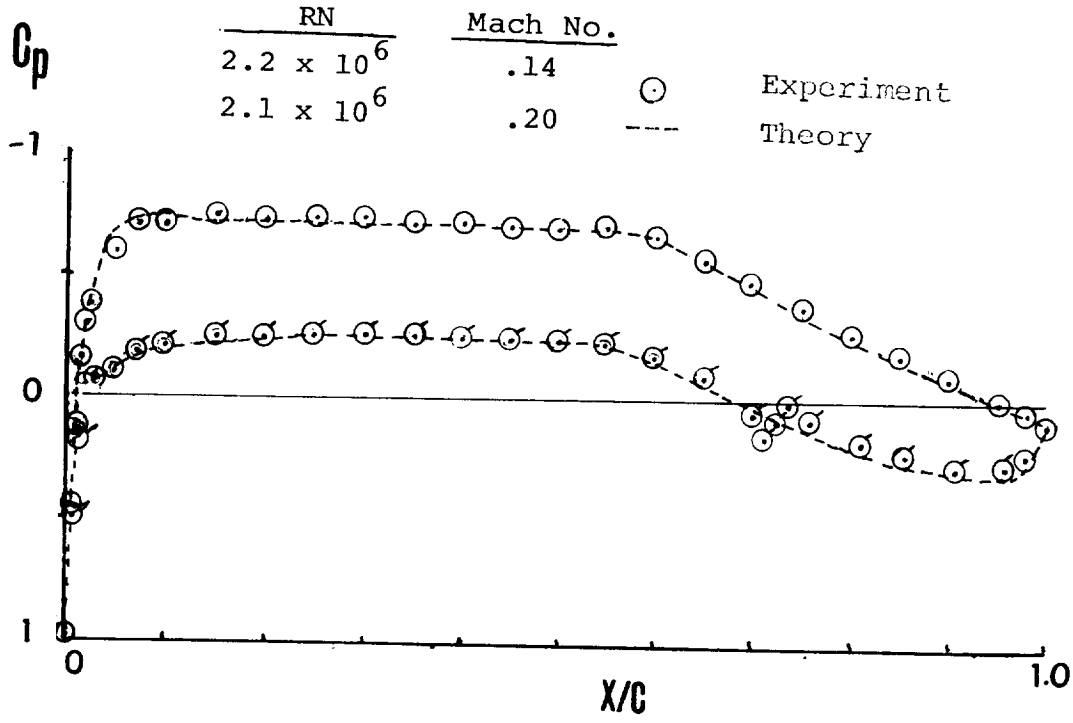

Figure 22 - Pressure Distribution, Flap Nested, $\alpha = 0°$

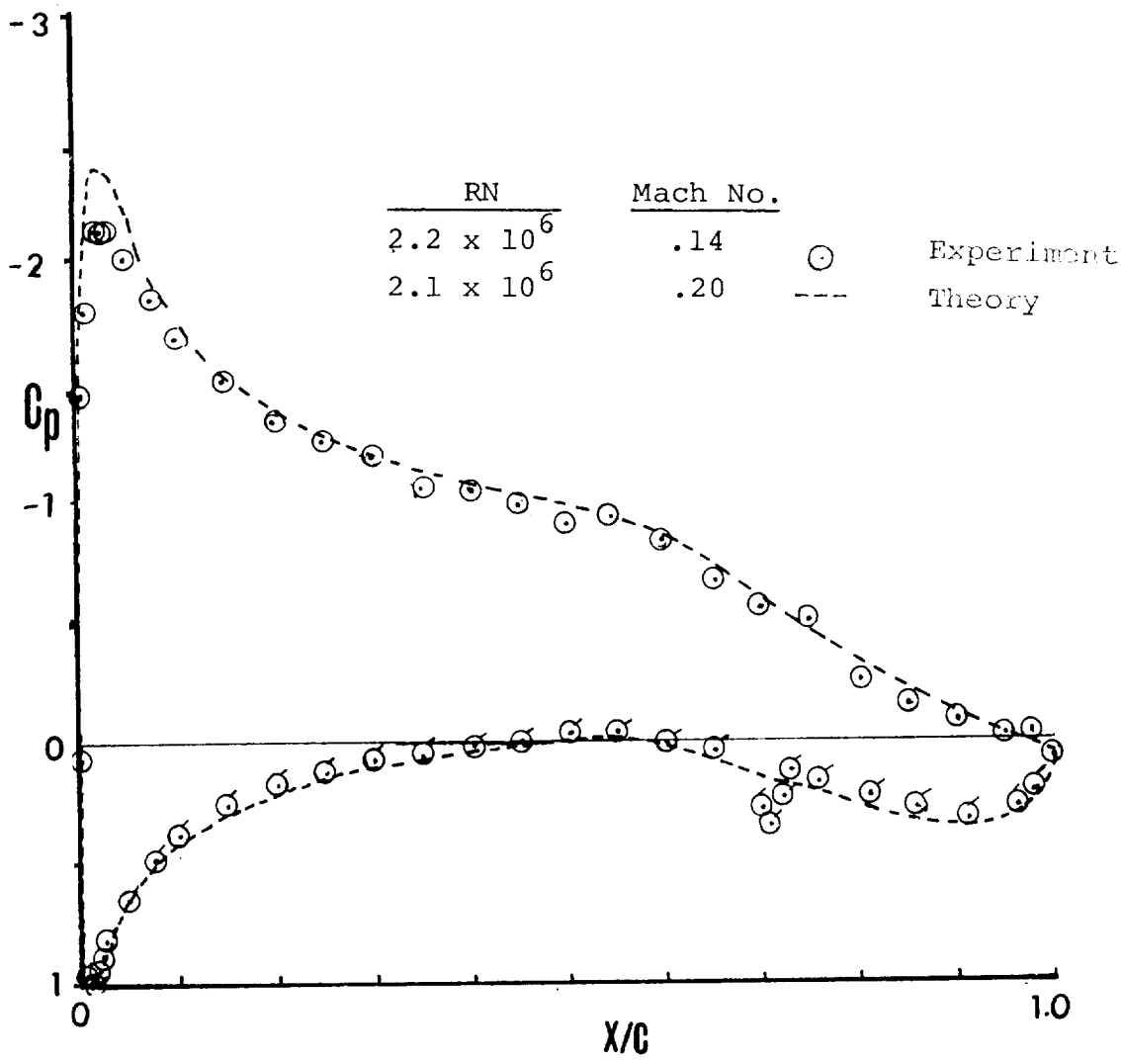

Figure 23 - Pressure Distribution, Flap Nested, $\alpha = 6°$

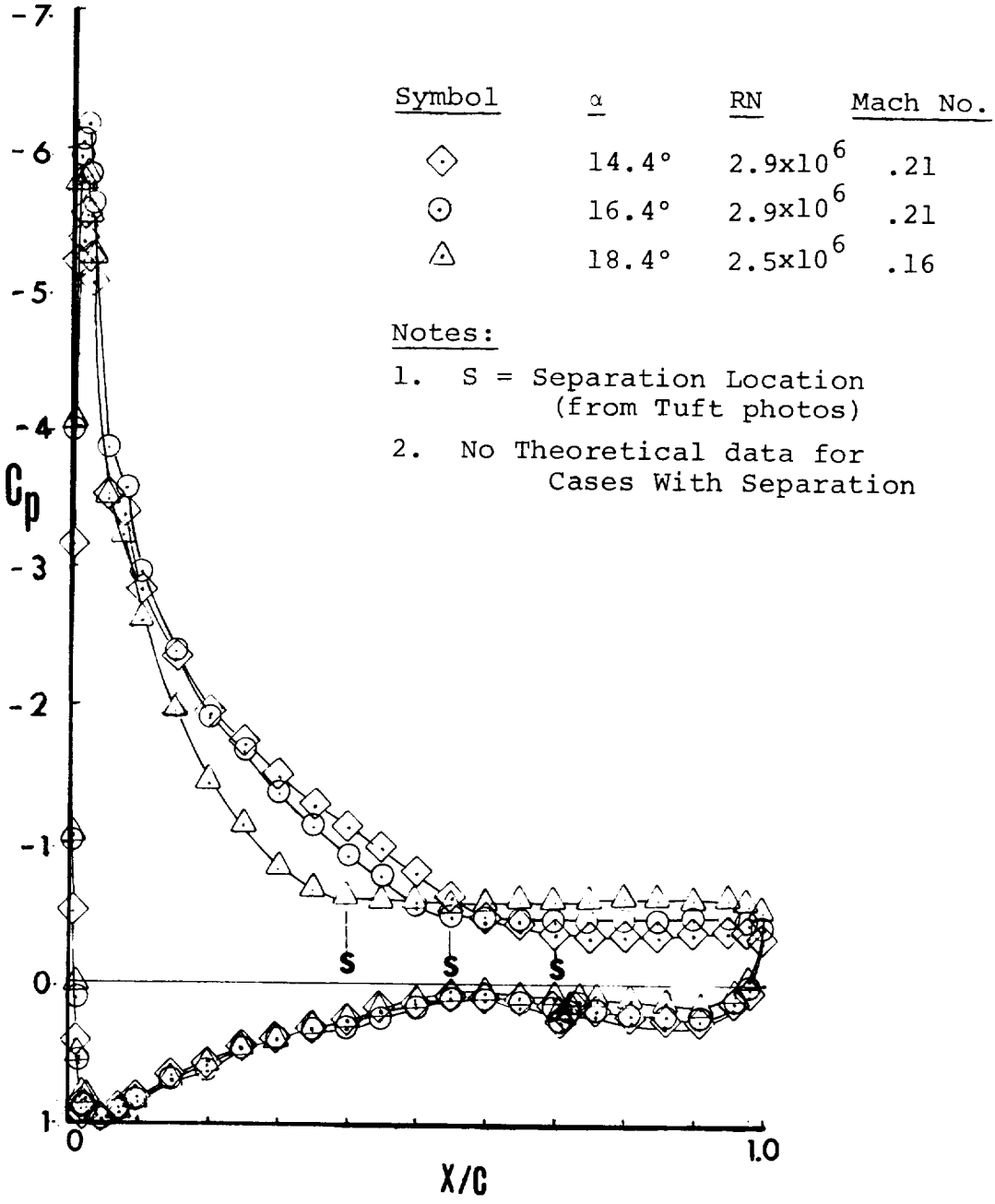

Figure 24 - Pressure Distributions, Flap Nested

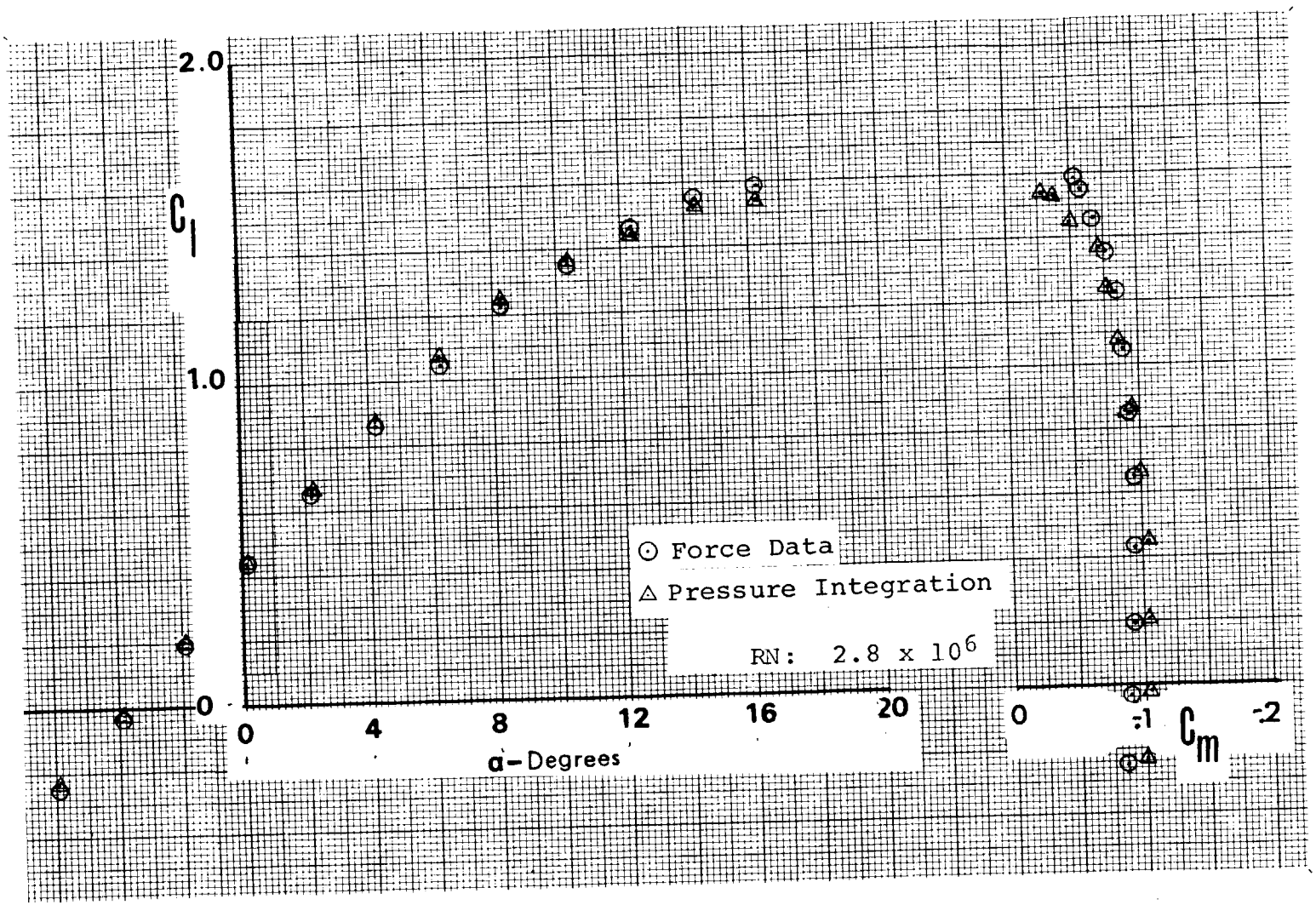

Figure 25 - Comparison of Integrated Pressures with Measured Forces and Moments, Flap Nested

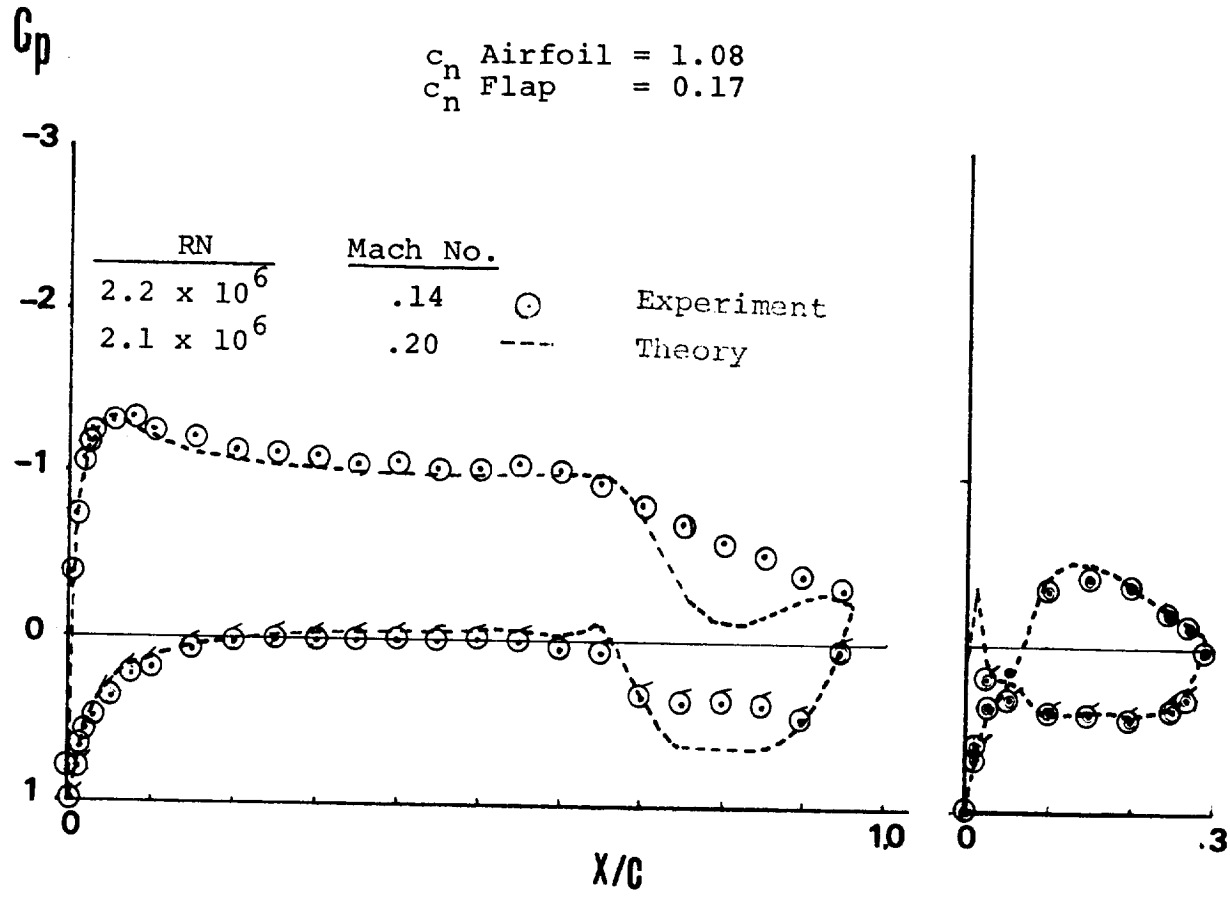

Figure 26 - Pressure Distribution, 29% c Model 10° Flap, α = 0°

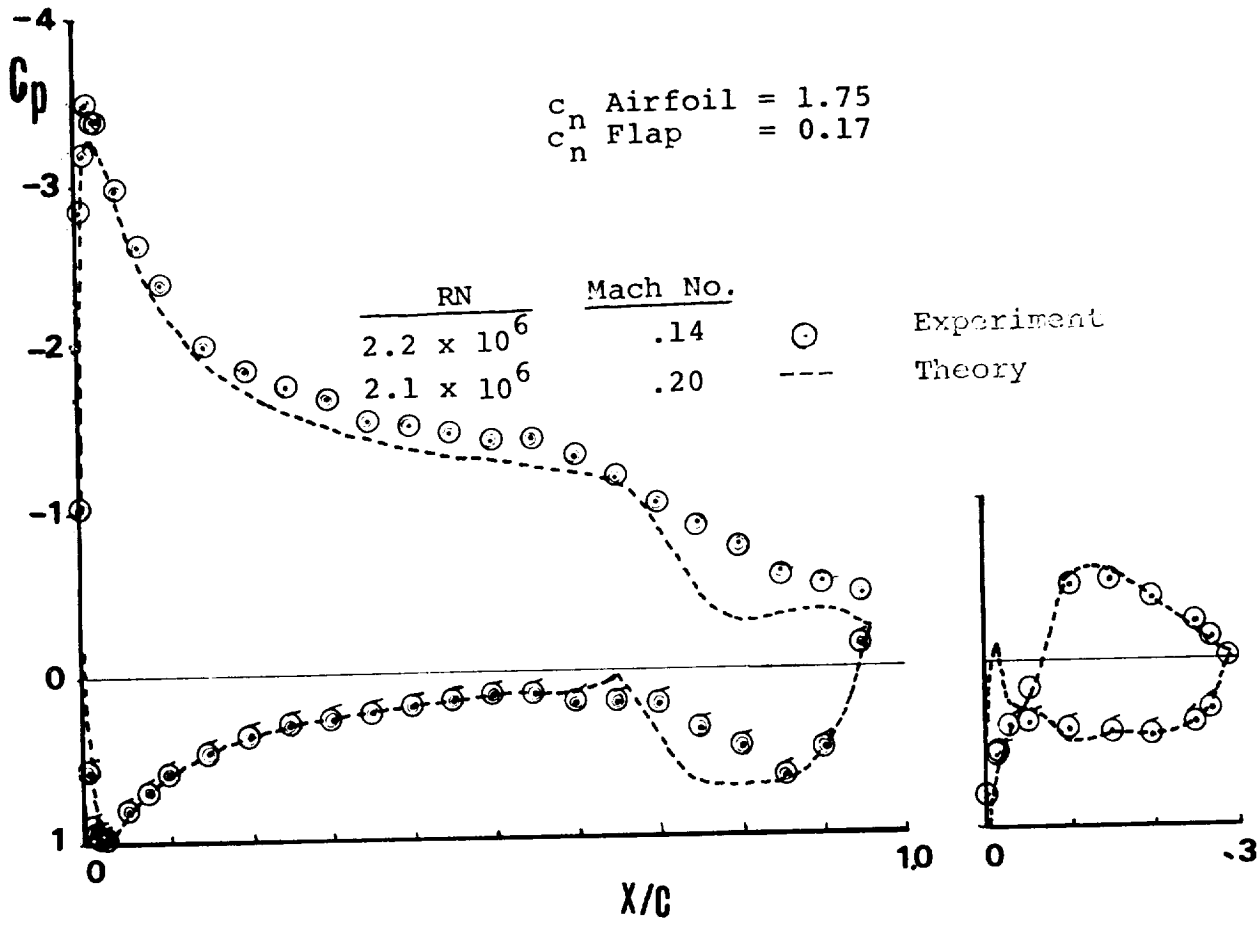

Figure 27 - Pressure Distribution, 29% c Model 10° Flap, α = 5°

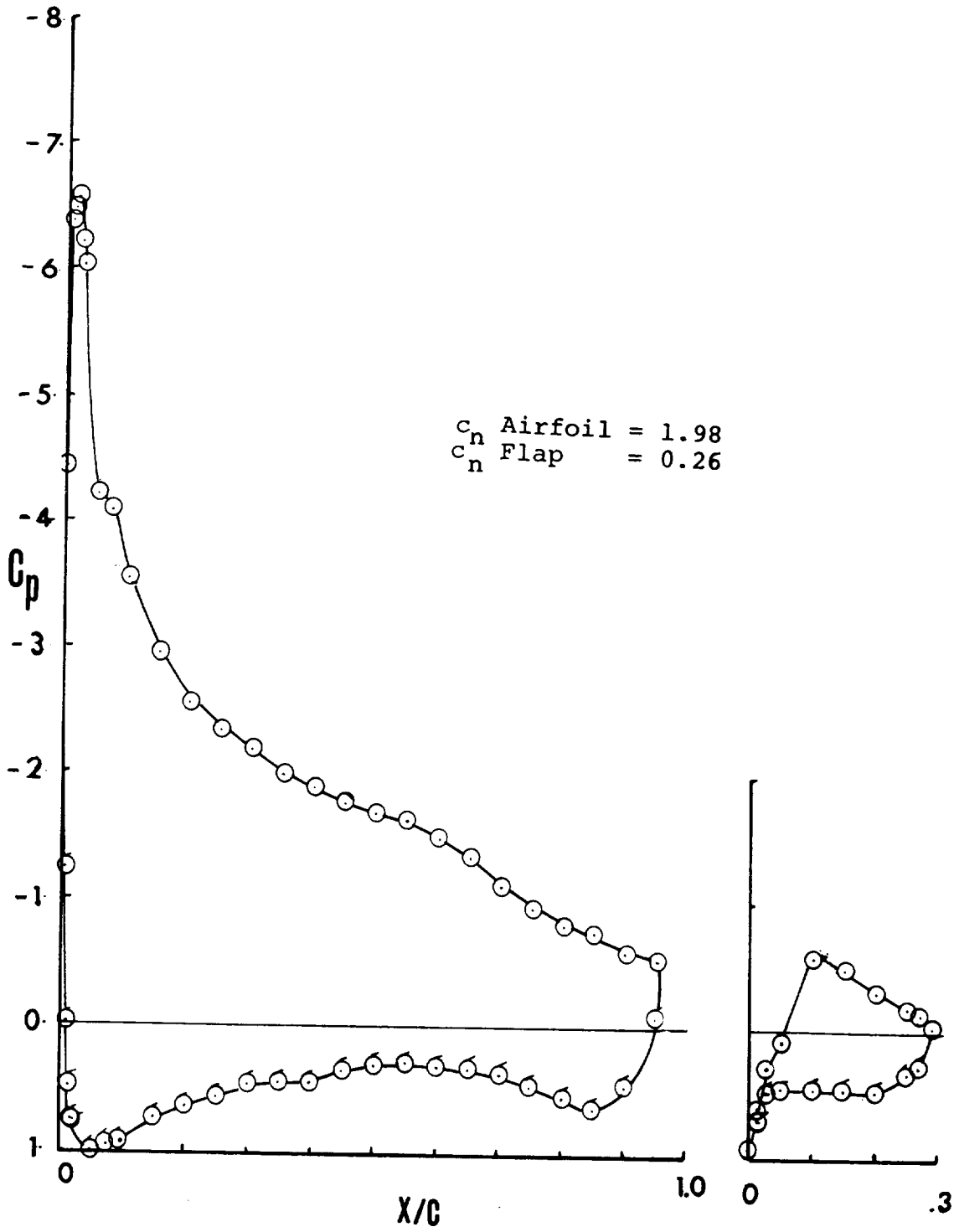

Figure 28 - Pressure Distribution, 29% c Model, 10° Flap, α = 15°

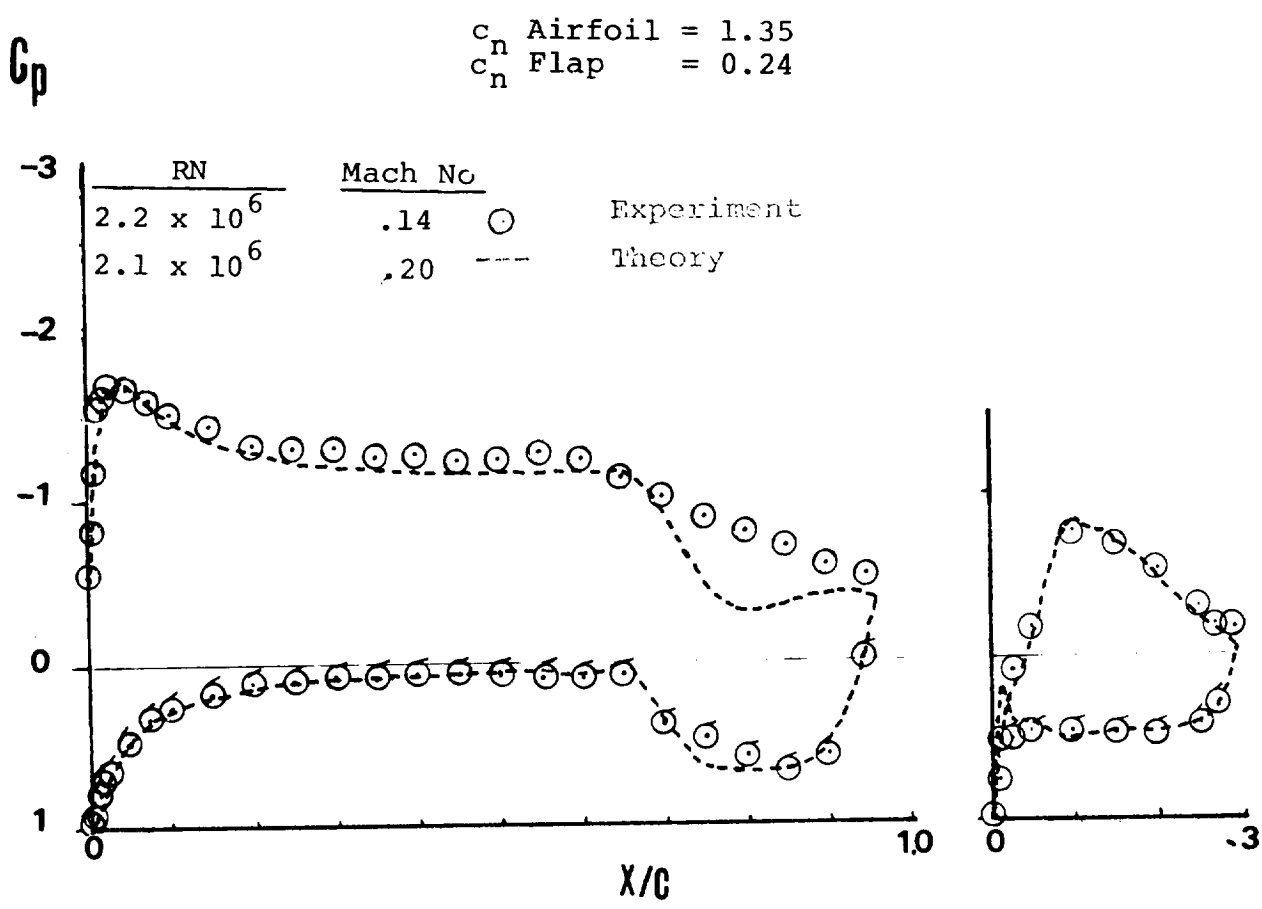

Figure 29 - Pressure Distribution, 29% c Model, 15° Flap, α = 0°

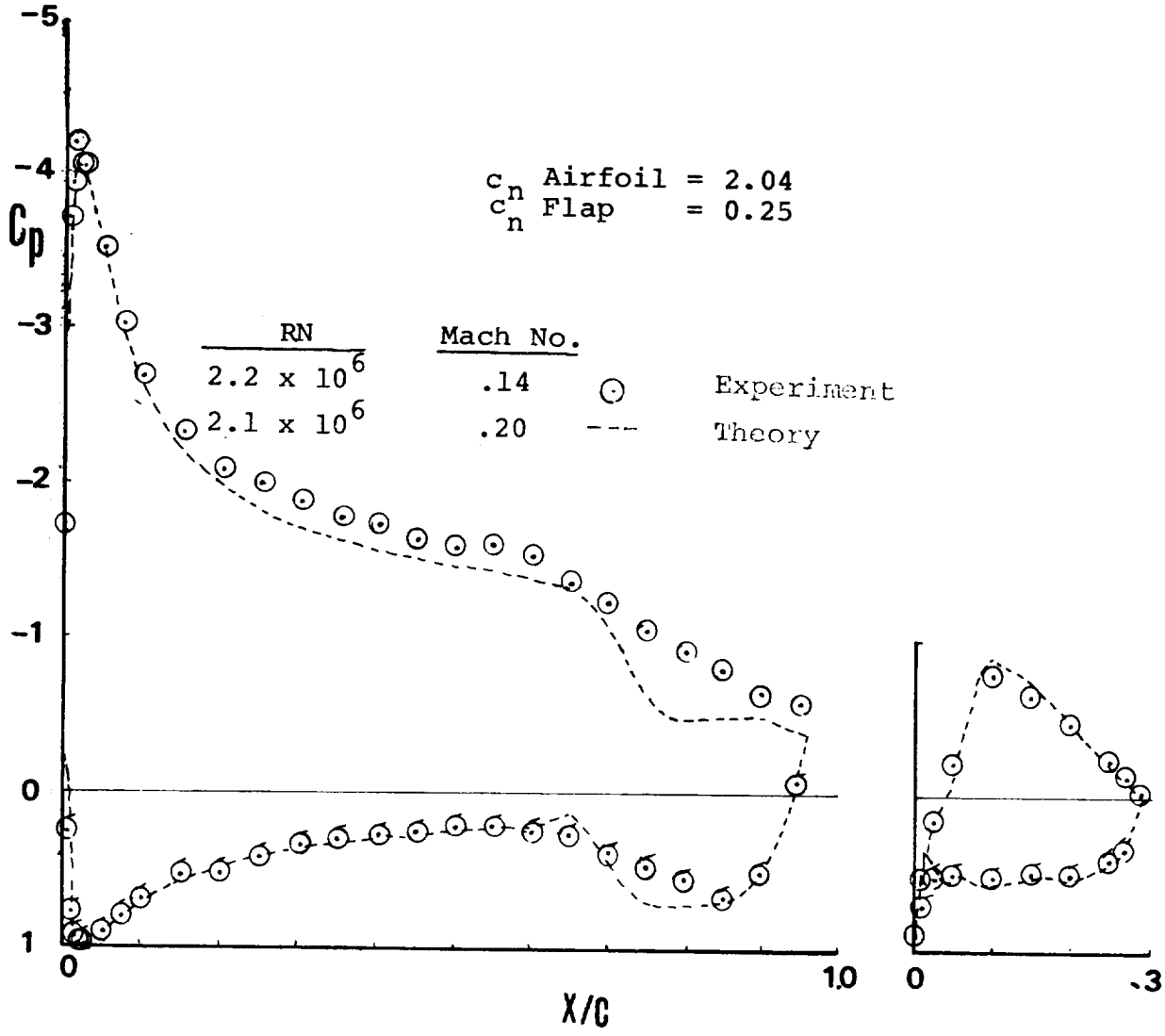

Figure 30 - Pressure Distribution, 29% c Model, 15° Flap, α = 5°

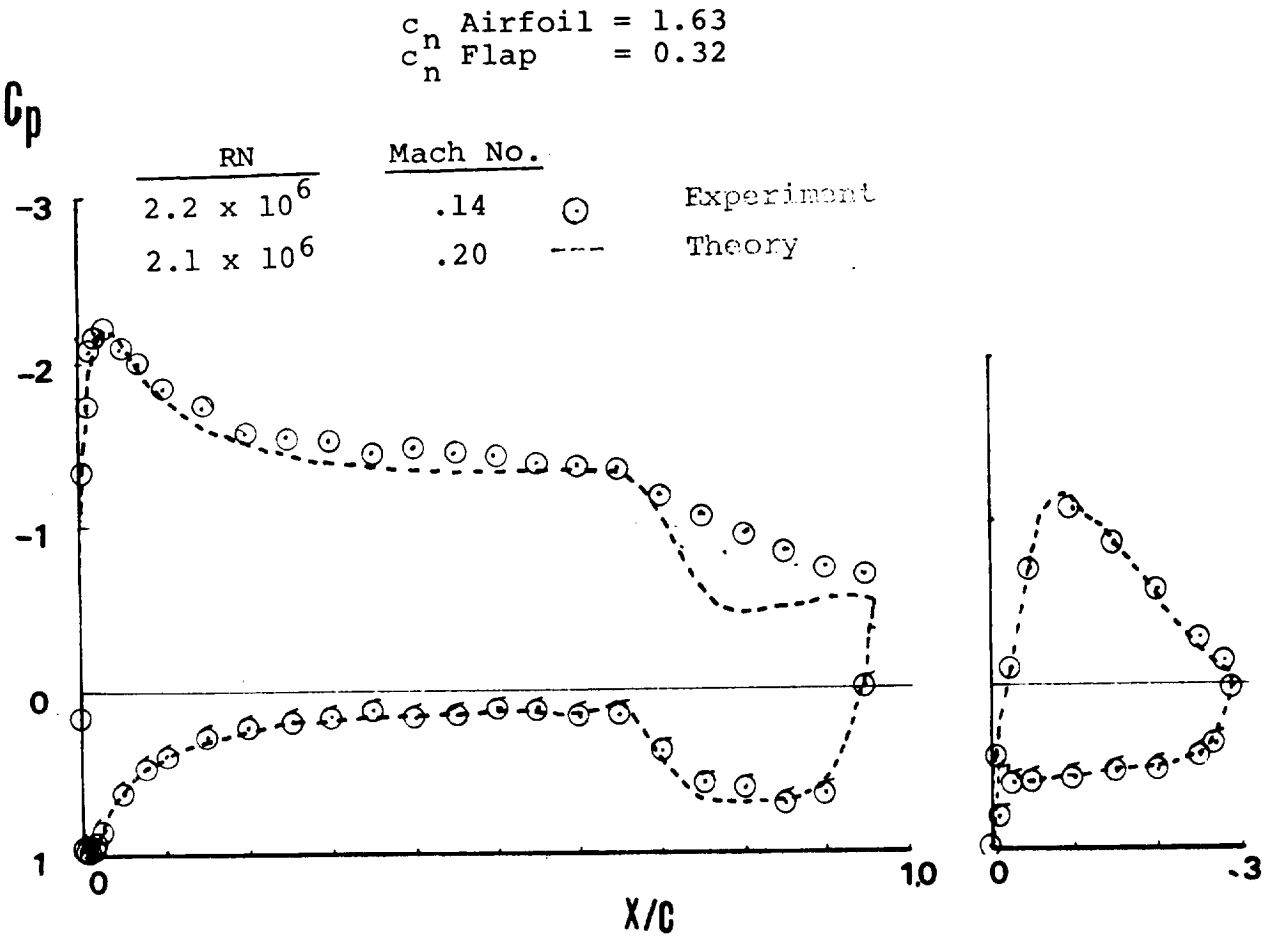

Figure 31 - Pressure Distribution, 29% c Model, 20° Flap, α = 0°

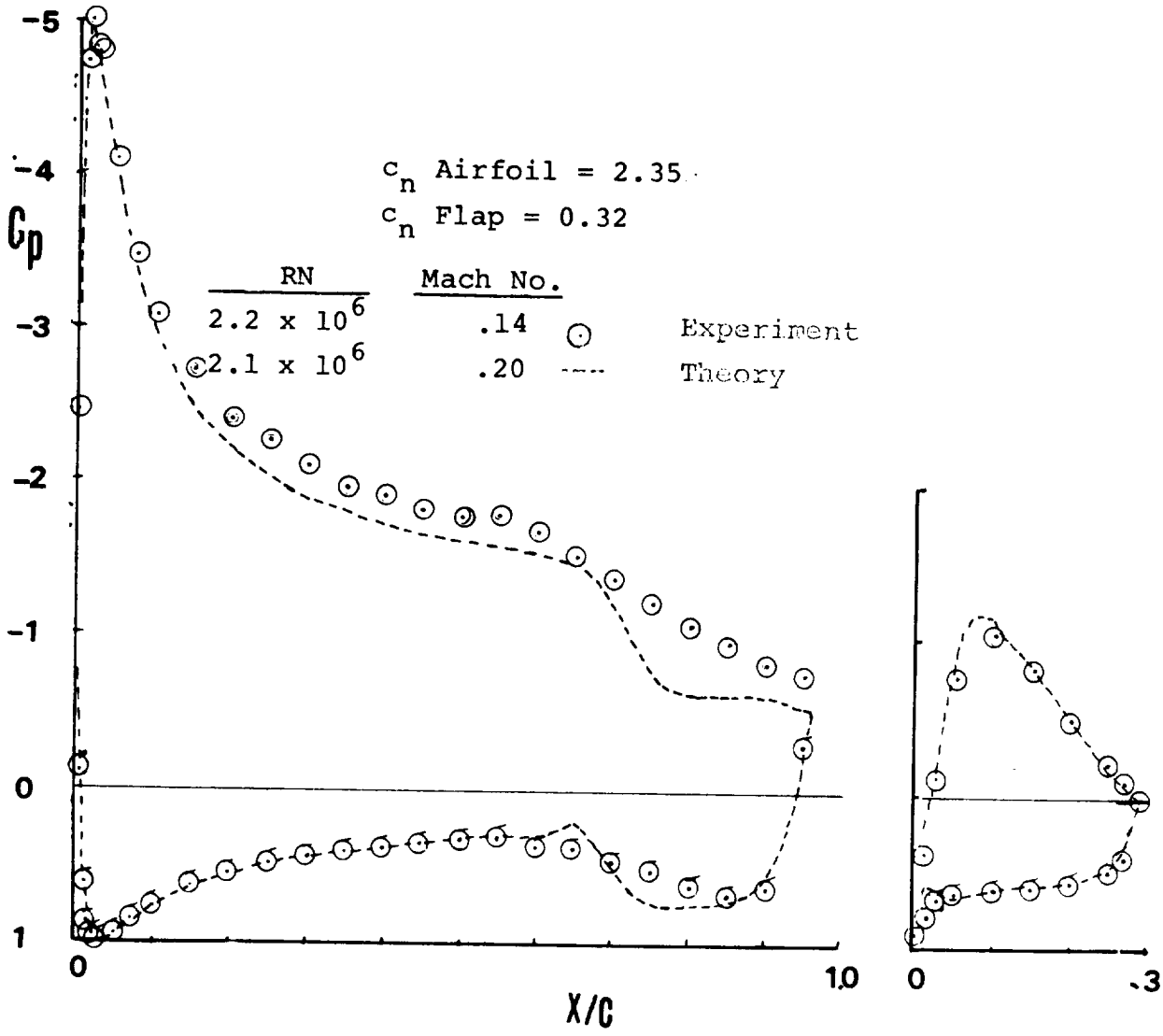

Figure 32 - Pressure Distribution, 29% c Model, 20° Flap, α = 5°

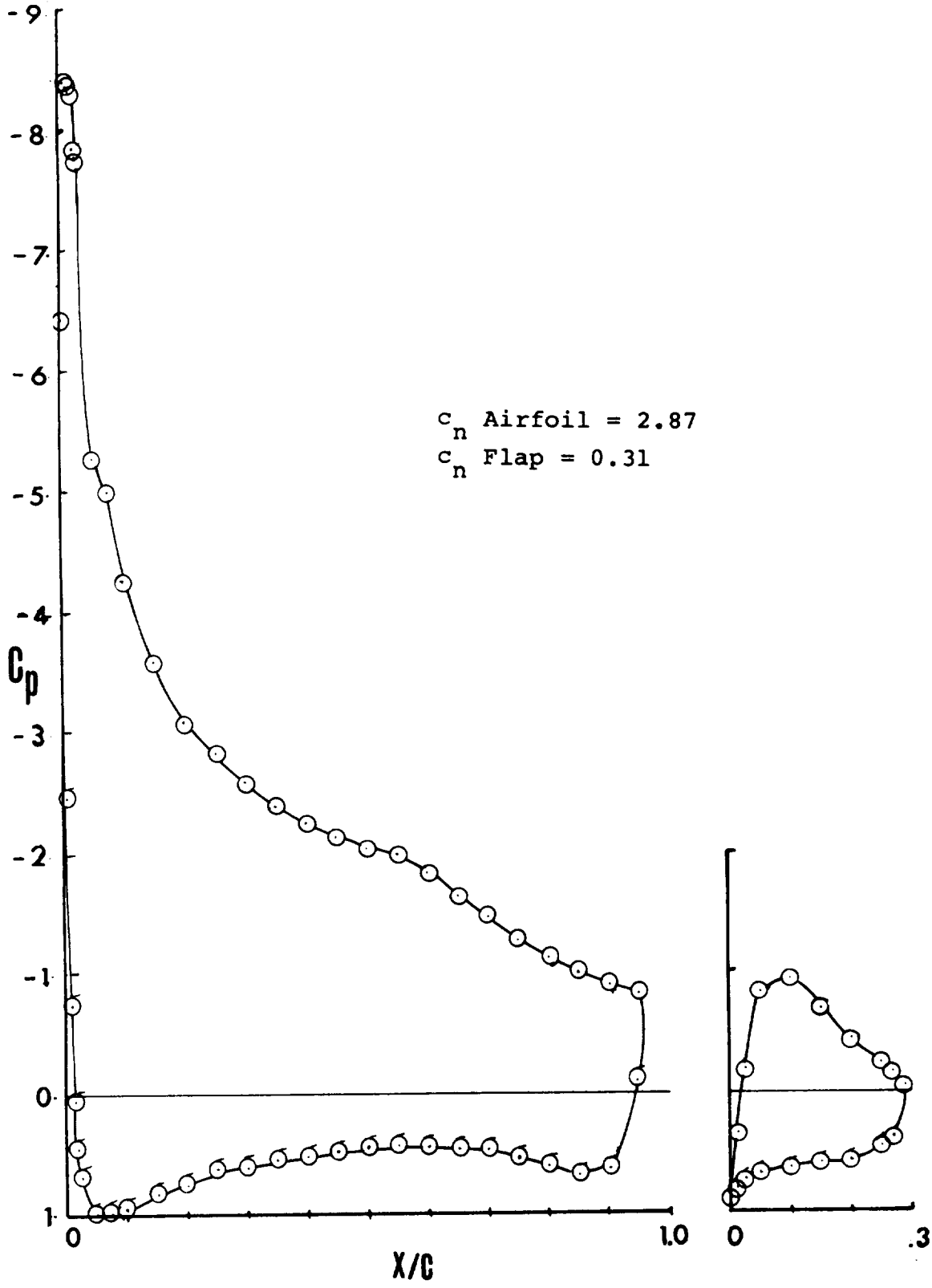

Figure 33 - Pressure Distribution, 29% c Model, 20° Flap, α = 10°

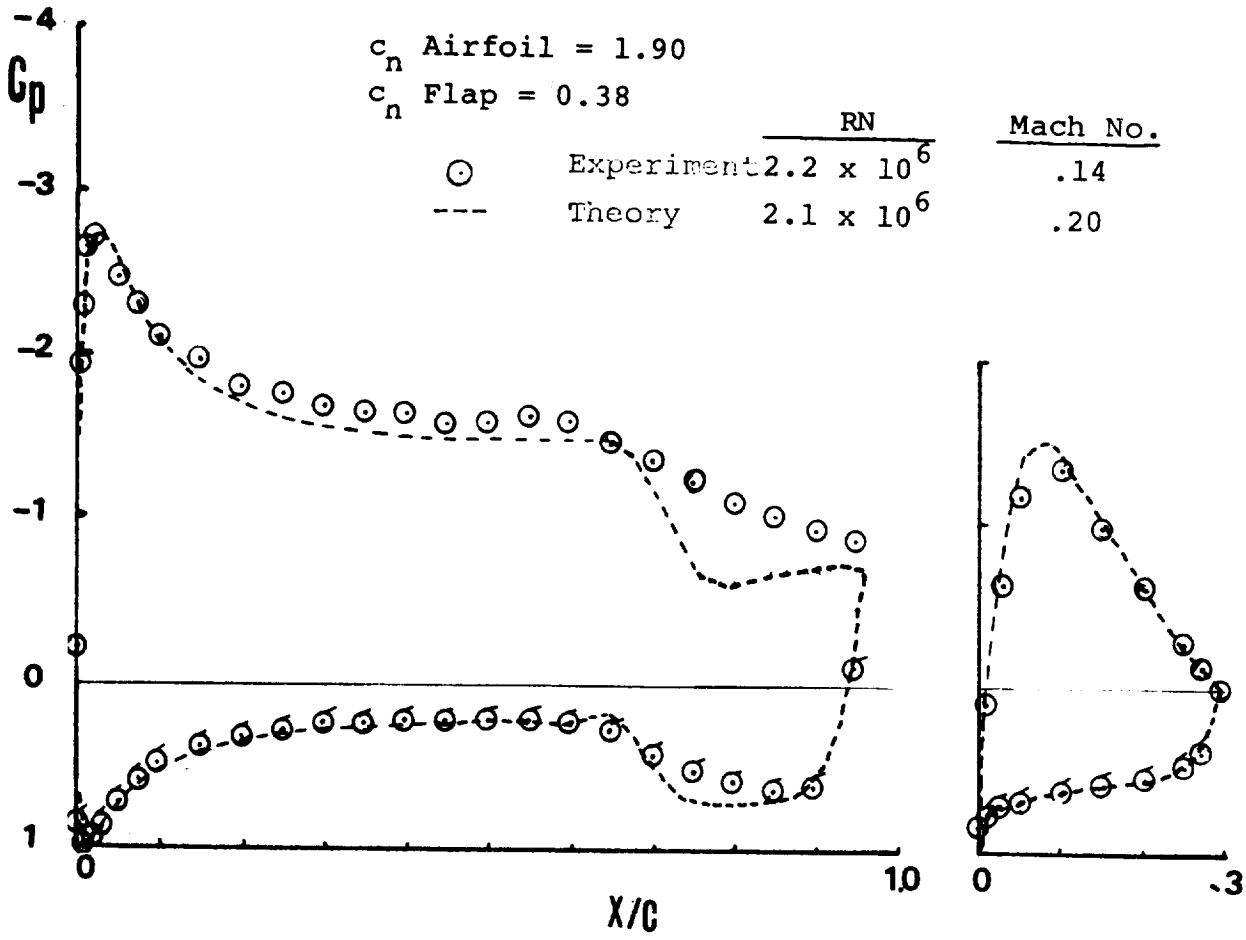

Figure 34 - Pressure Distribution, 29% c Model, 25° Flap, α = 0°

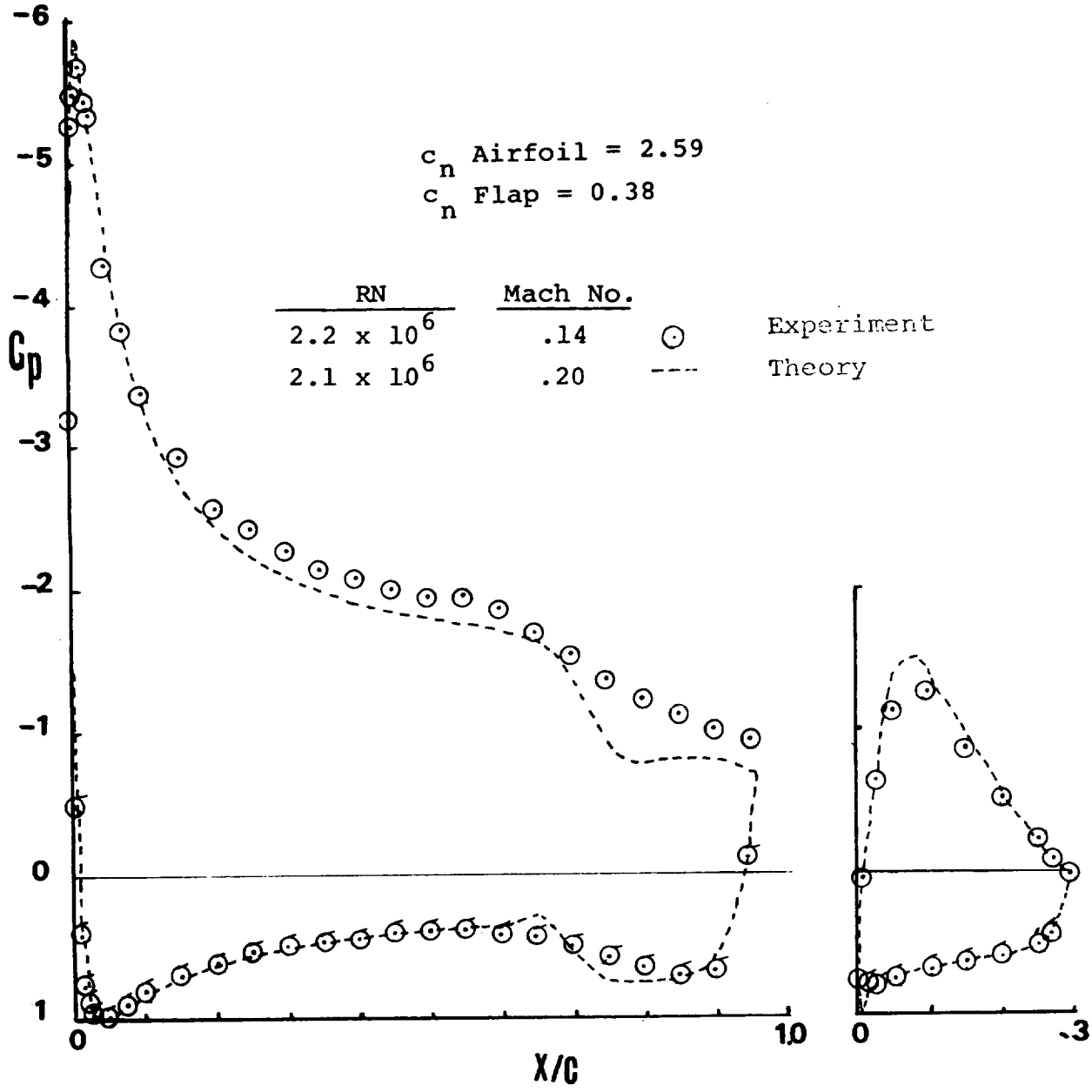

Figure 35 - Pressure Distribution, 29% c Model, 25° Flap, α = 5°

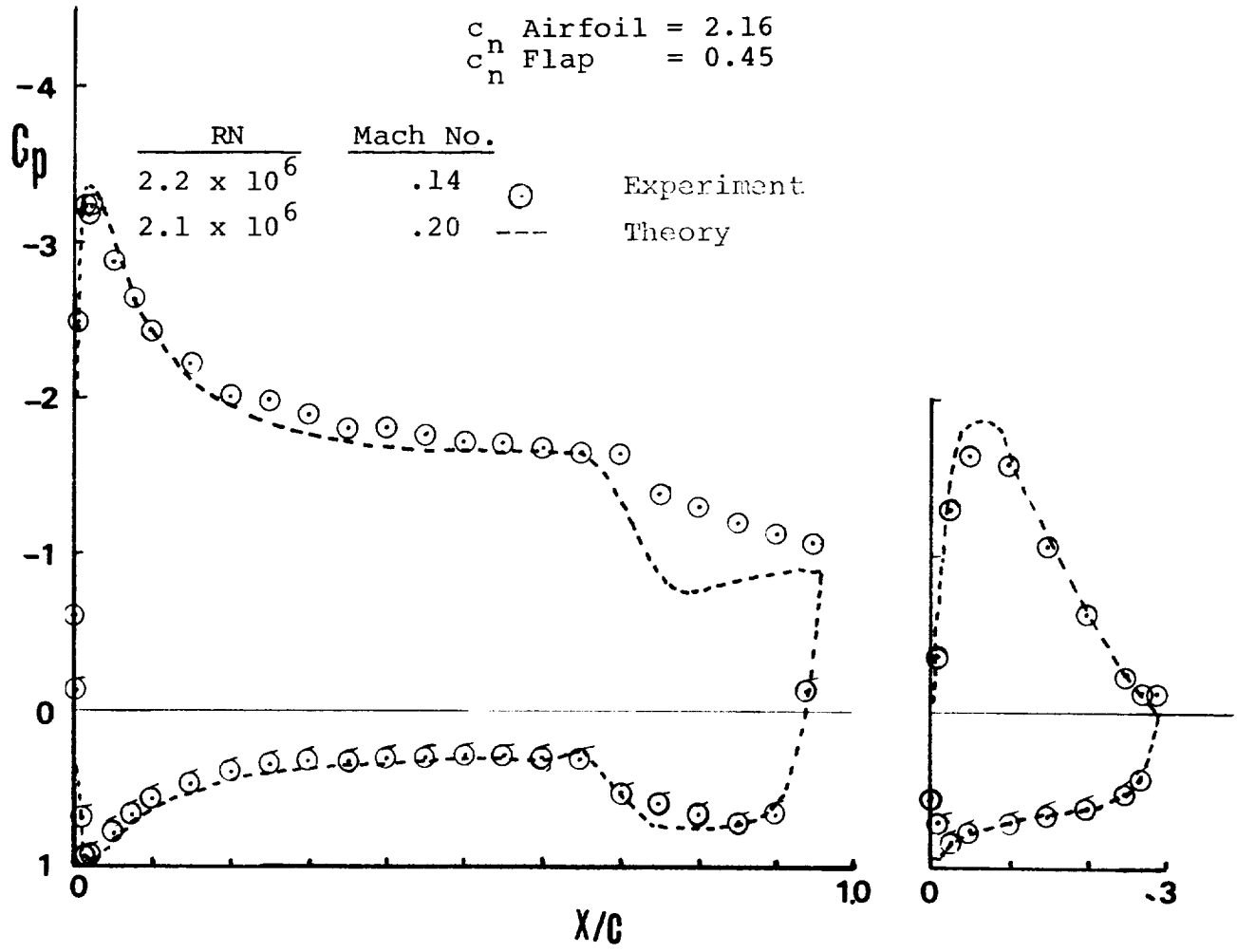

Figure 36 - Pressure Distribution, 29% c Model, 30° Flap, α = 0°

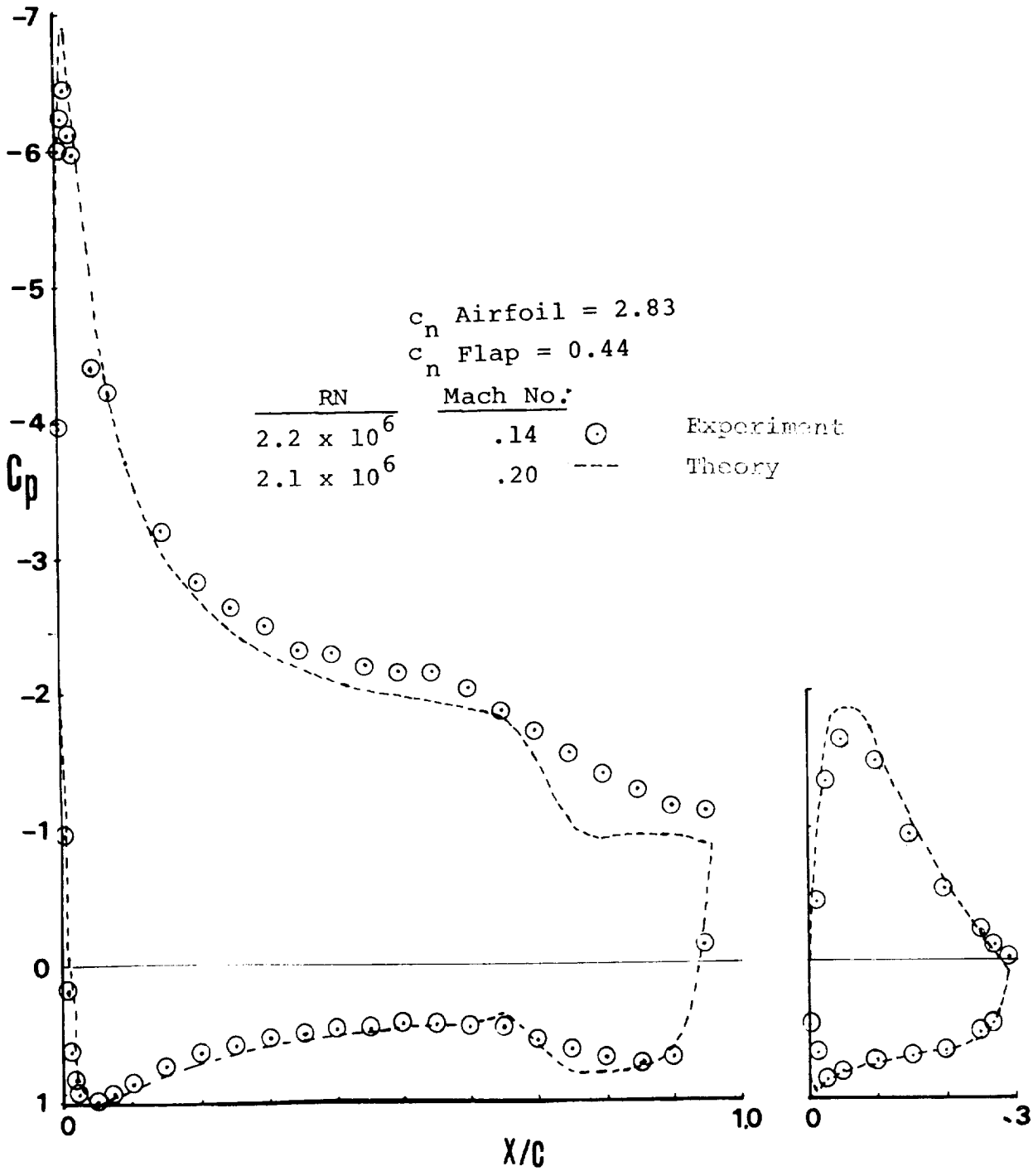

Figure 37 - Pressure Distribution, 29% c Model, 30° Flap, α = 5°

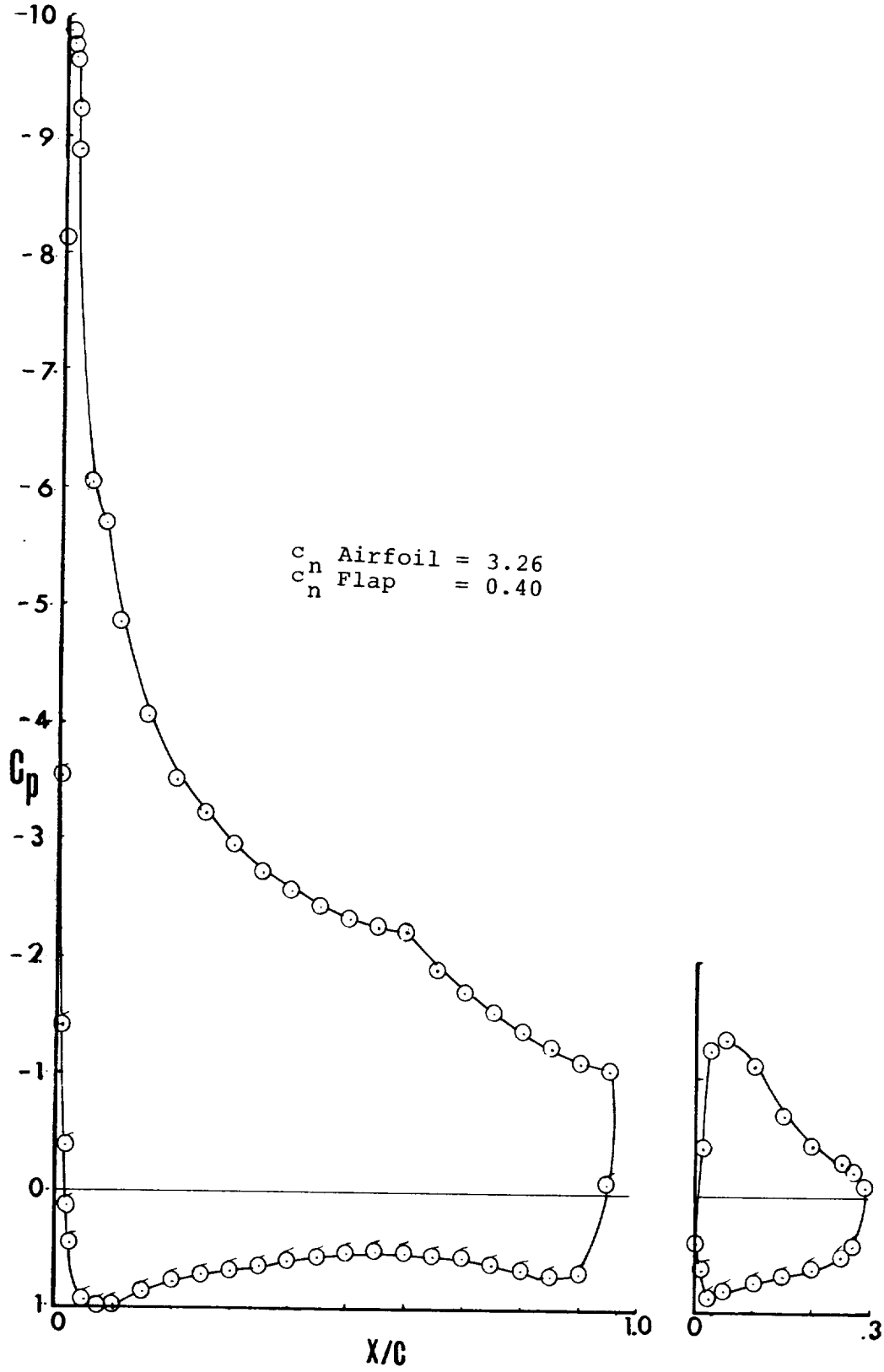

Figure 38 - Pressure Distribution, 29% c Model, 30° Flap, α = 10°

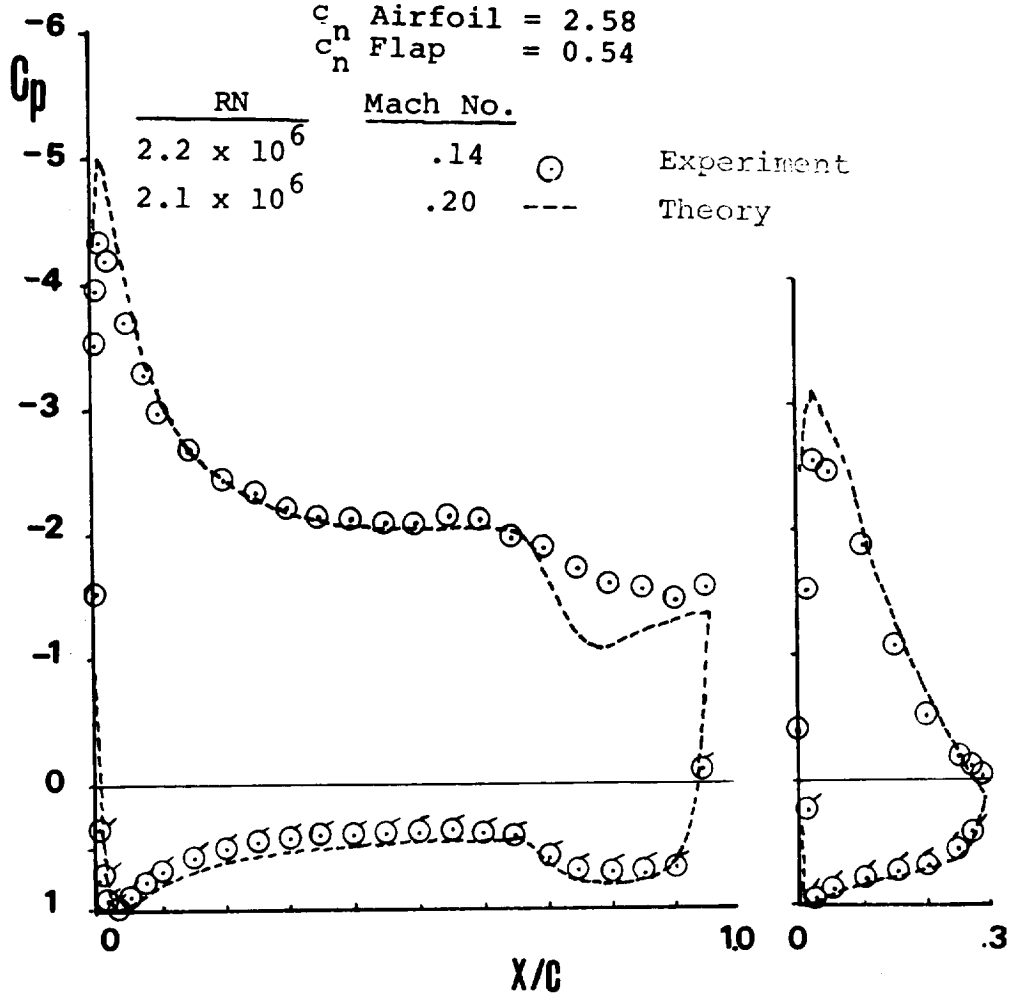

Figure 39 - Pressure Distribution, 29% c Model, 40° Flap, α = 0°

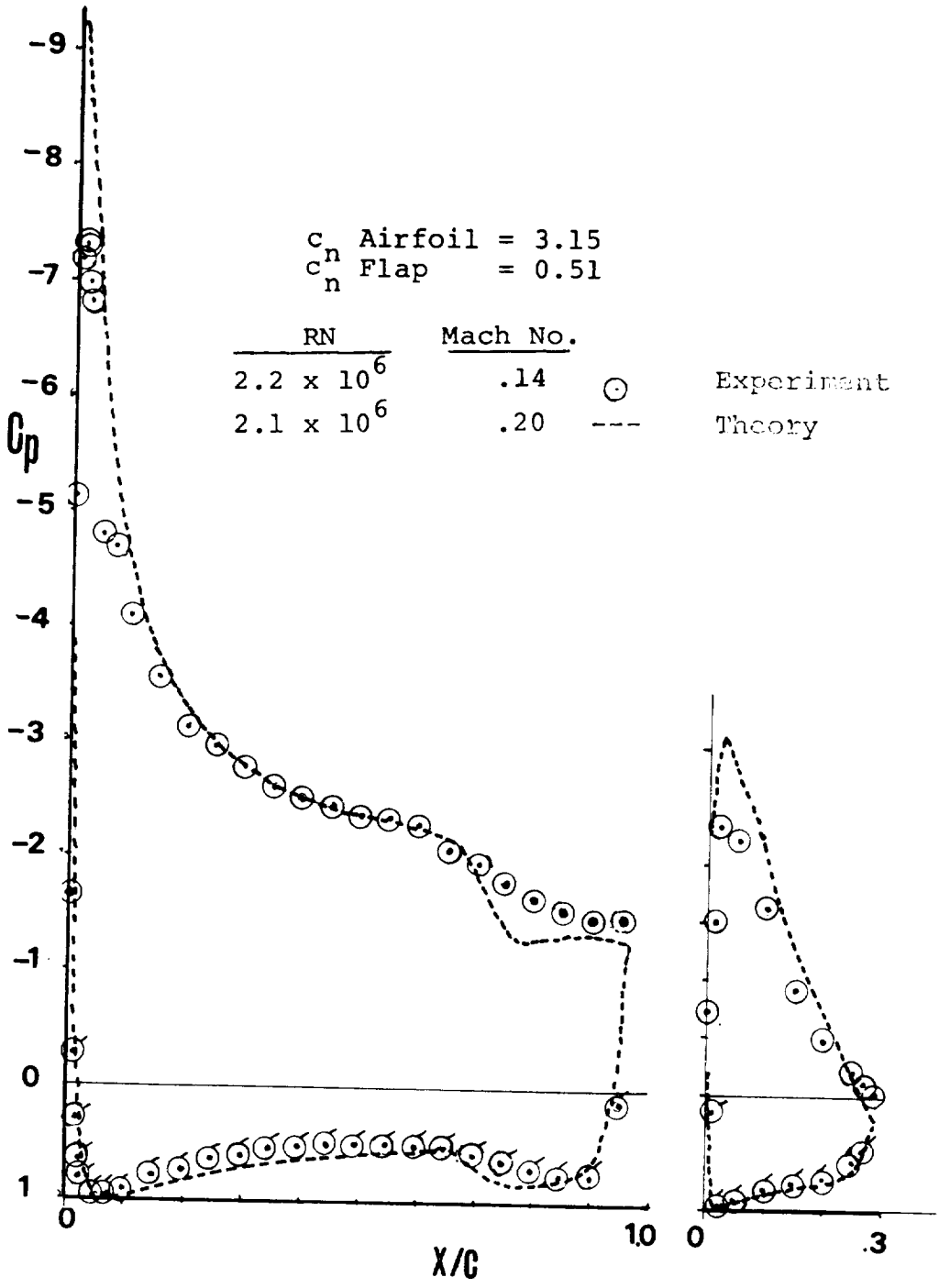

Figure 40 - Pressure Distribution, 29% c Model, 40° Flap, α = 5°

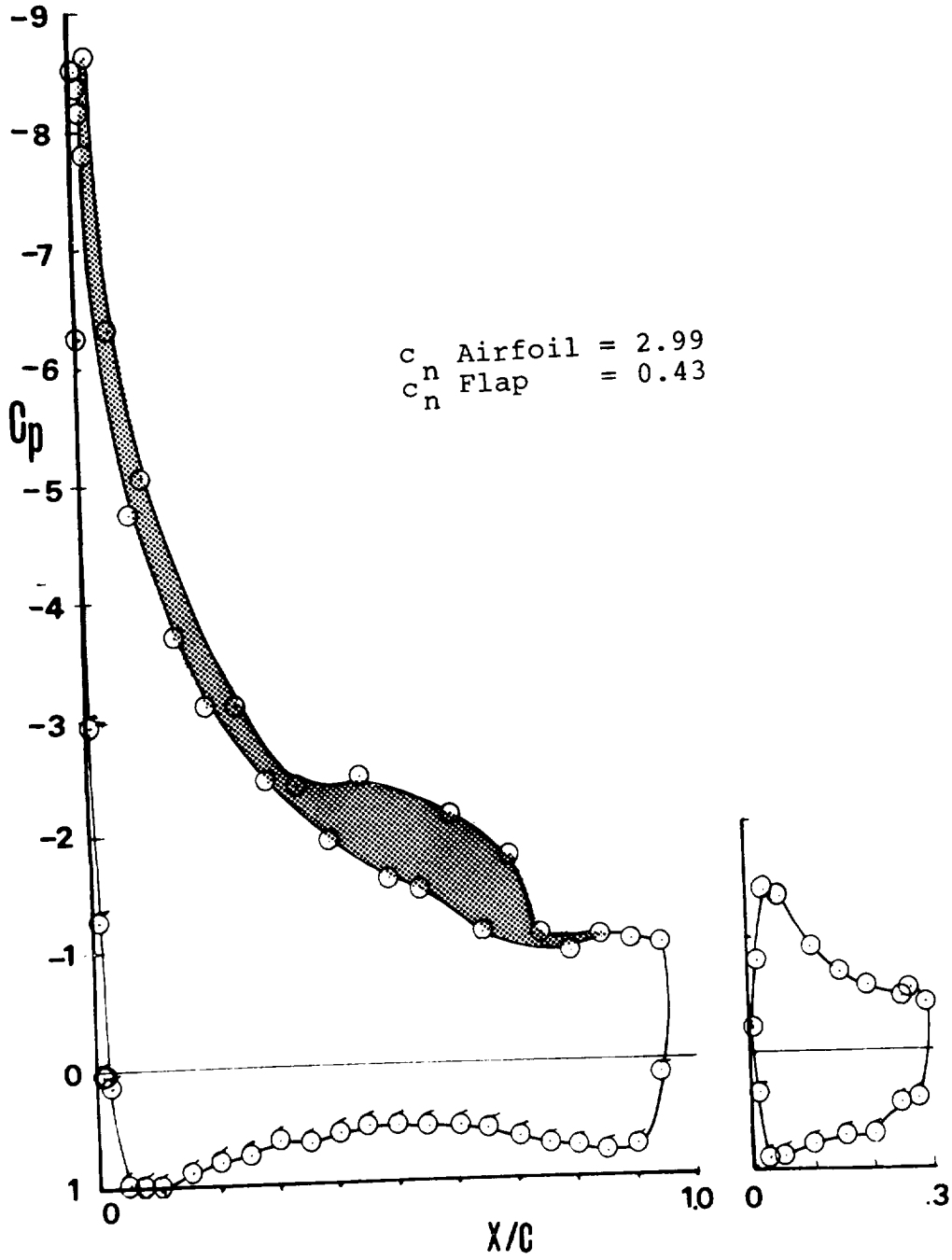

Figure 41 - Pressure Distribution, 29% c Model, 40° Flap, α = 10°

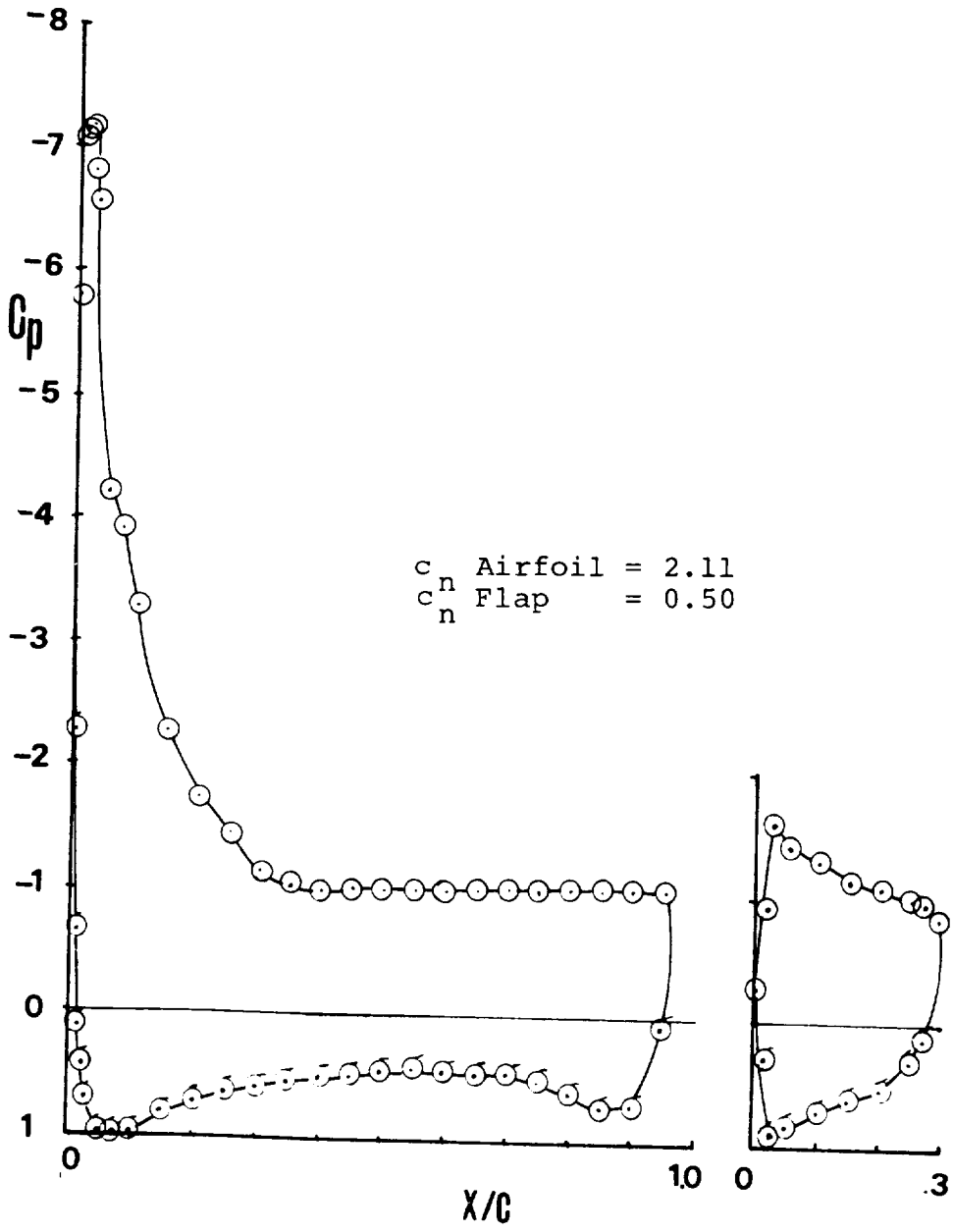

Figure 42 - Pressure Distribution, 29% c Model, 40° Flap, α = 15°

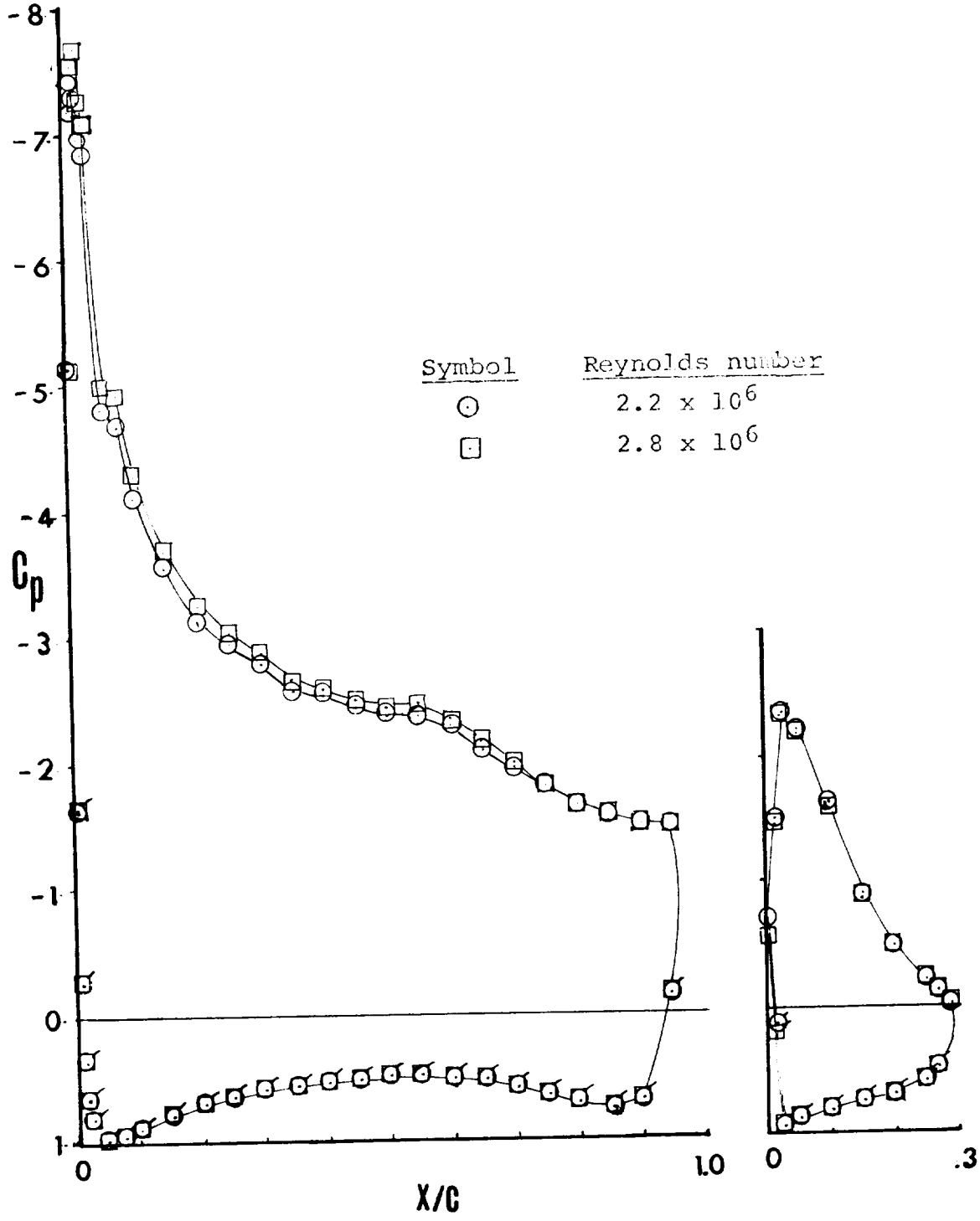

Figure 43 - Effect of Reynolds Number on Pressure Distribution, 40° Flap, α = 5°

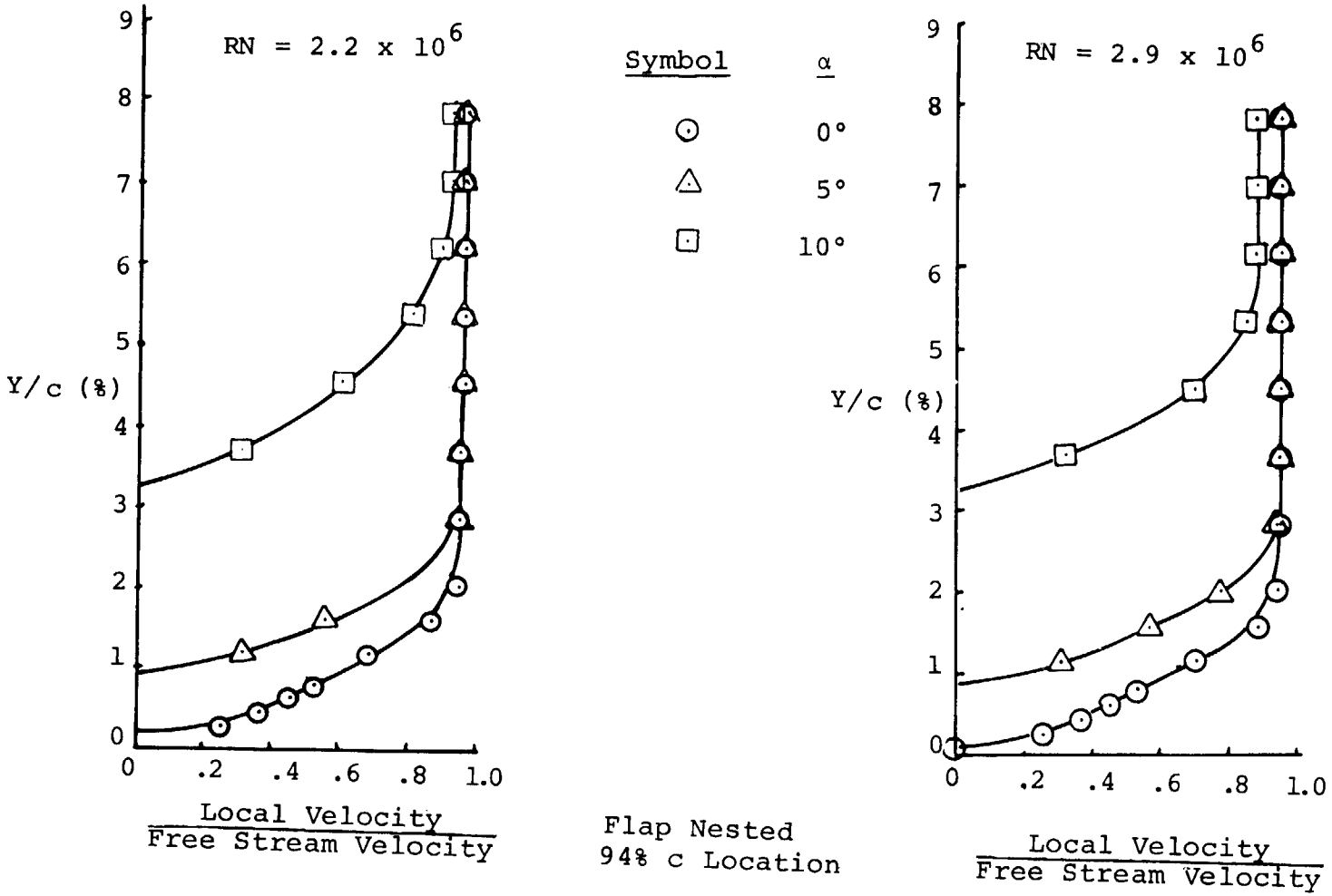

Figure 44 - Boundary Layer Profiles

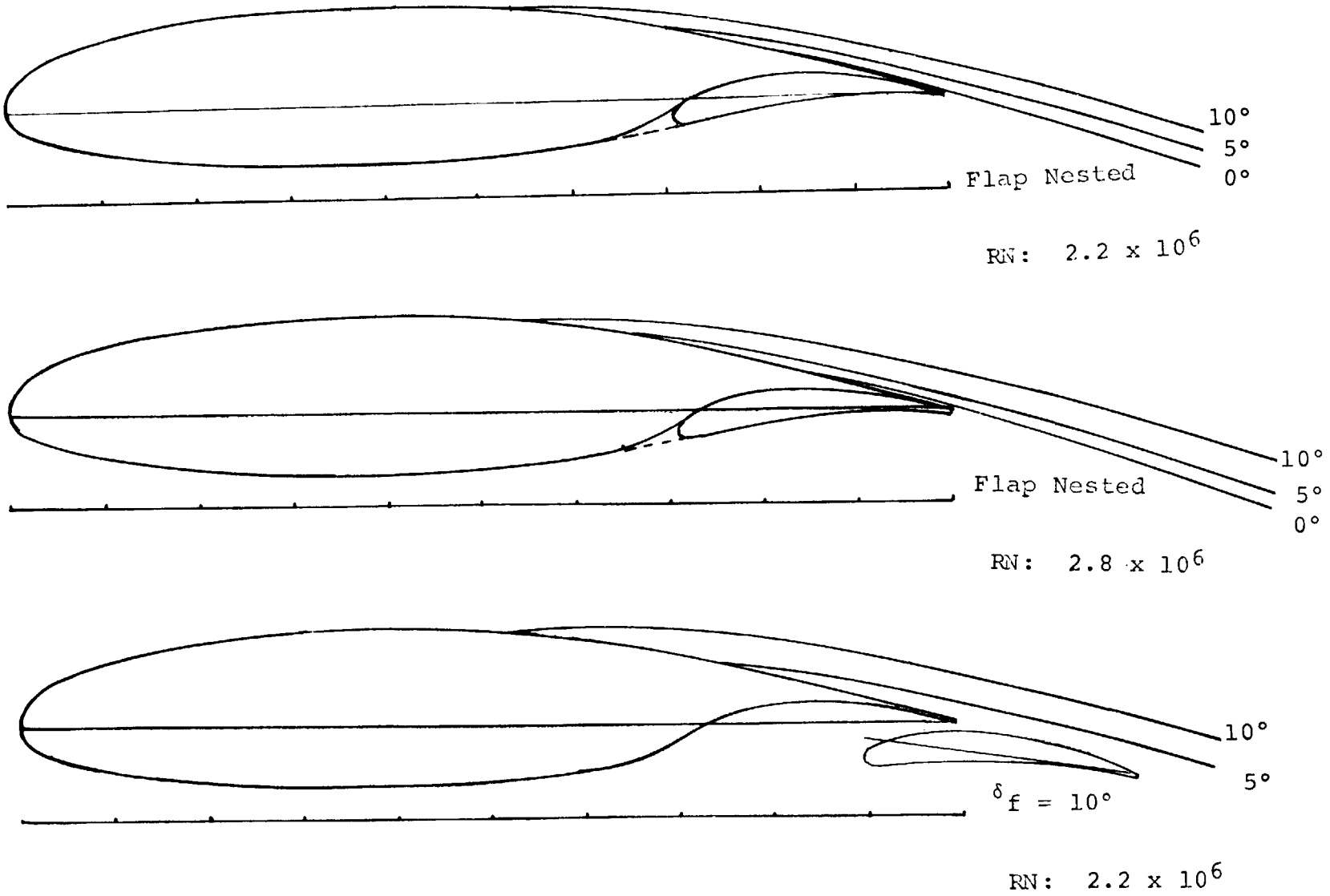

Figure 45 - Reversed Flow Region, 30% c Model

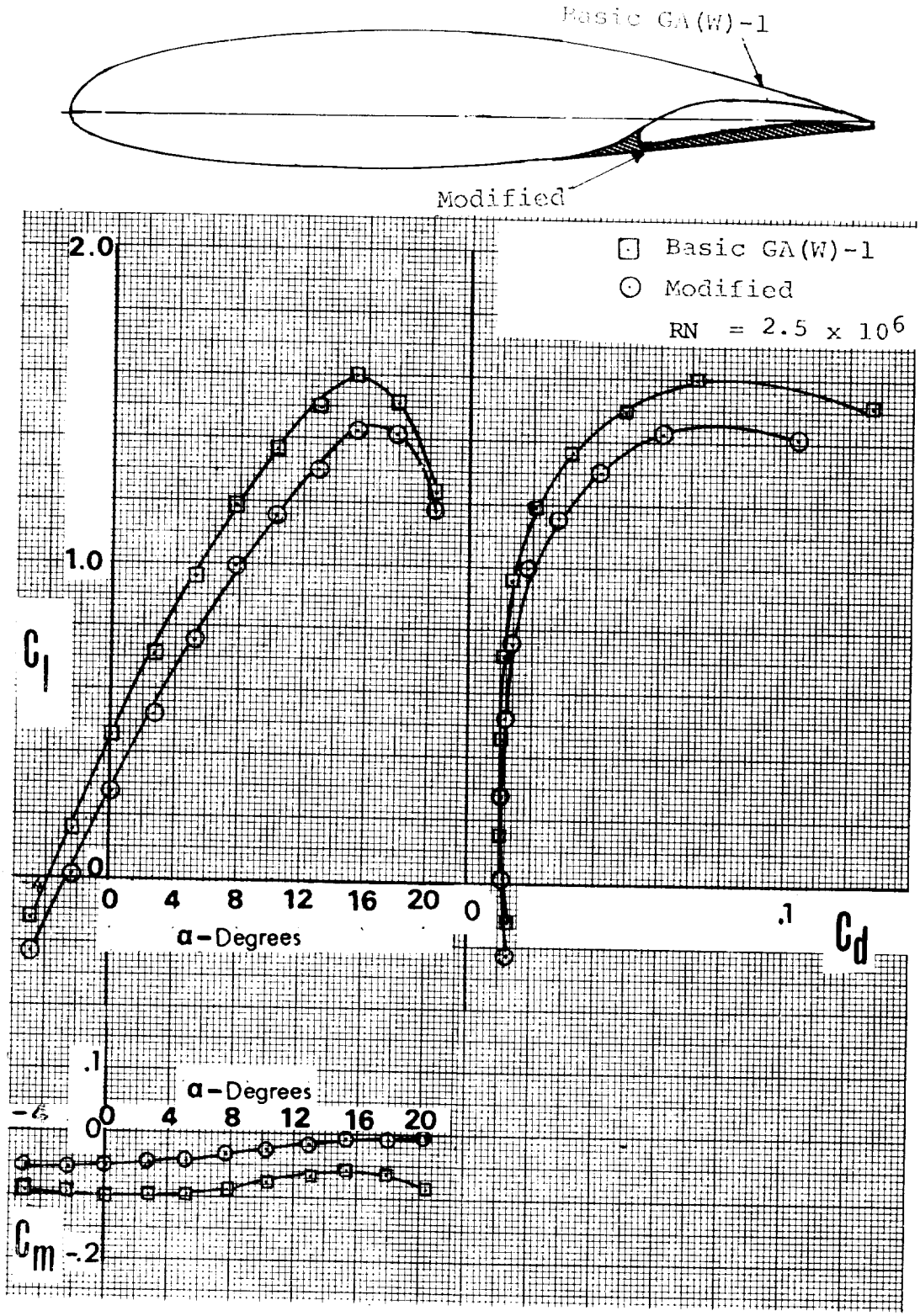

Figure 46 - Effects of Recontouring Airfoil Lower Surface

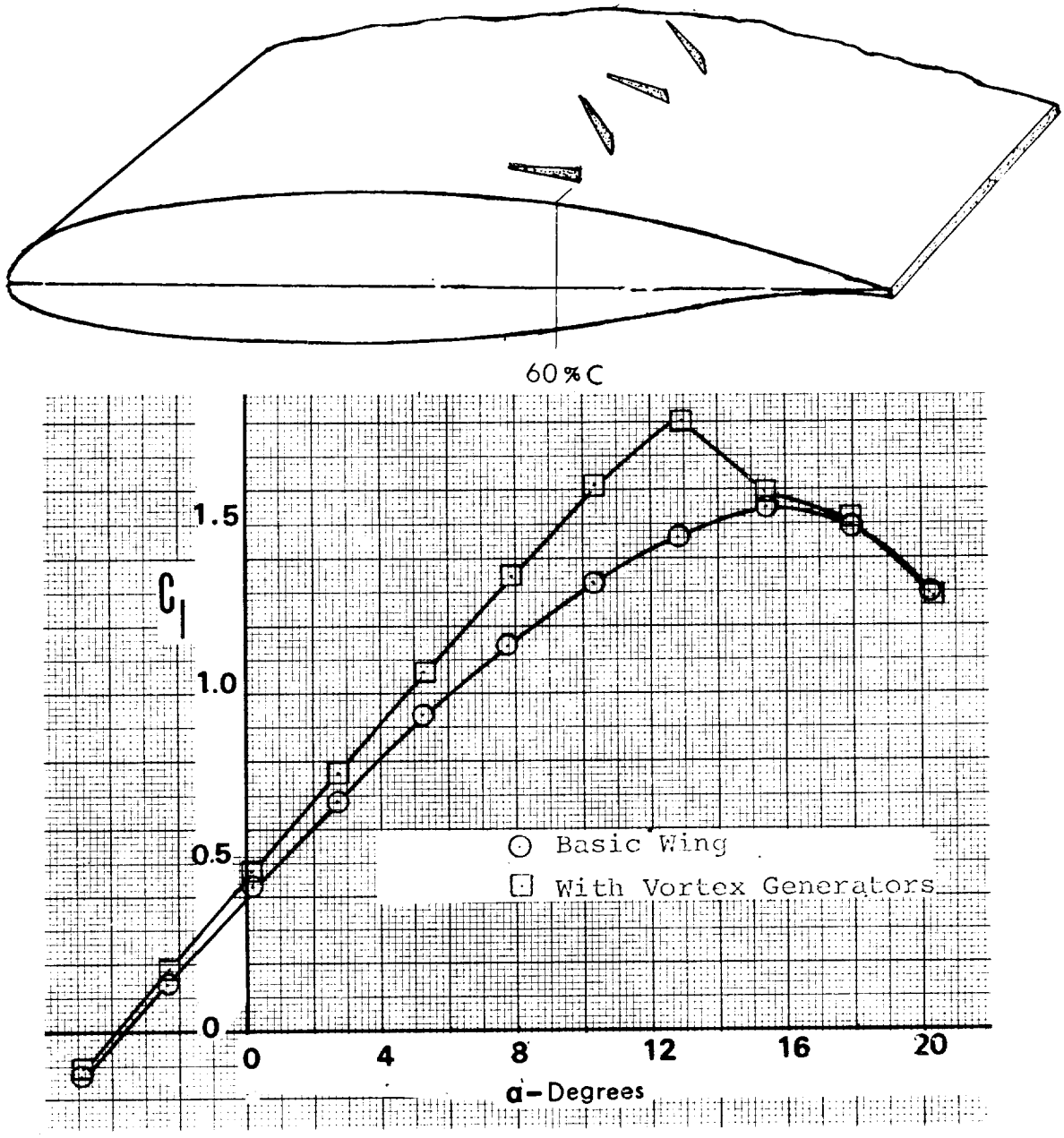

Figure 47 - Effect of Vortex Generators on Lift, Flap Nested

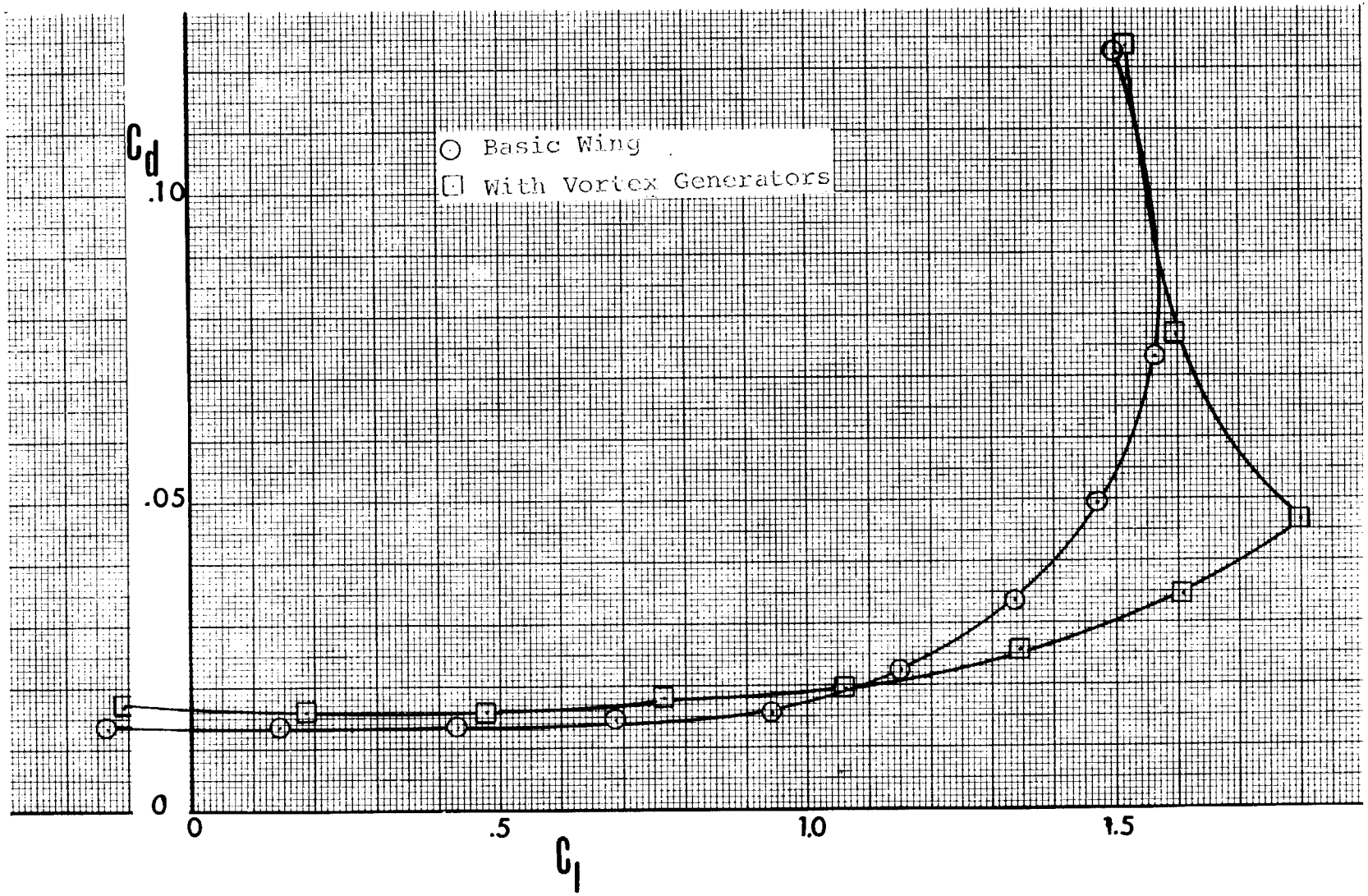

Figure 48 - Effect of Vortex Generators Drag, Flap Nested

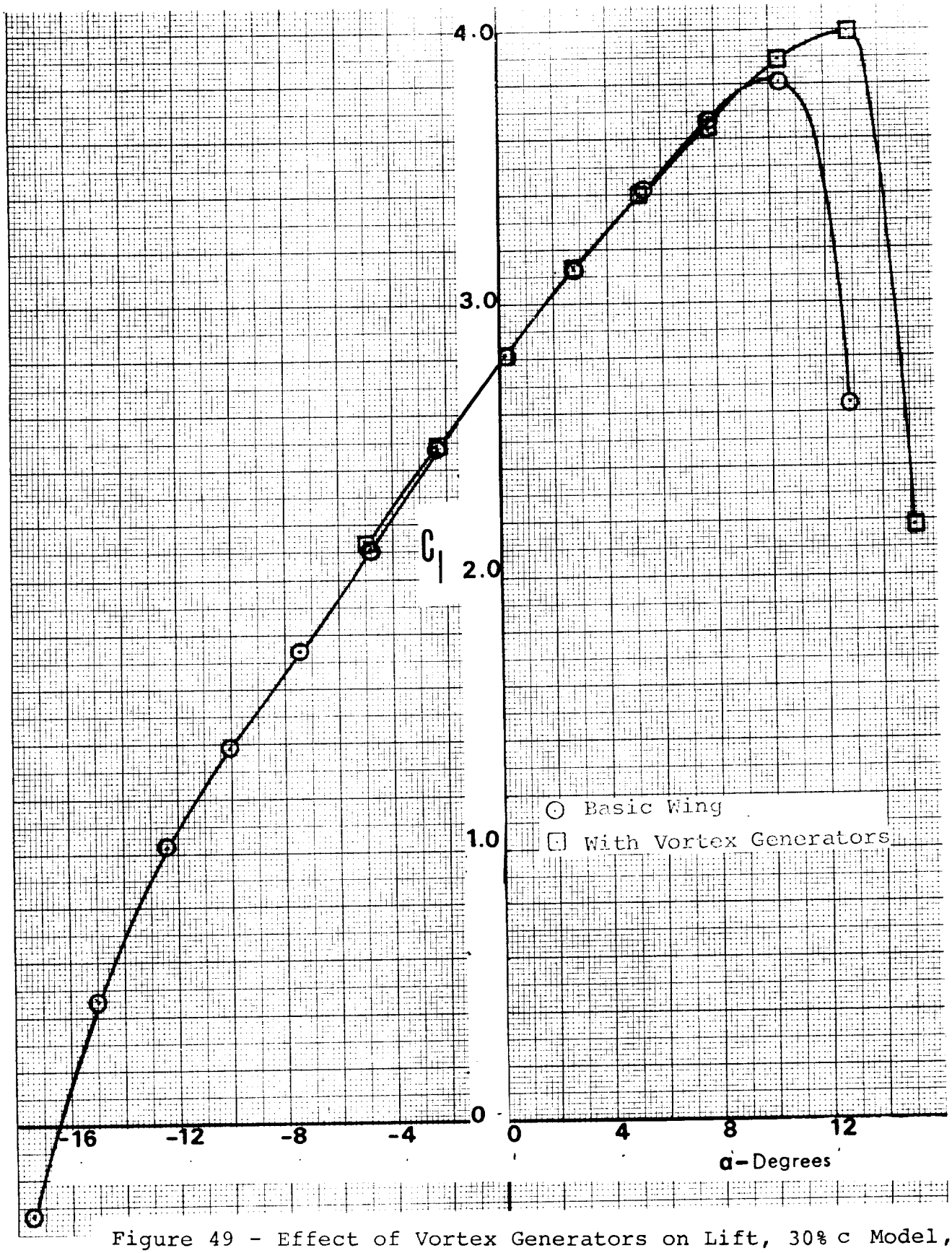

Figure 49 - Effect of Vortex Generators on Lift, 30% c Model, 40° Flap

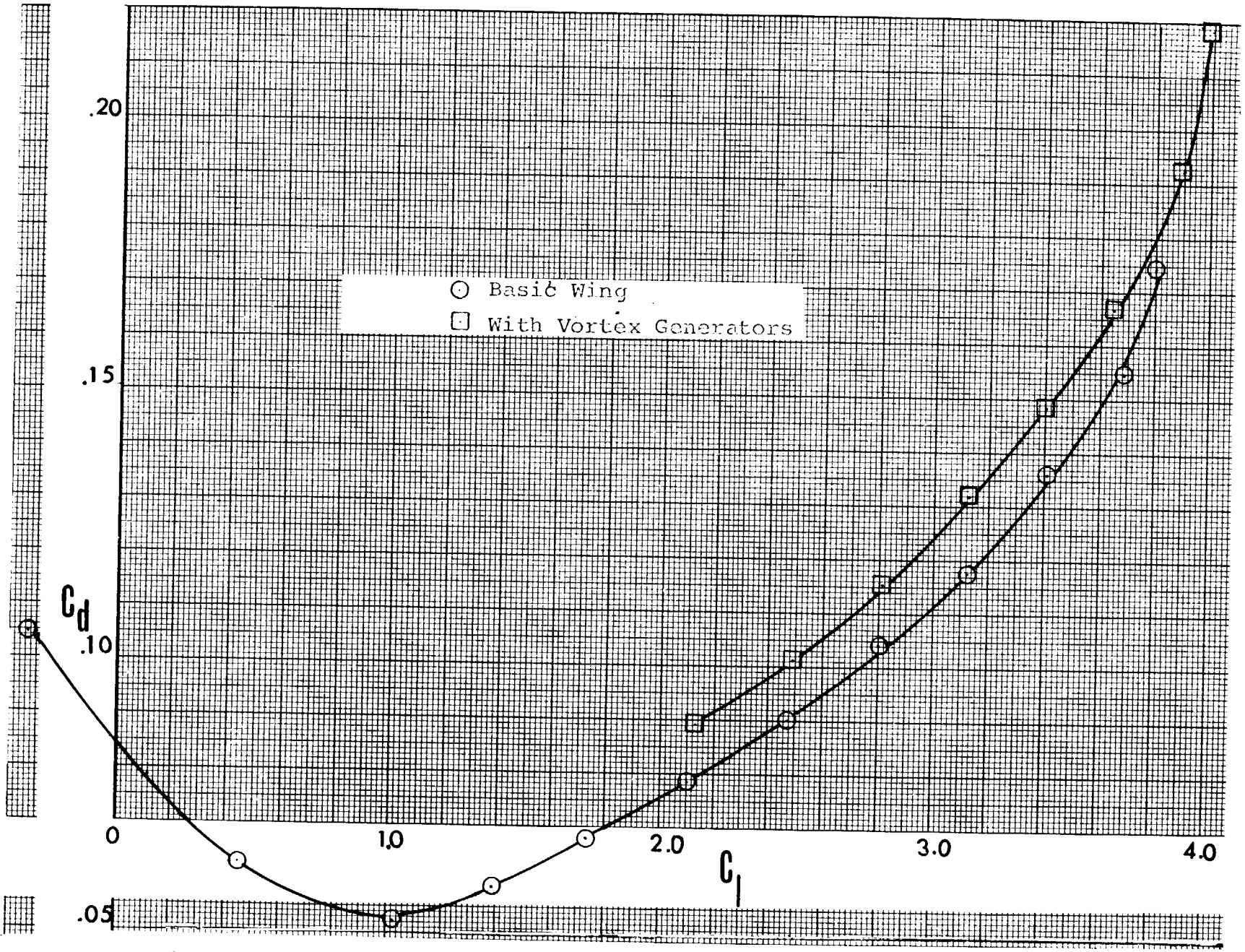

Figure 50 - Effect of Vortex Generators on Drag, 30% c Model, 40° Flap

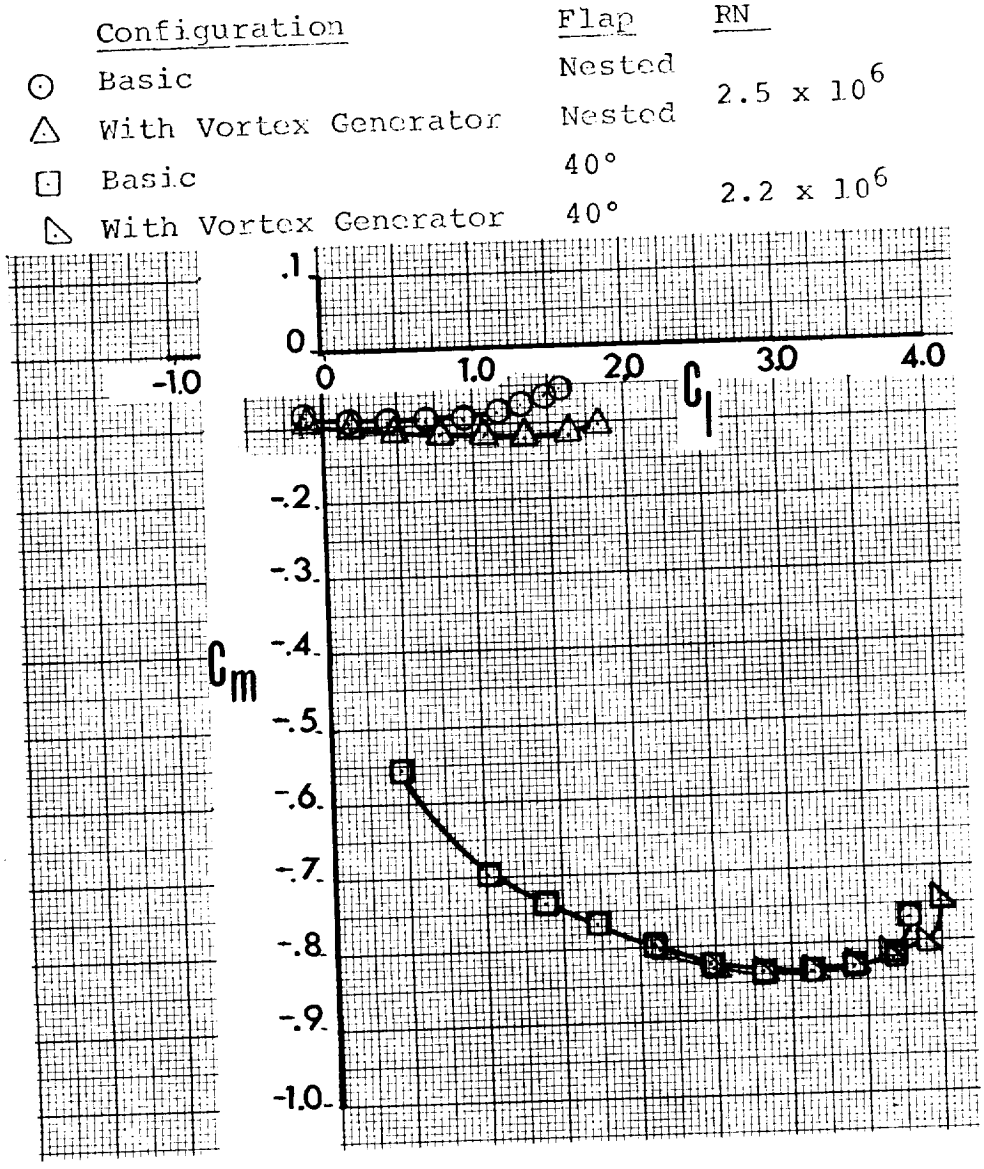

Figure 51 - Effect of Vortex Generators on Pitching Moment, 30% c Model

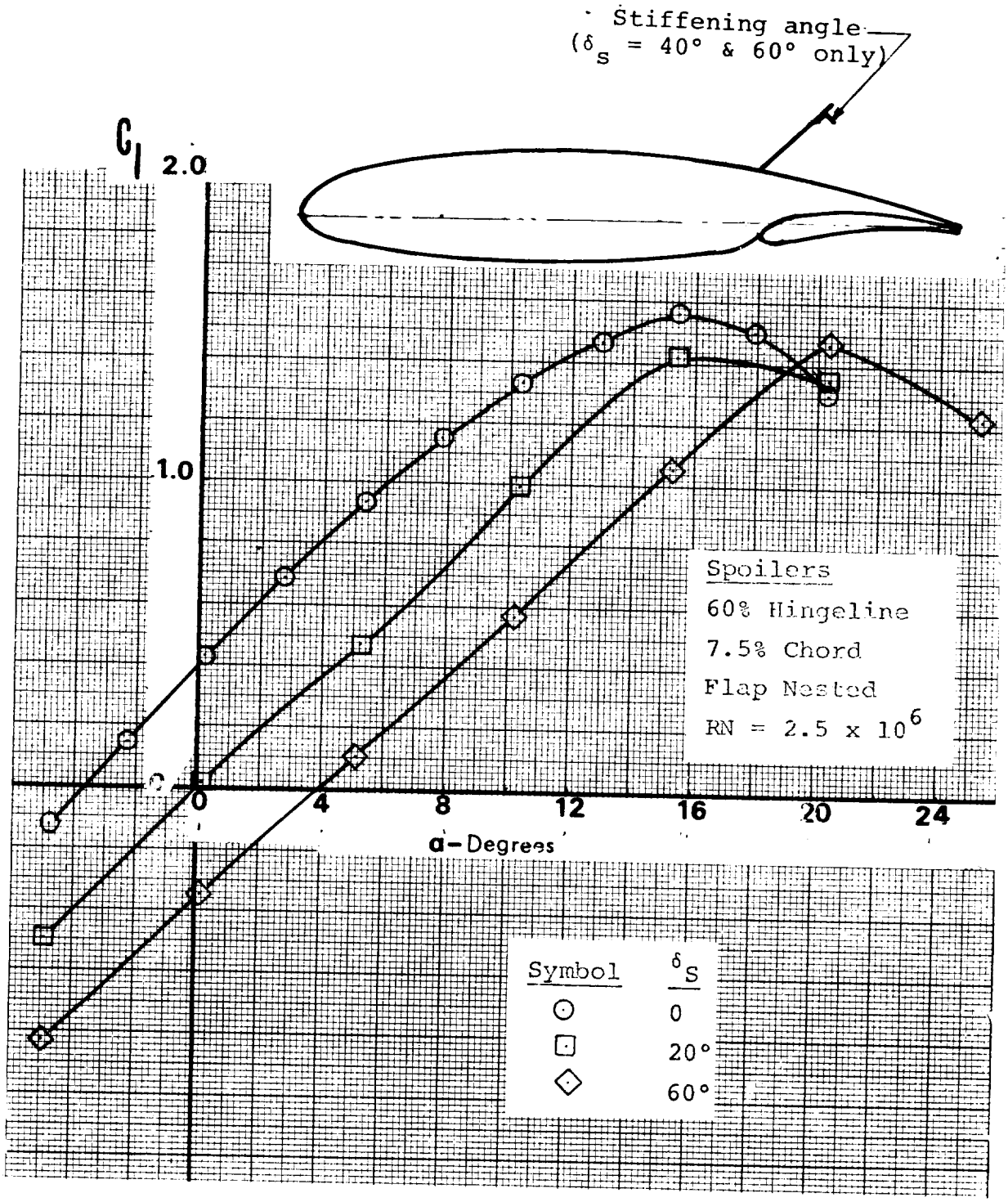

Figure 52 - Effect of Spoilers on Lift

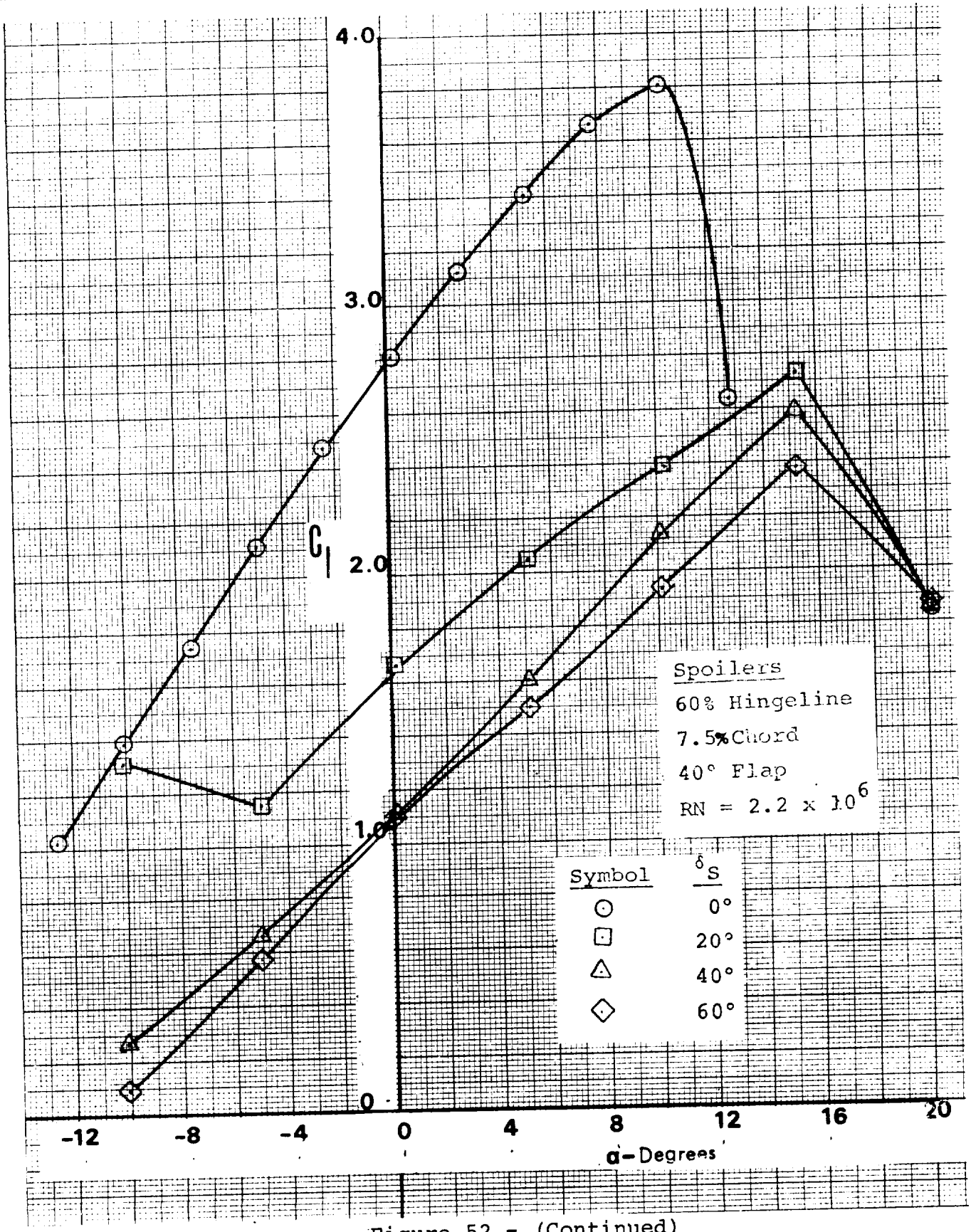

Figure 52 - (Continued)

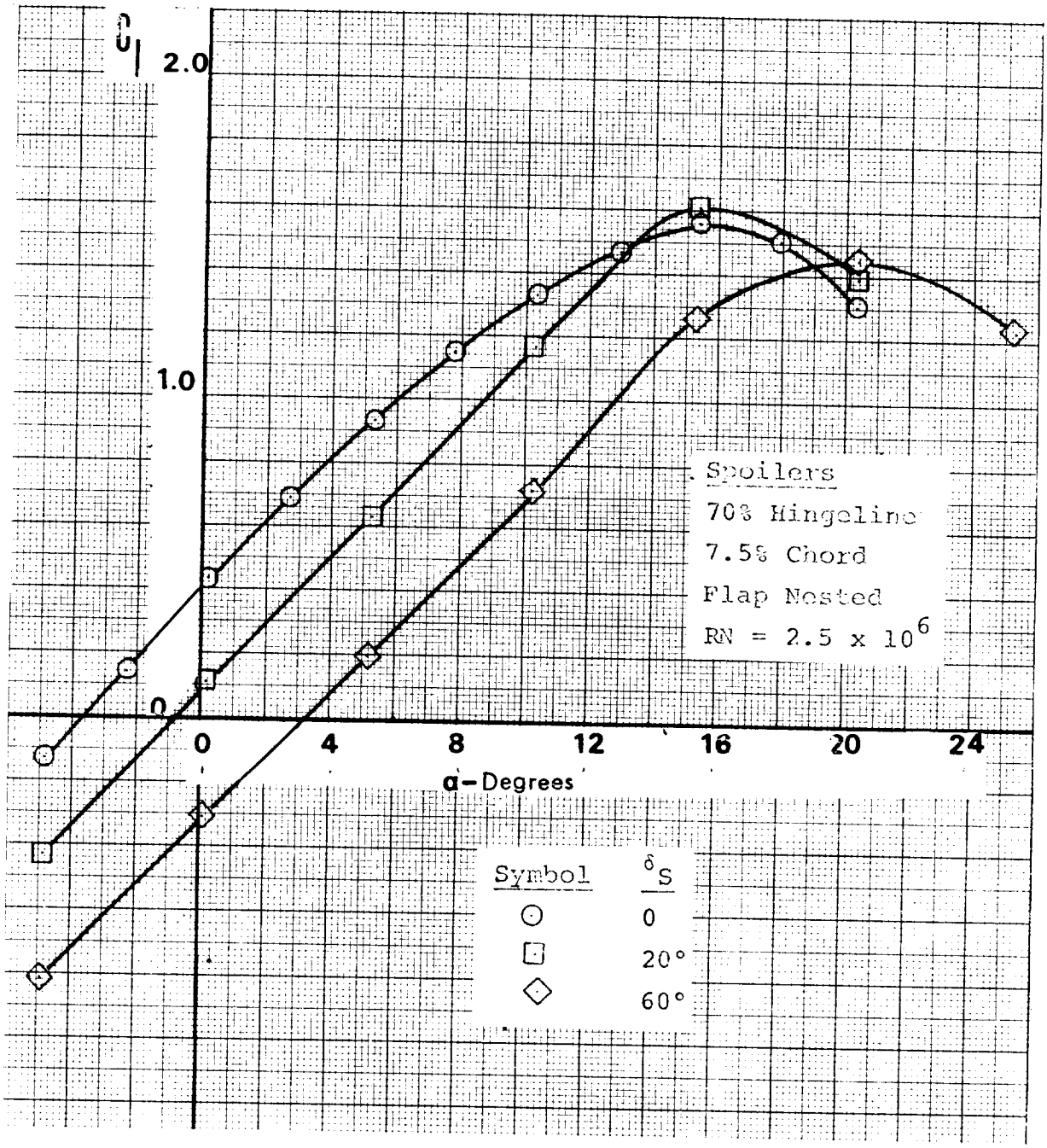

Figure 52 - (Continued)

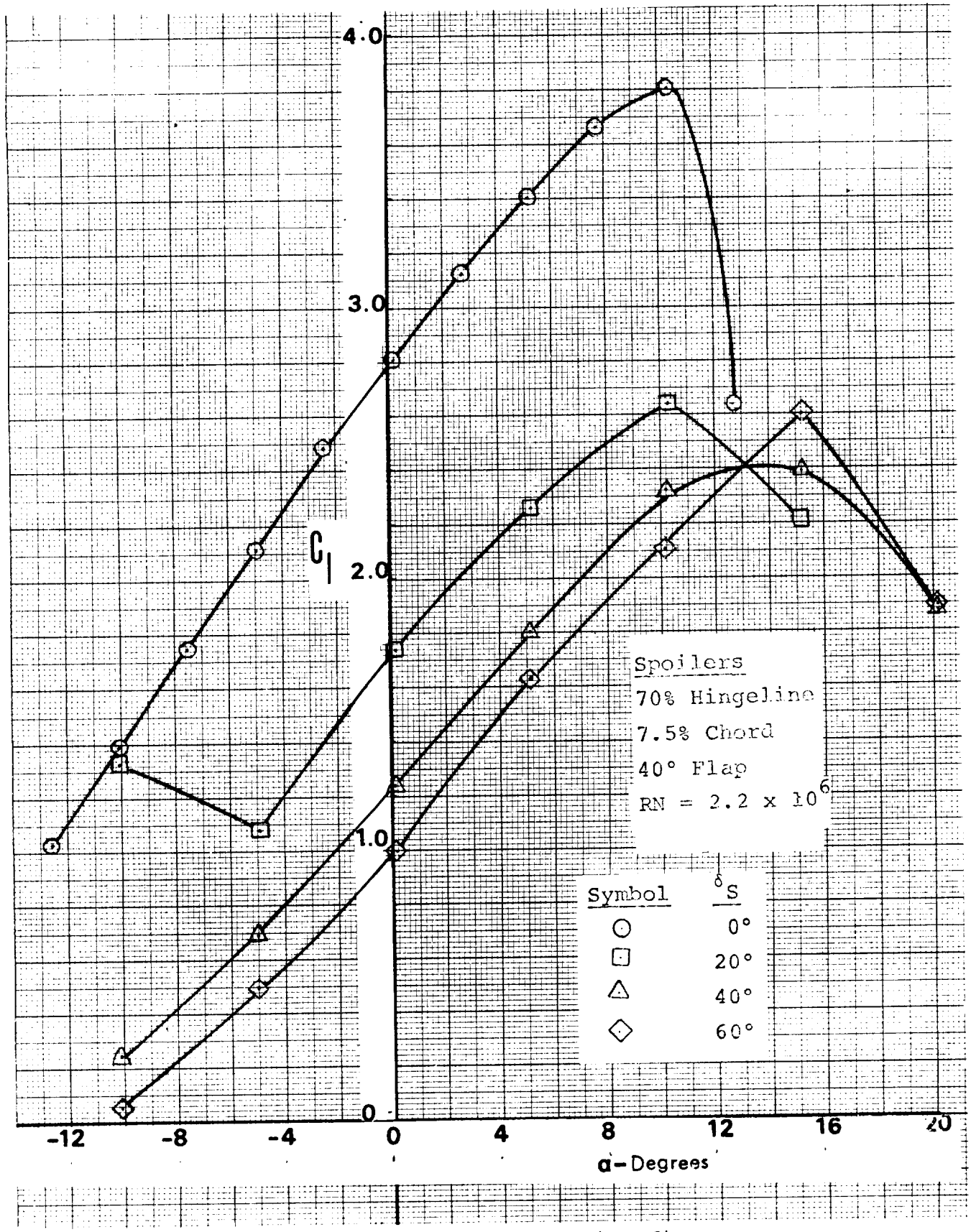

Figure 52 - (Continued)

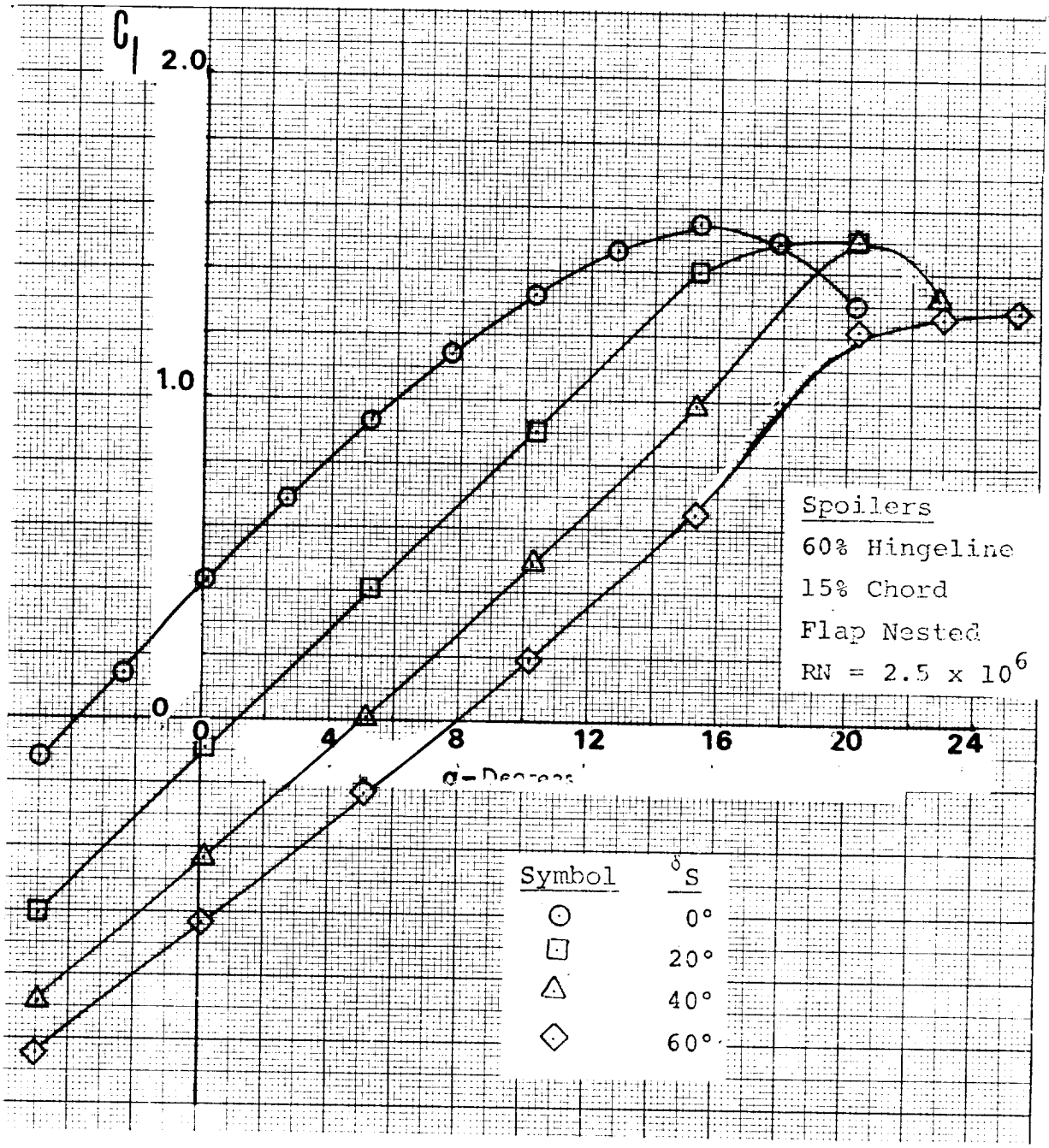

Figure 52 - (Continued)

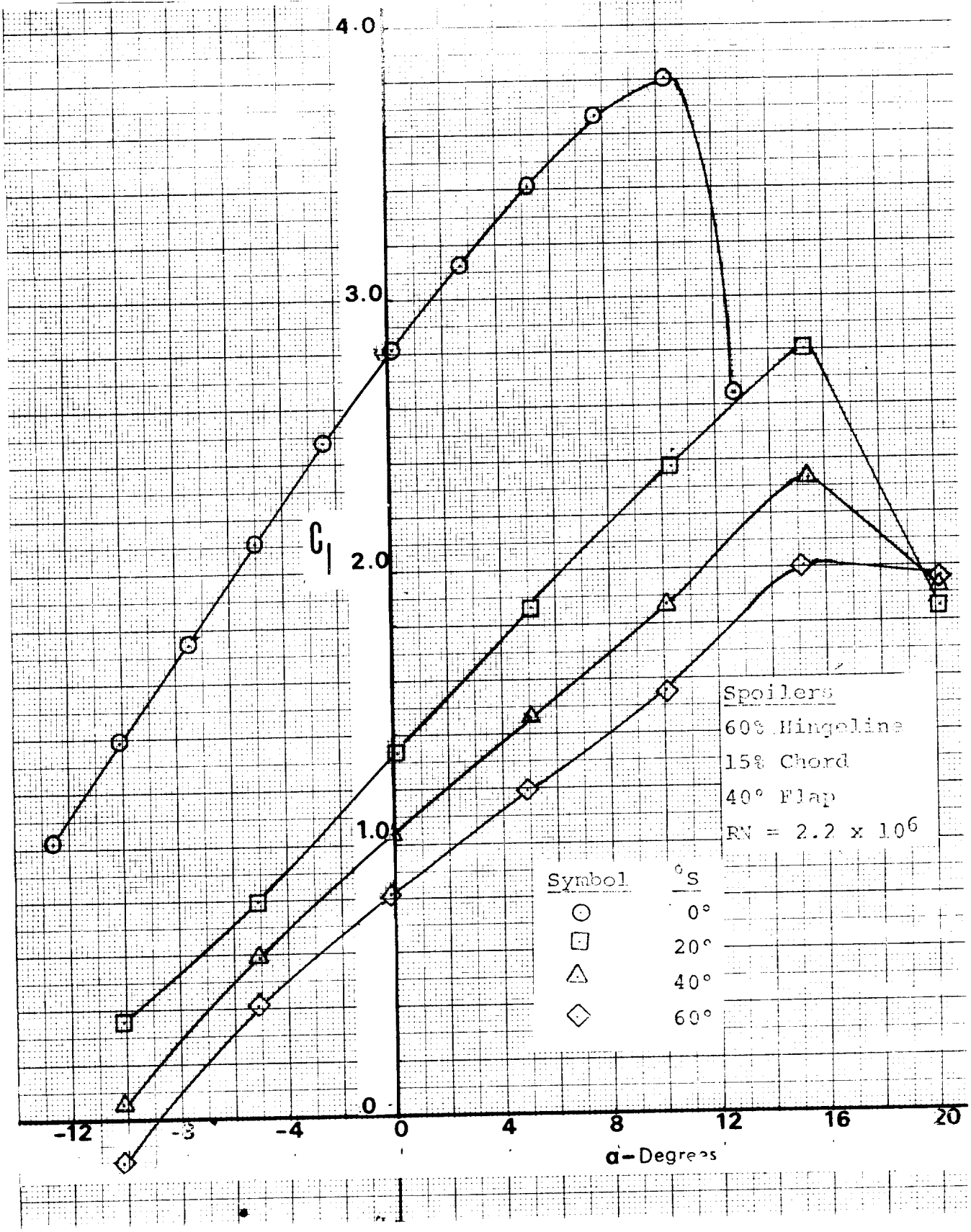

Figure 52 - (Continued)

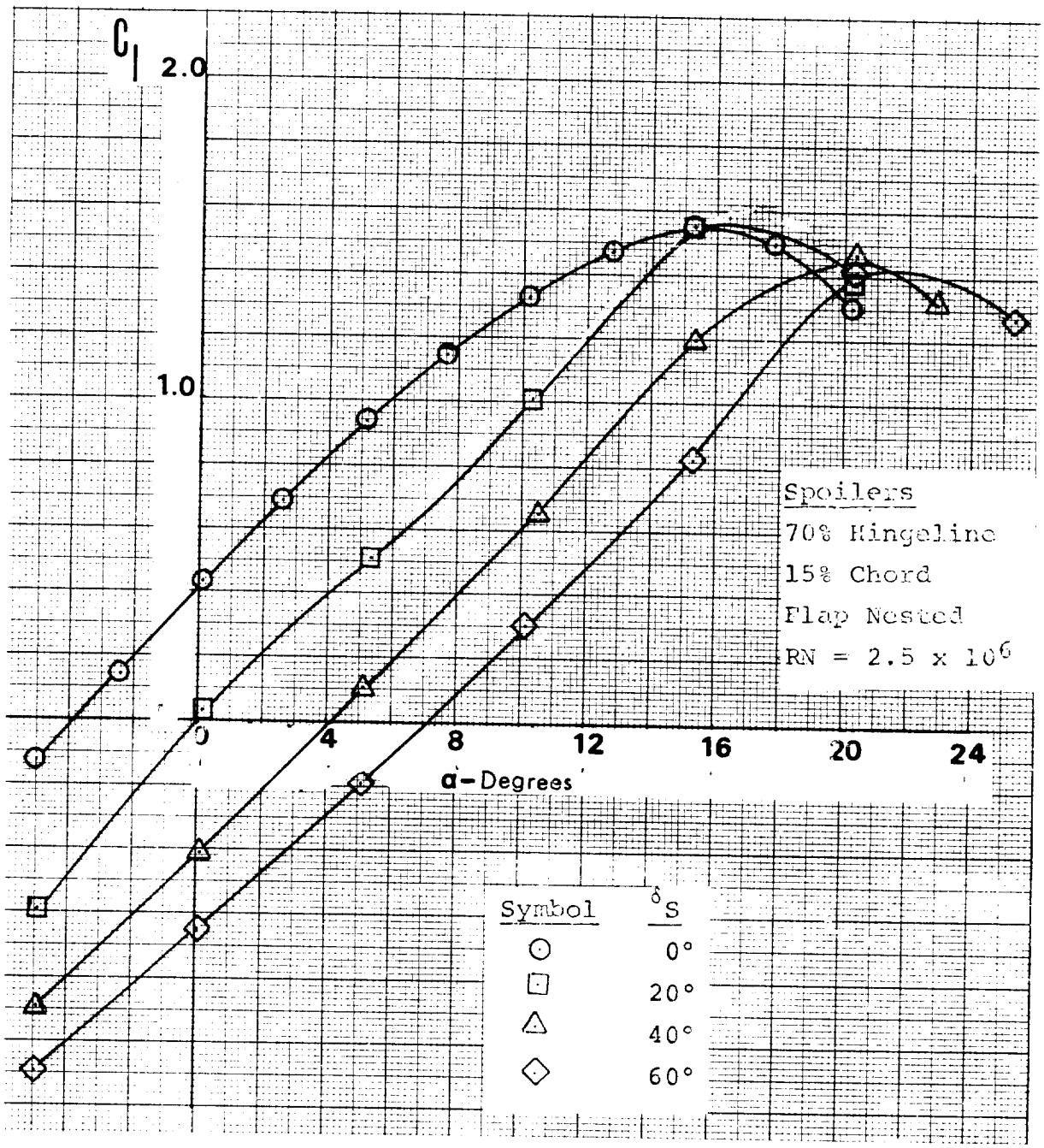

Figure 52 - (Continued)

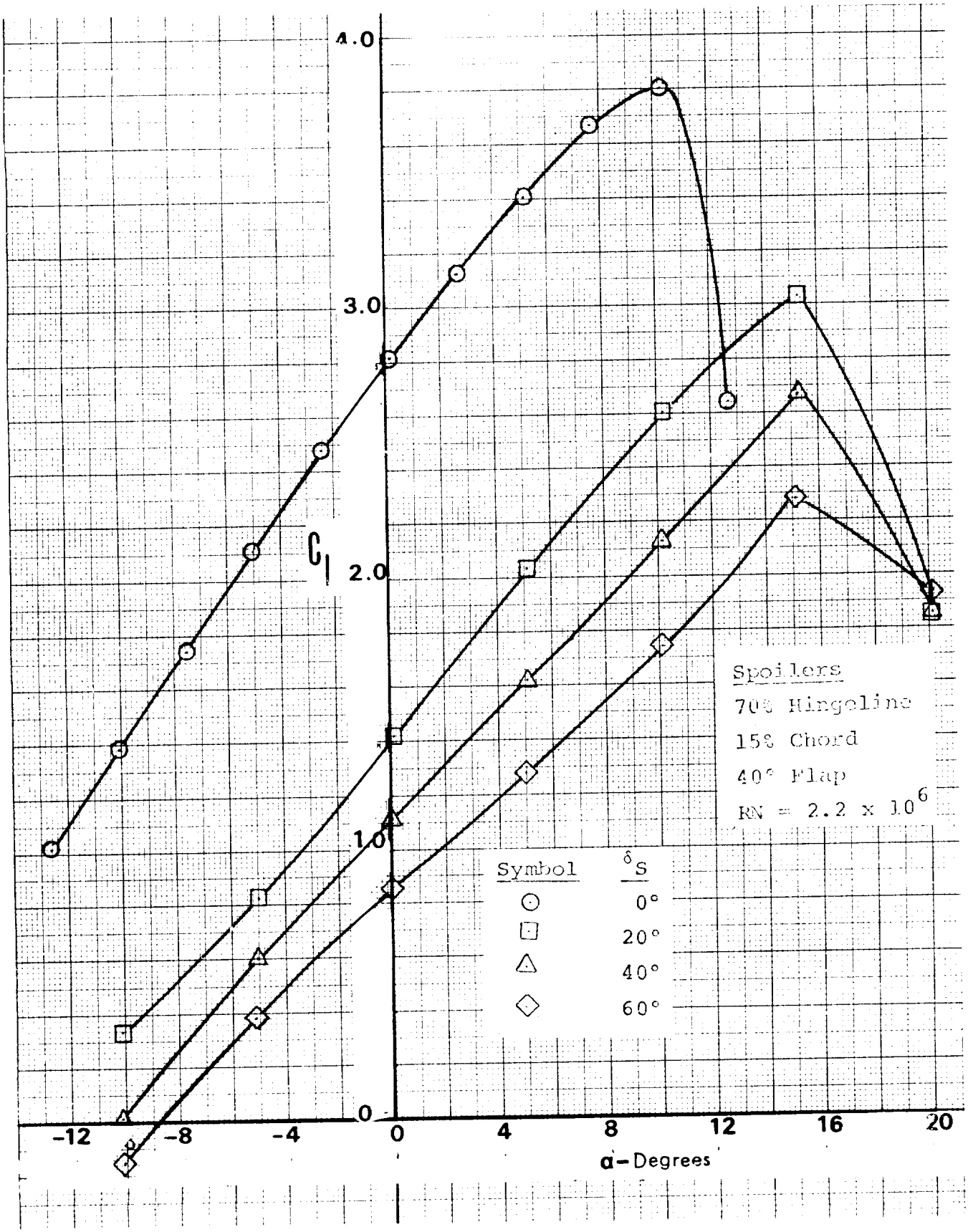

Figure 52 - (Concluded)

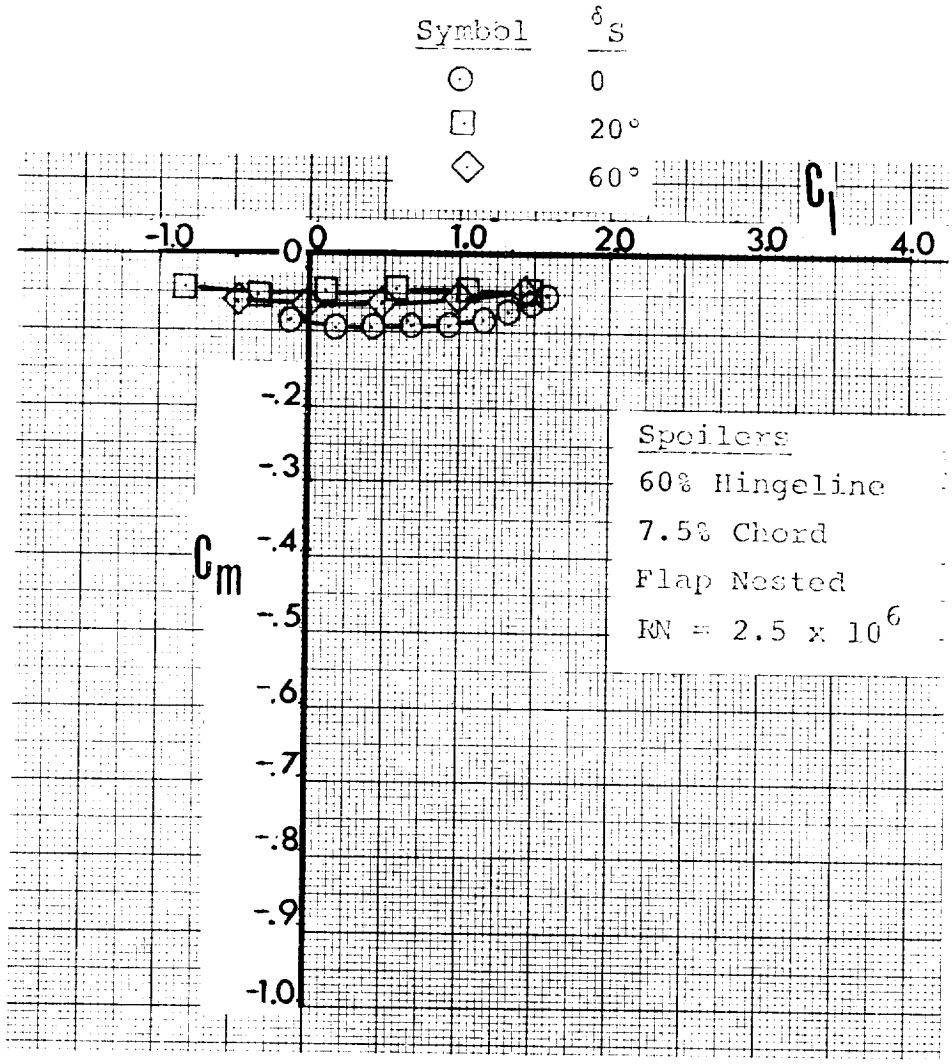

Figure 53 - Effect of Spoilers on Pitching Moments

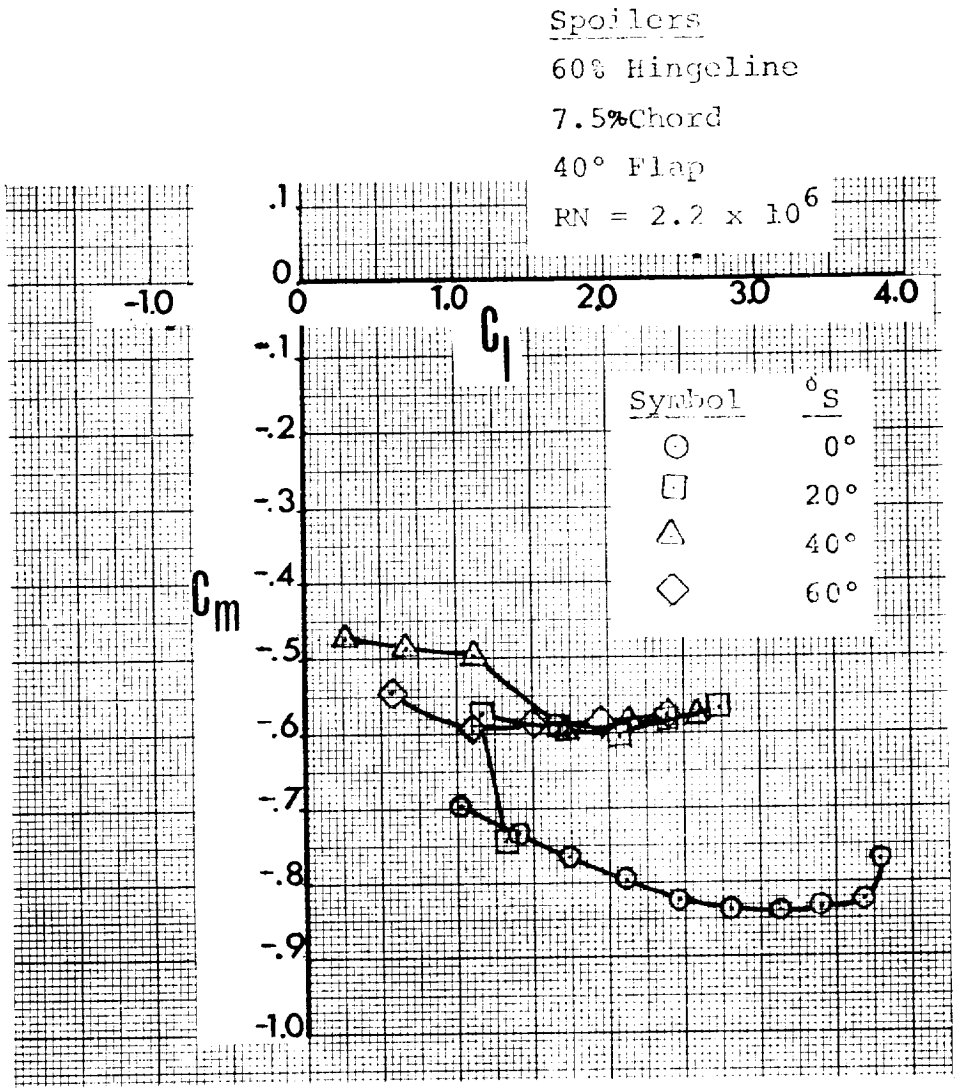

Figure 53 - (Continued)

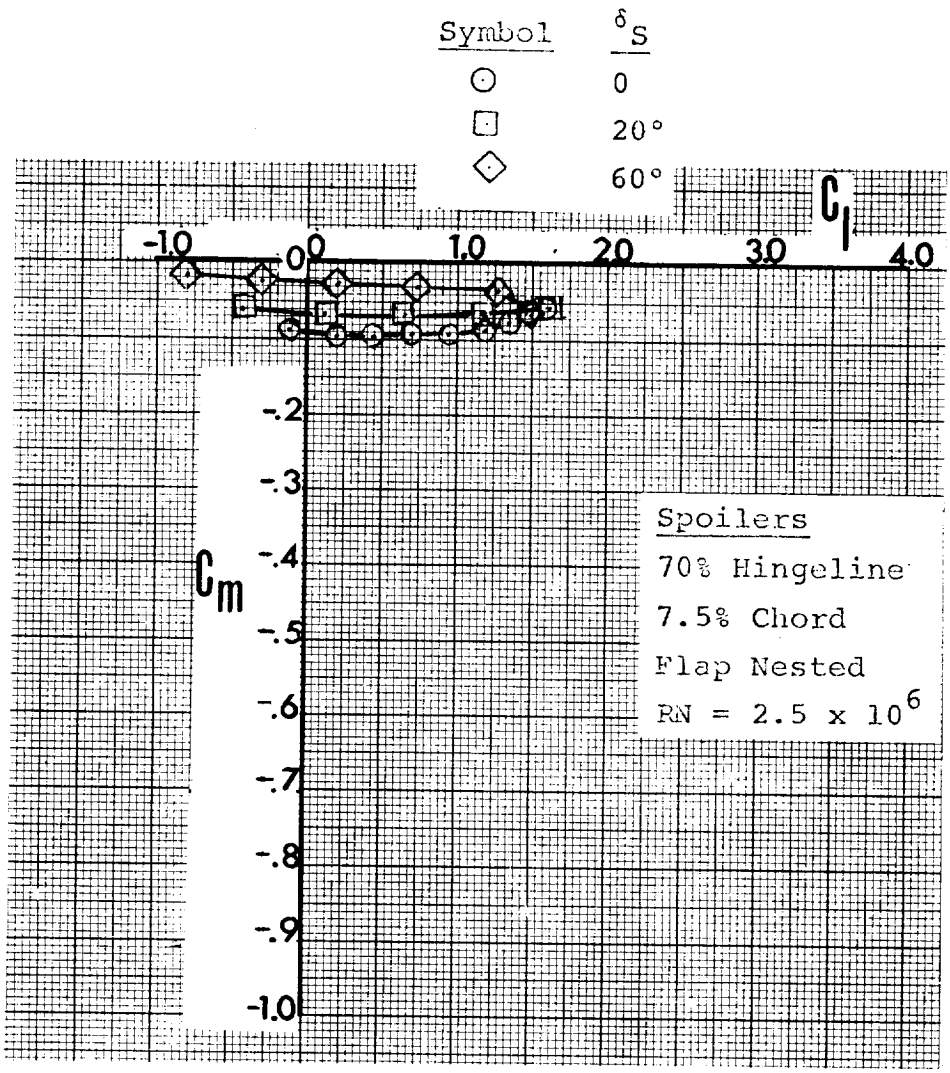

Figure 53 - (Continued)

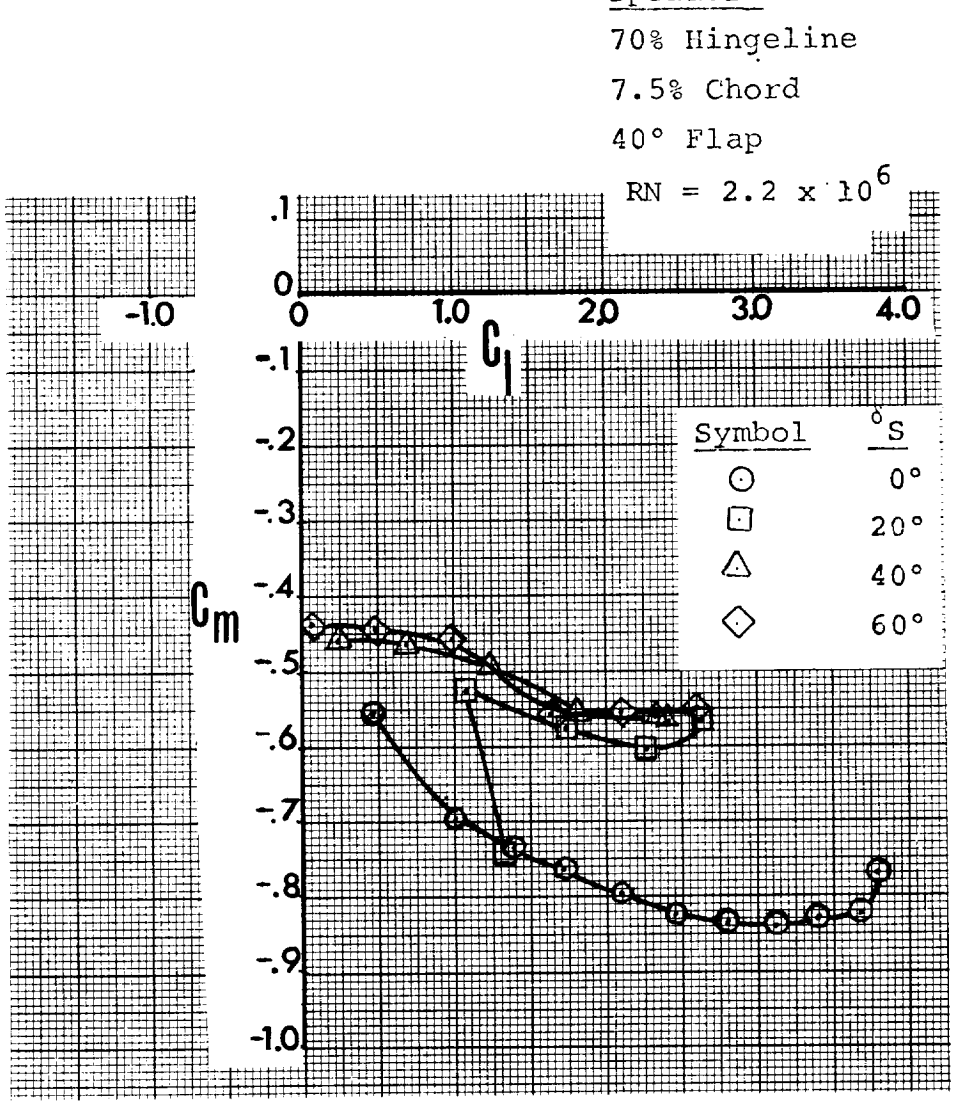

Figure 53 - (Continued)

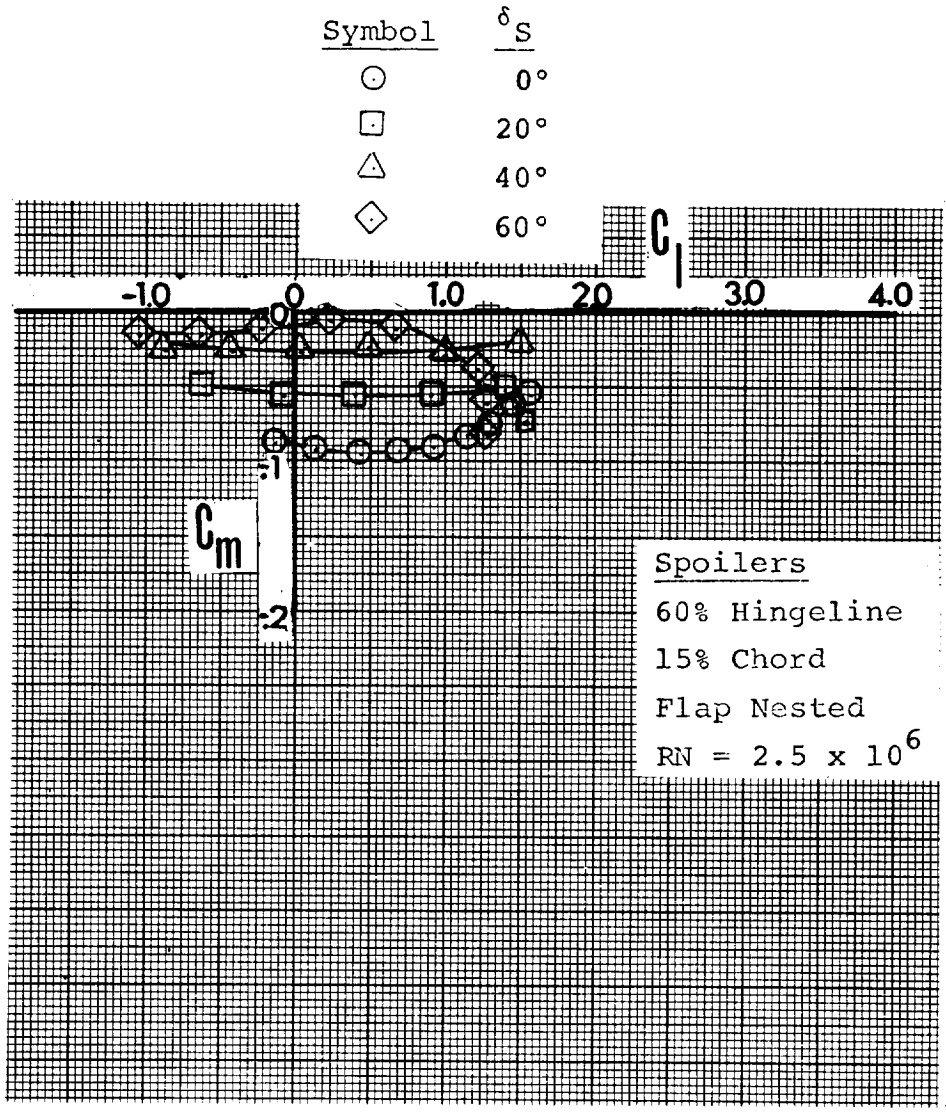

Figure 53 - (Continued)

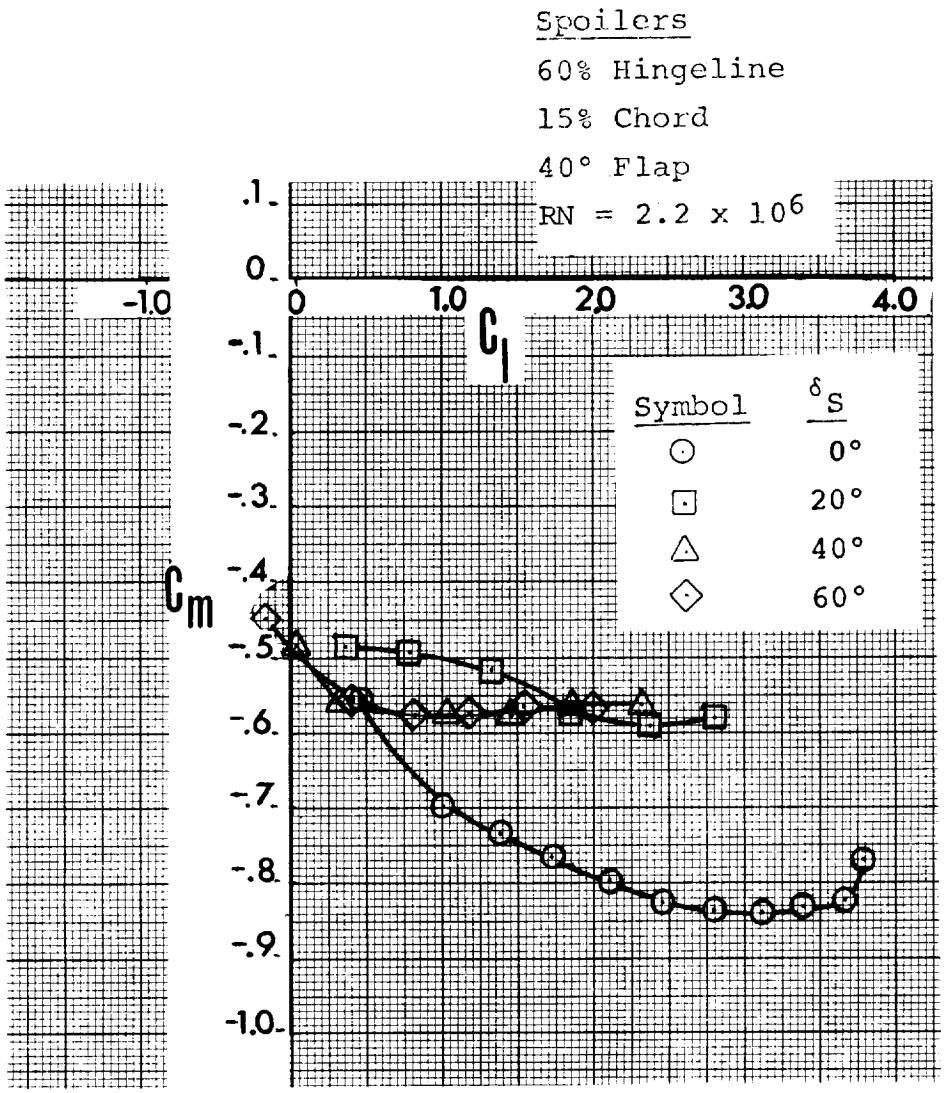

Figure 53 - (Continued)

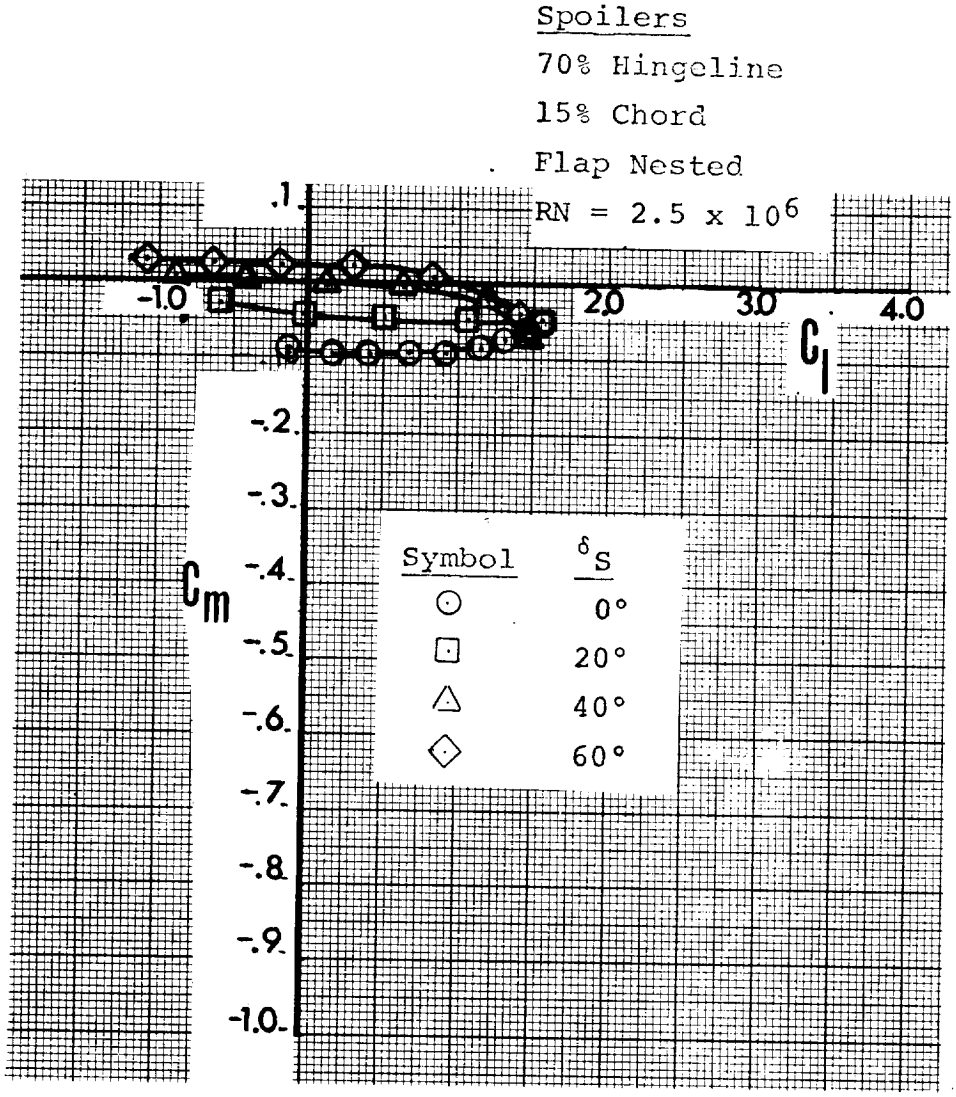

Figure 53 - (Continued)

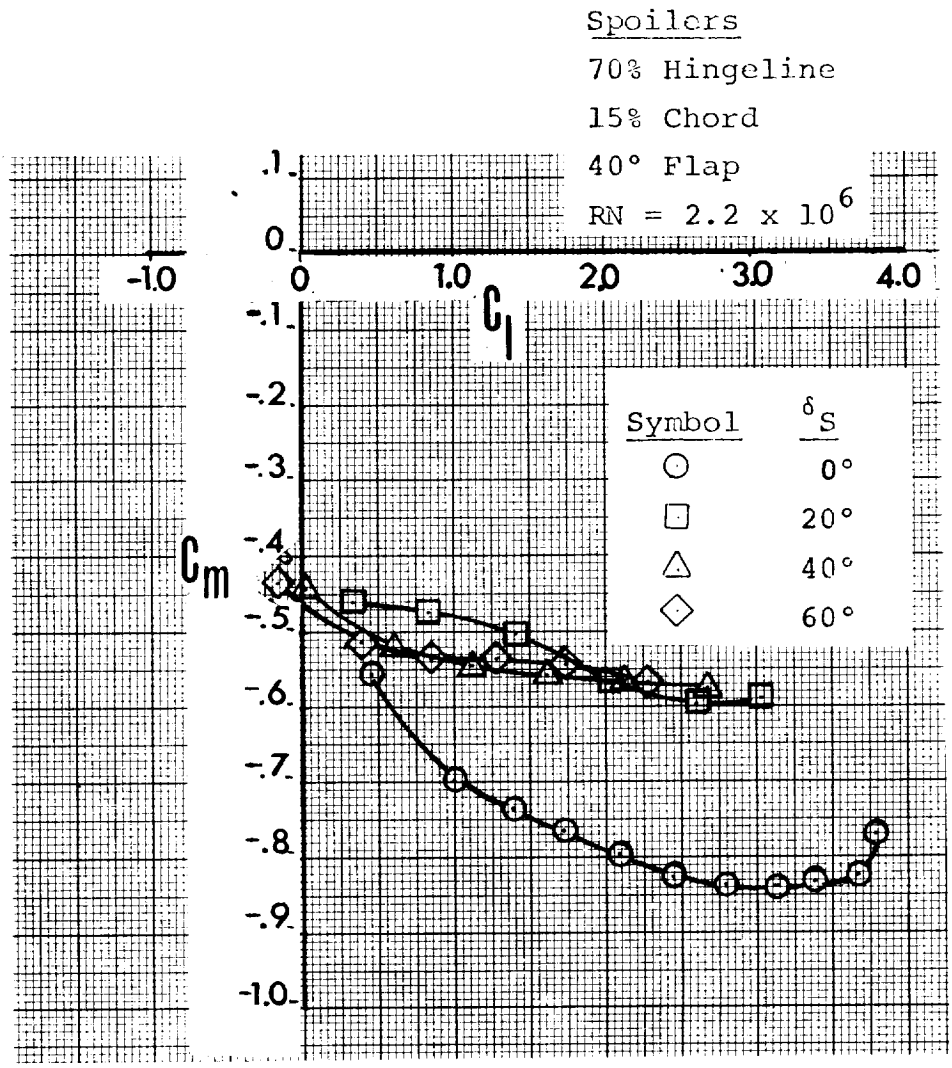

Figure 53 - (Concluded)

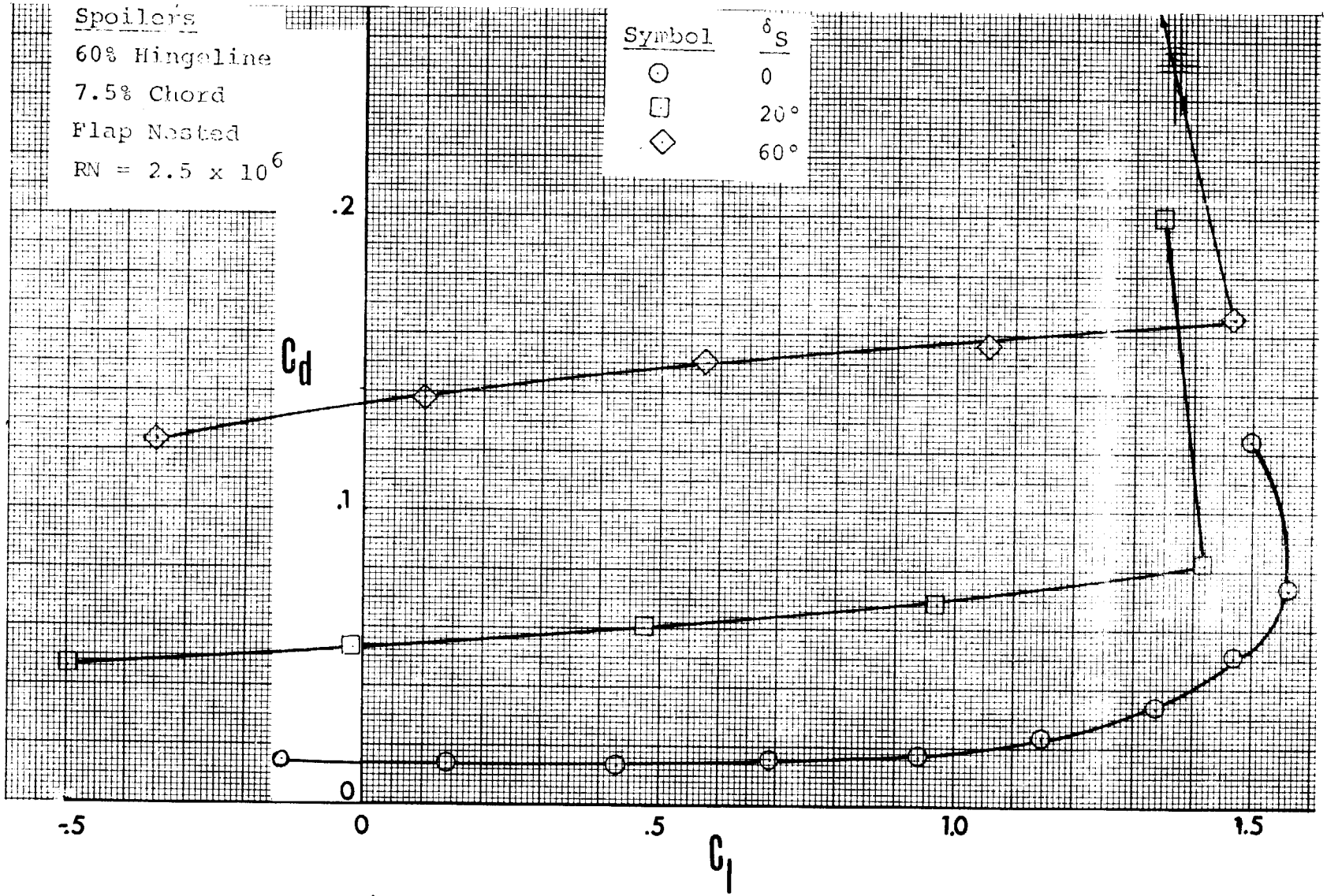

Figure 54 - Effect of Spoilers on Drag

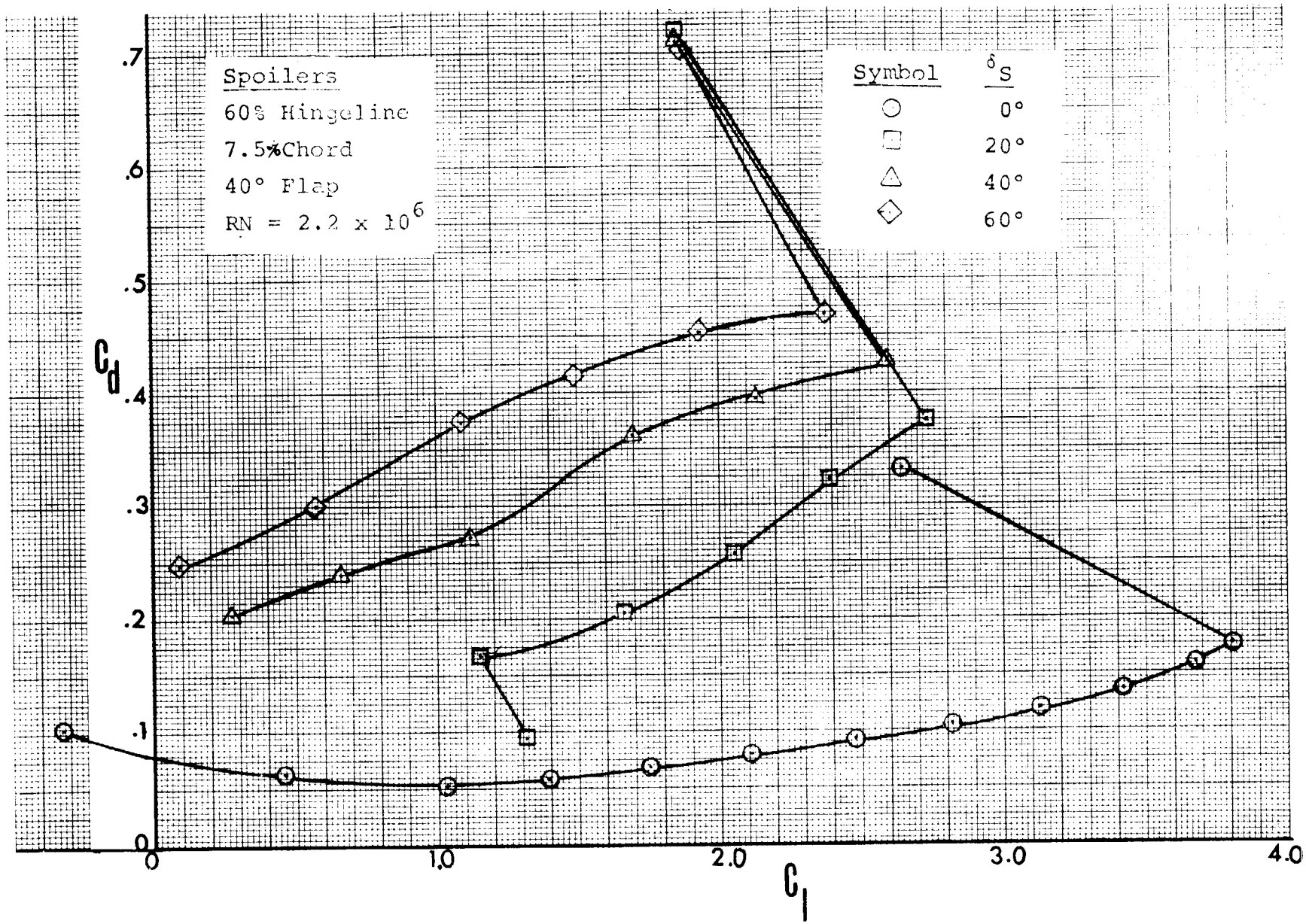

Figure 54 - (Continued)

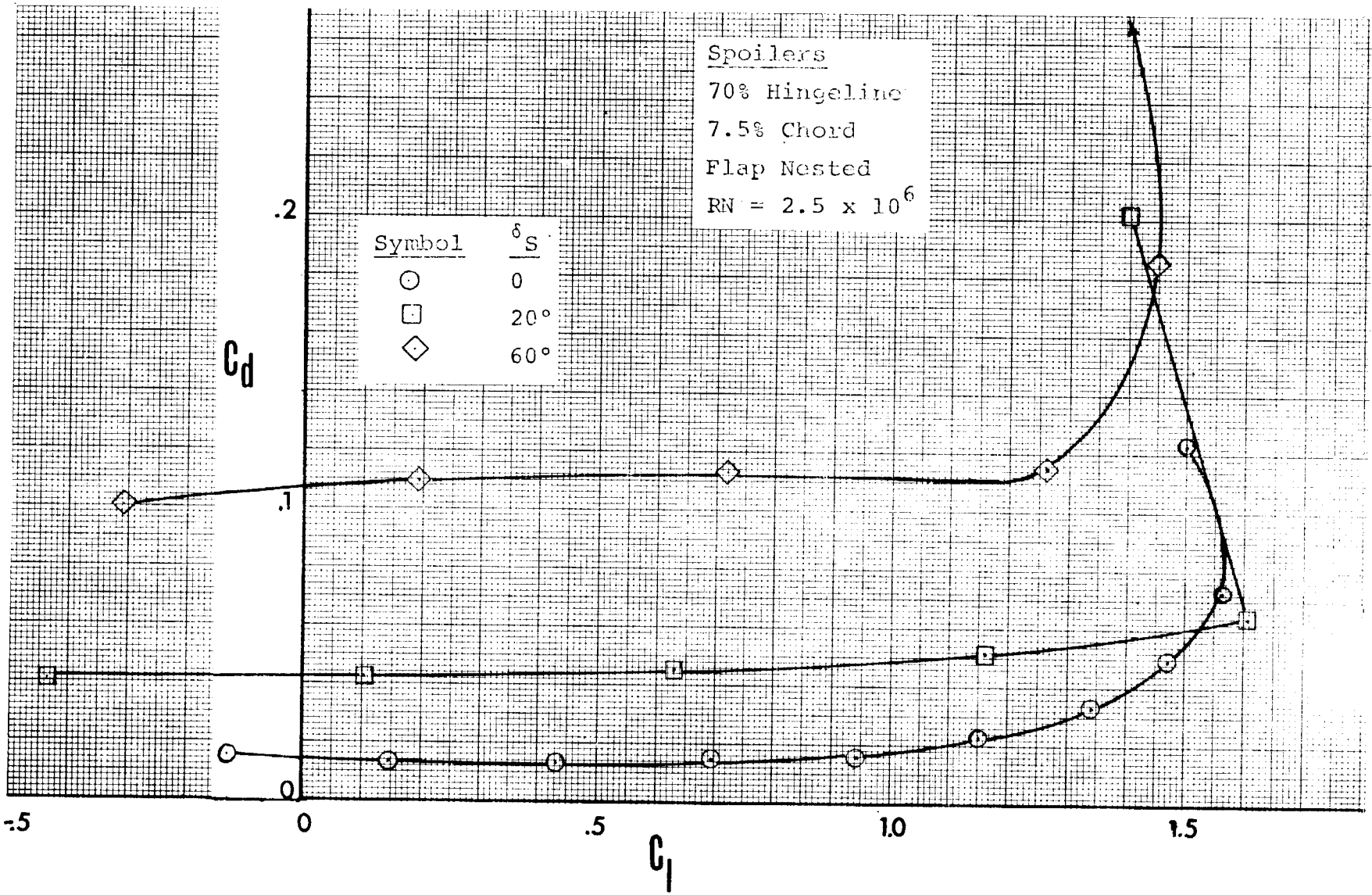

Figure 54 - (Continued)

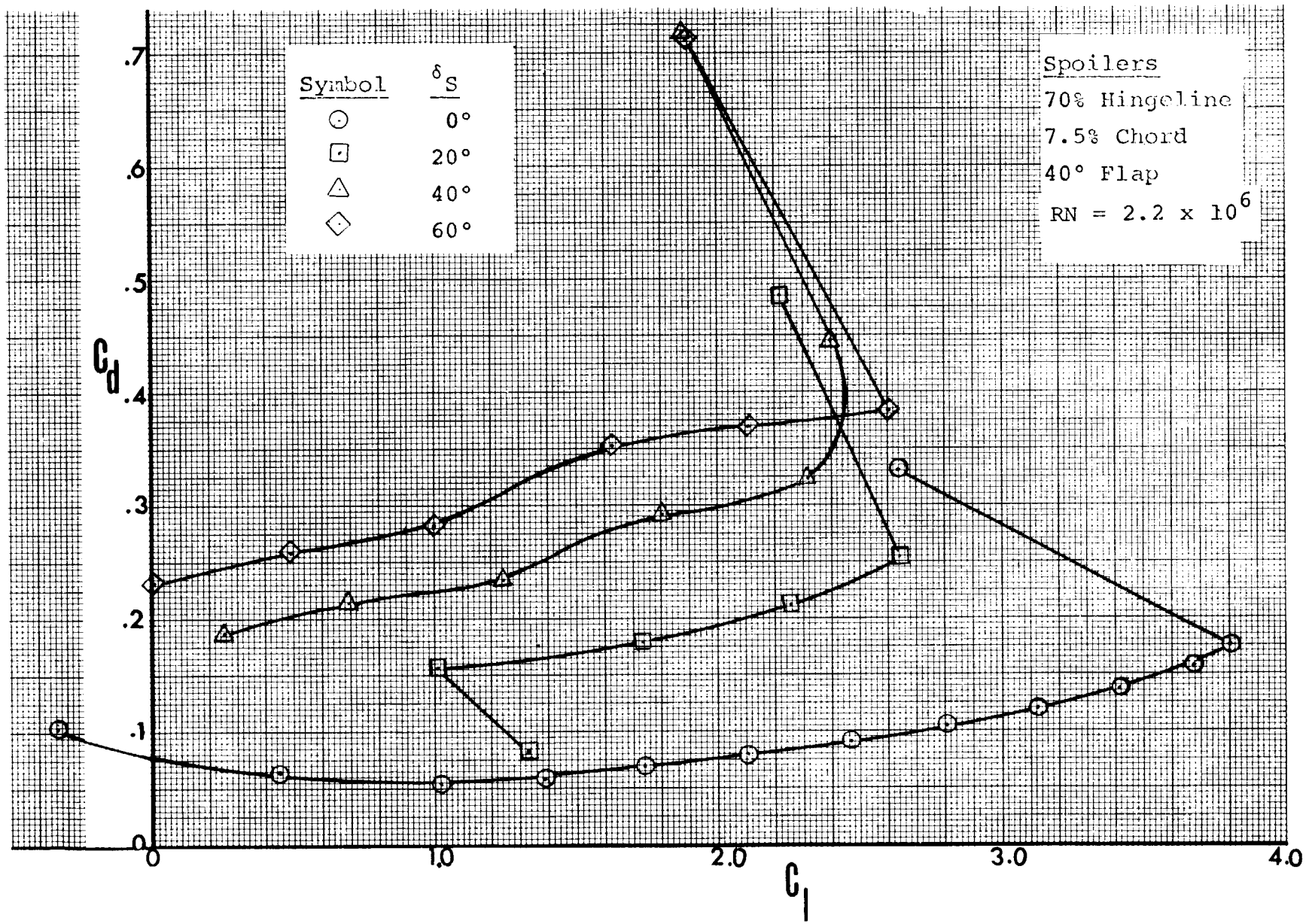

Figure 54 - (Continued)

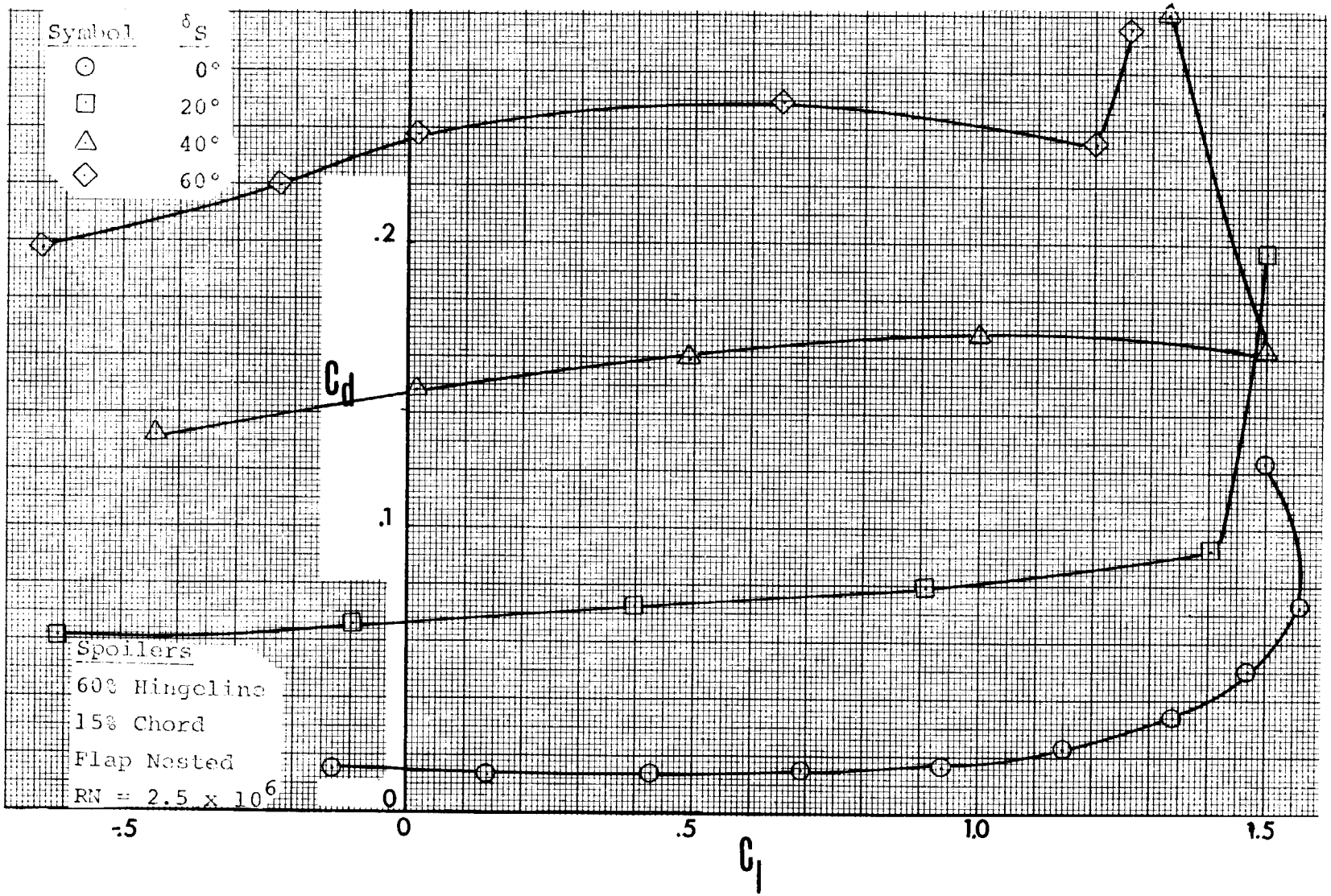

Figure 54 - (Continued)

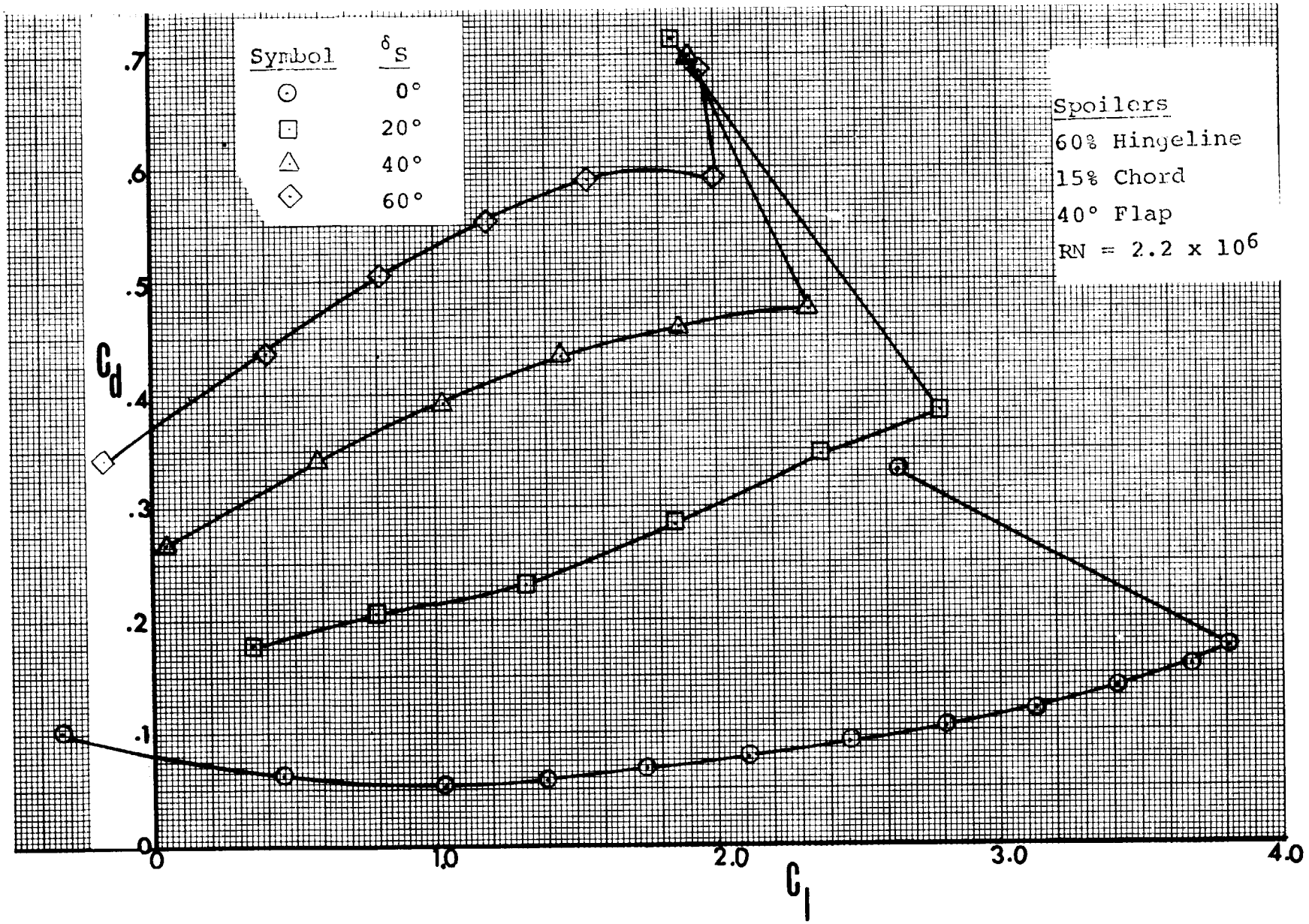

Figure 54 - (Continued)

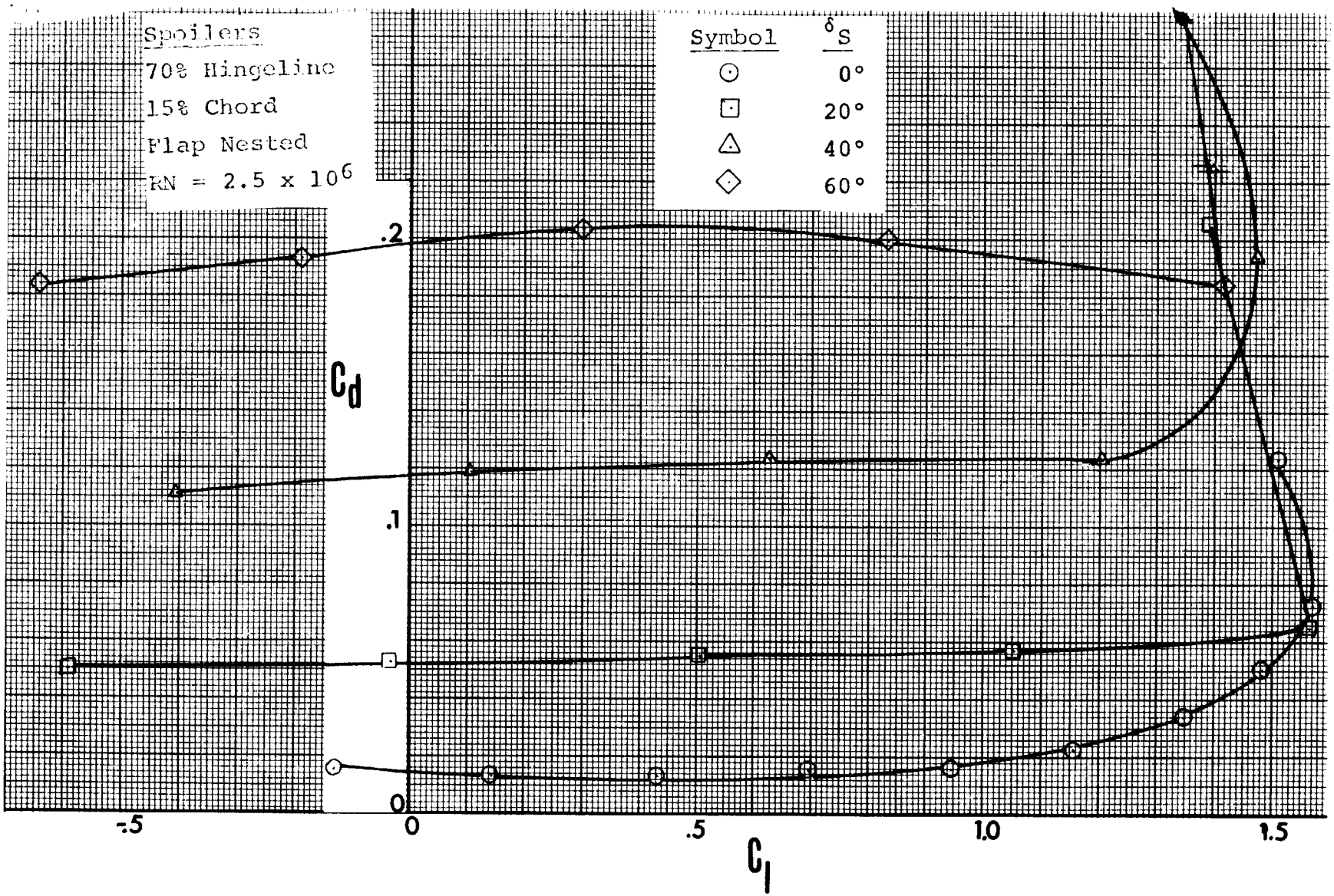

Figure 54 - (Continued)

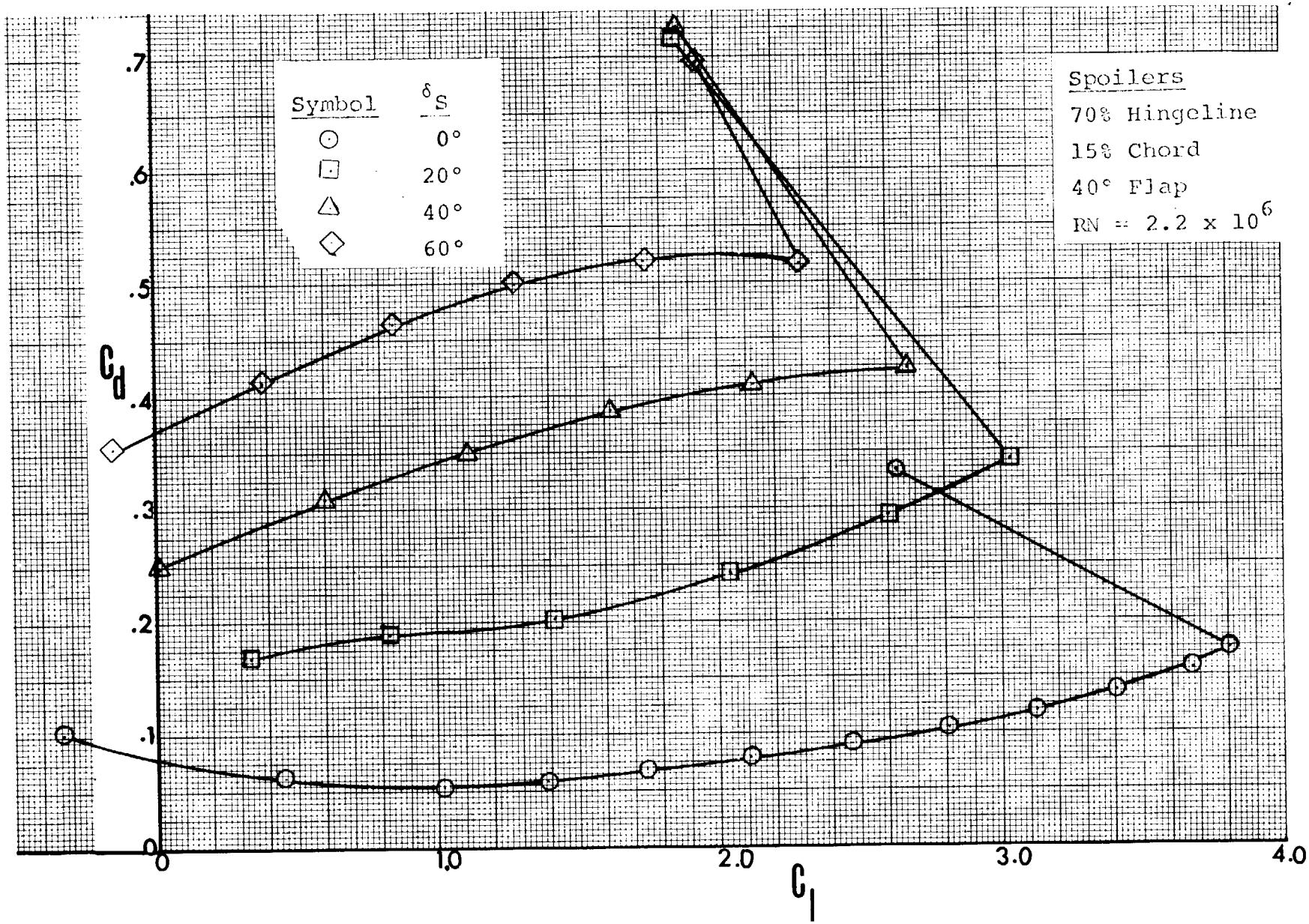

Figure 54 - (Concluded)

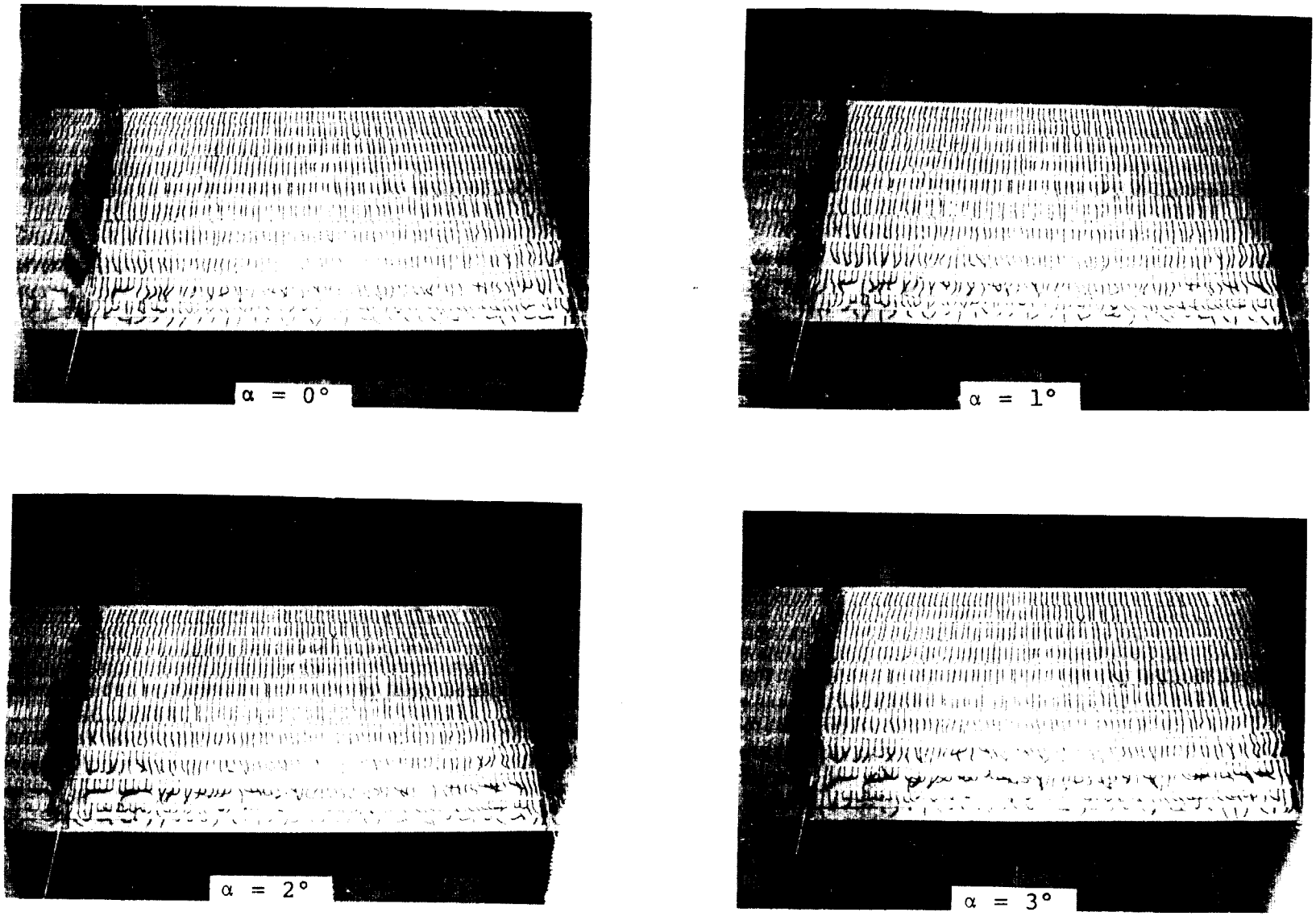

Figure 55 - Flow Visualization, Flap Nested (a) α = 0° to 3°

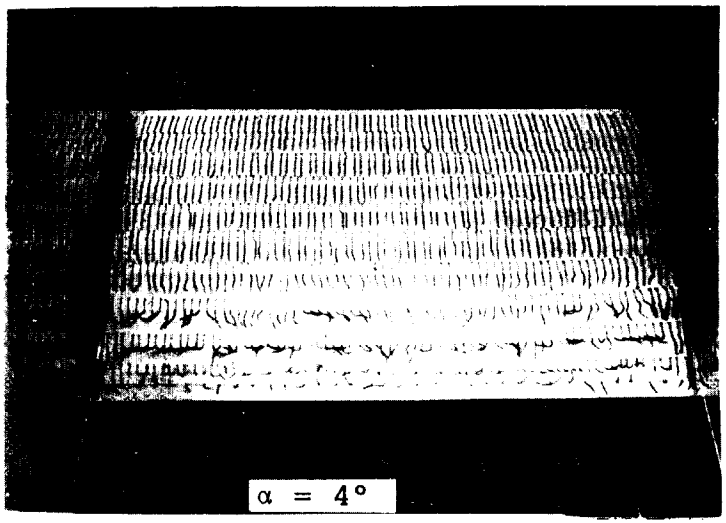

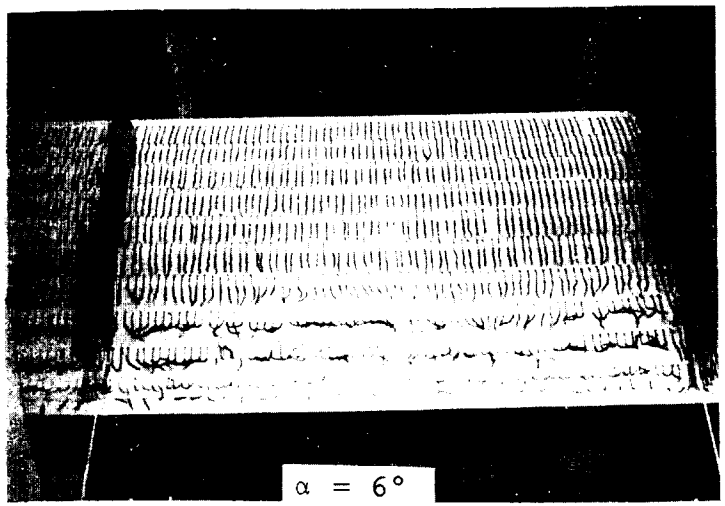

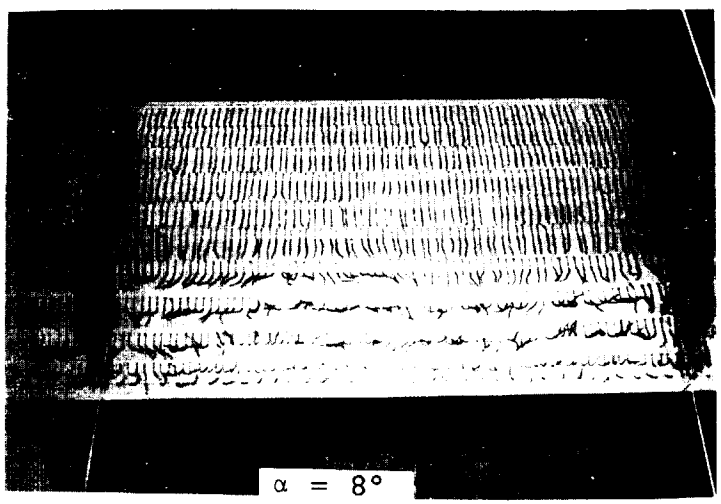

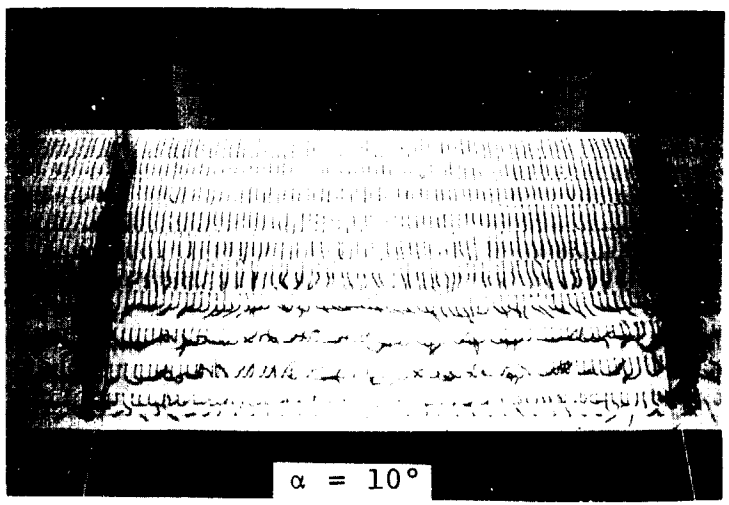

Figure 55 - (Continued) (b) α = 4° to 10°

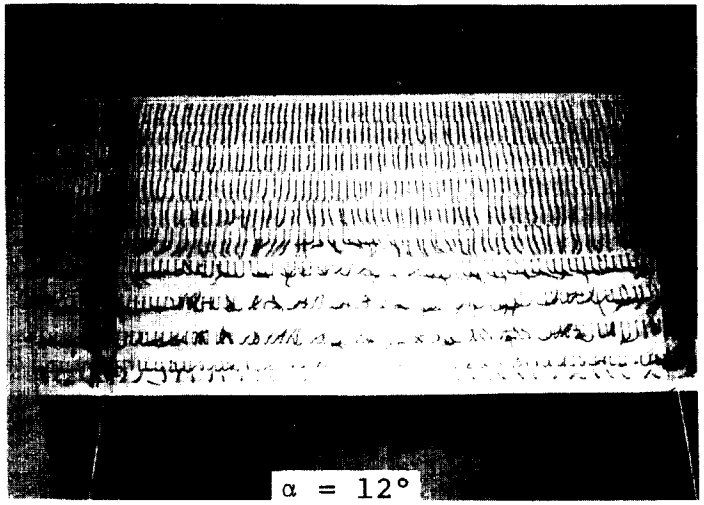

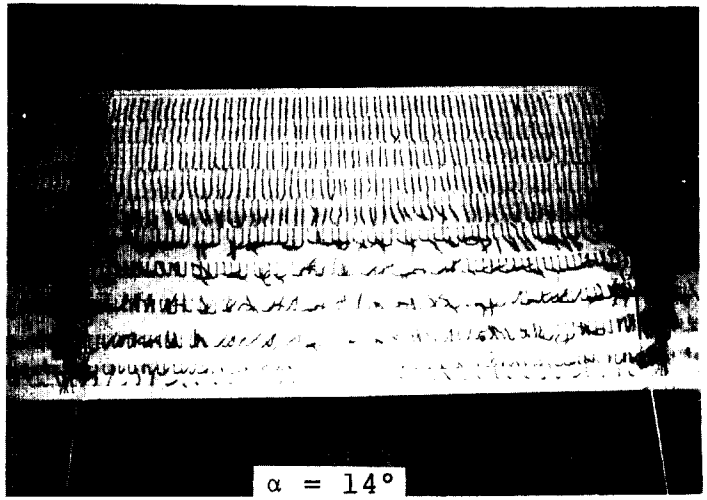

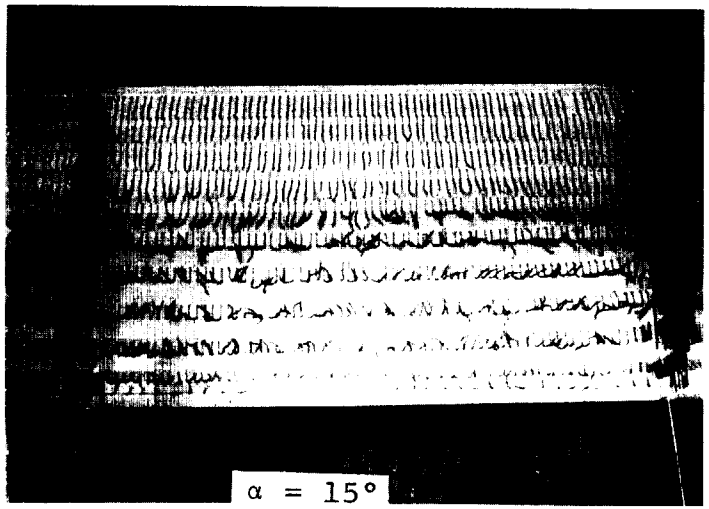

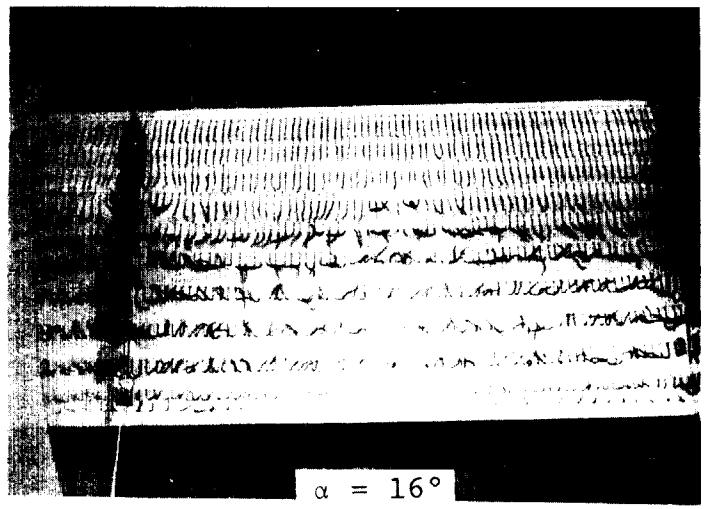

Figure 55 - (Concluded) (c) α = 12° to 16°

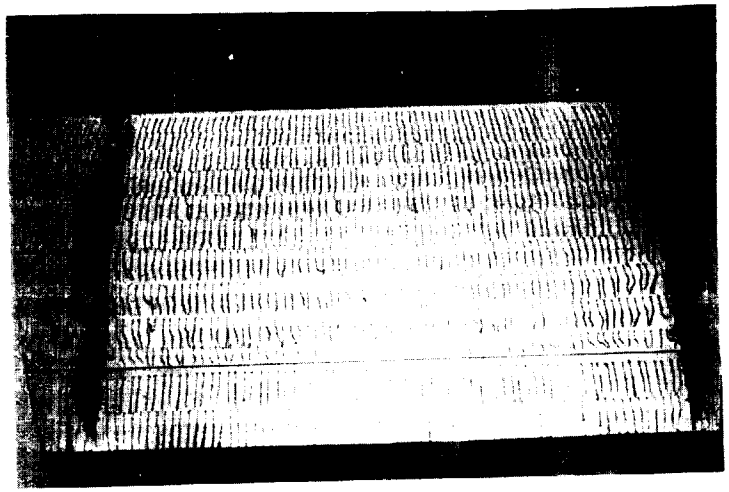

29% c Flap, α = 0°

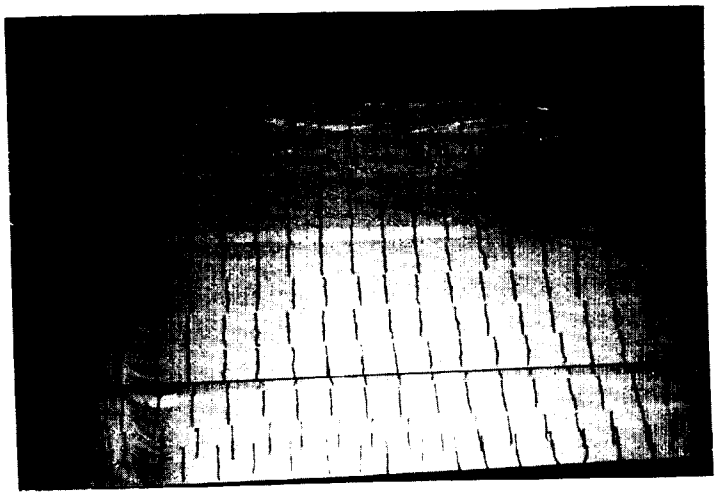

30% c Flap, α = 0°

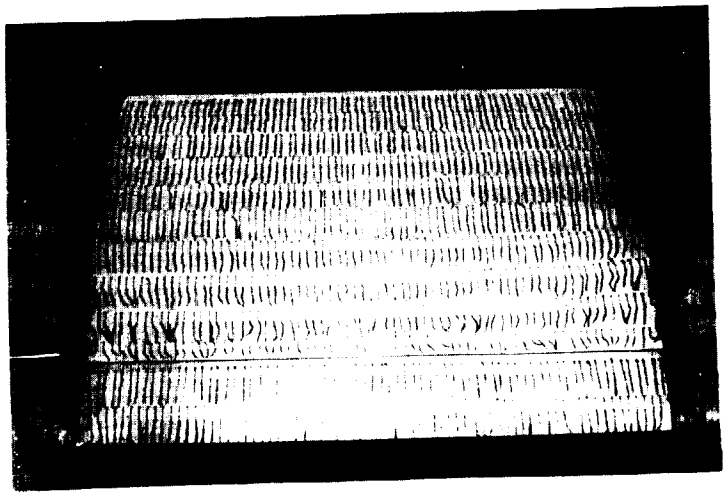

29% c Flap, α = 2.5°

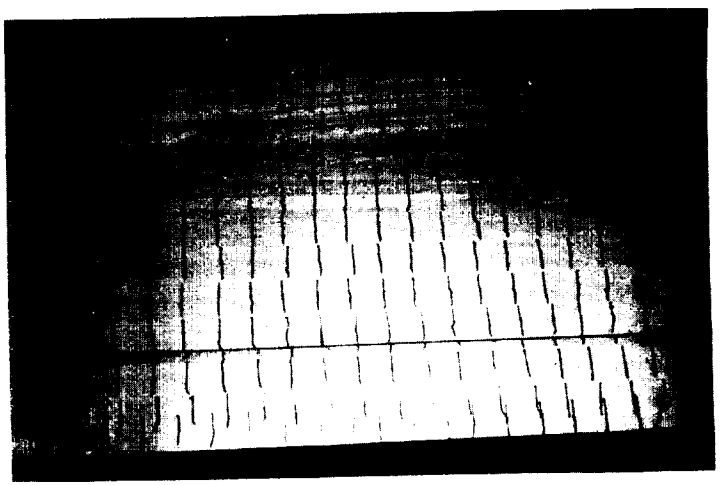

30% c Flap, α = 2.5°

Figure 56 - Flow Visualization, 10° Flap (a) α = 0° and 2.5°

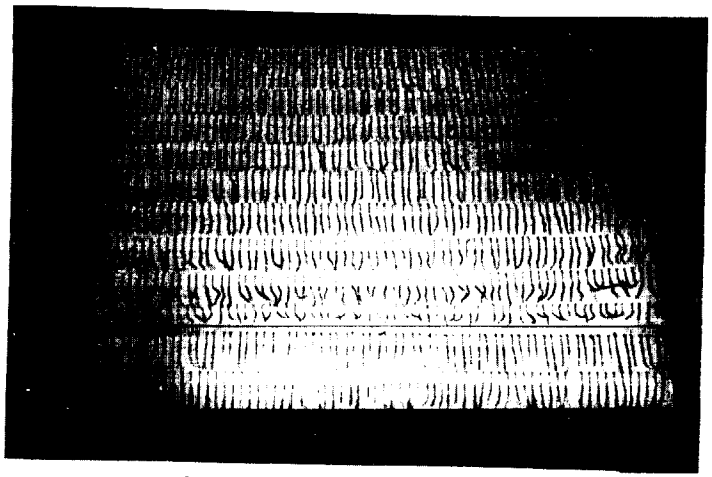

29% c Flap, α = 5°

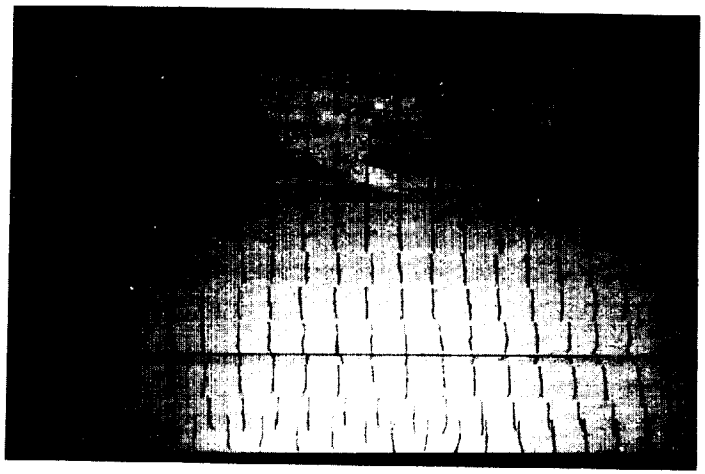

30% c Flap, α = 5°

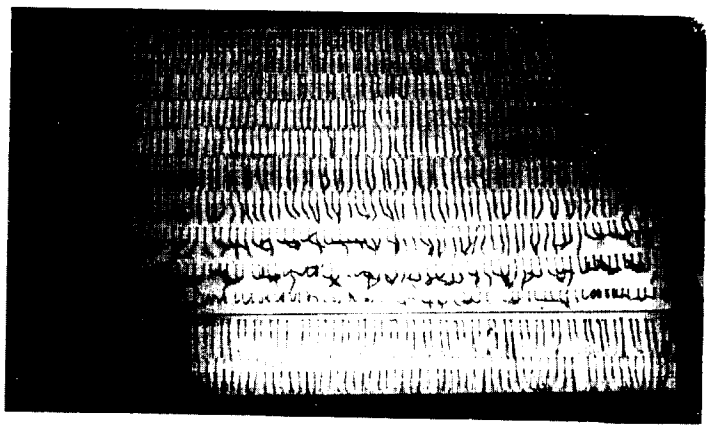

29% c Flap, α = 7.5°

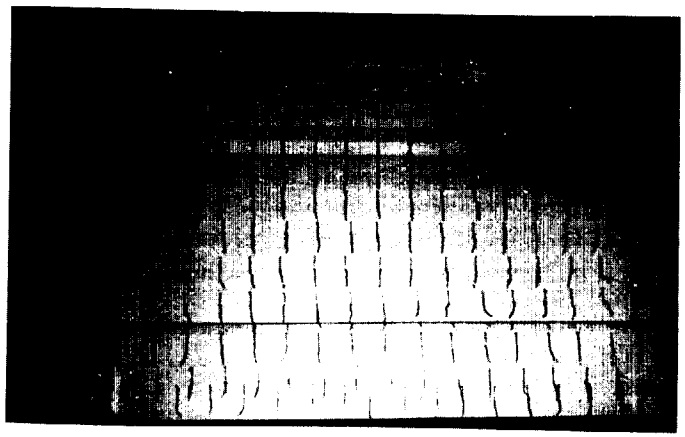

30% c Flap, α = 7.5°

Figure 56 – (Continued) (b) α = 5° and 7.5°

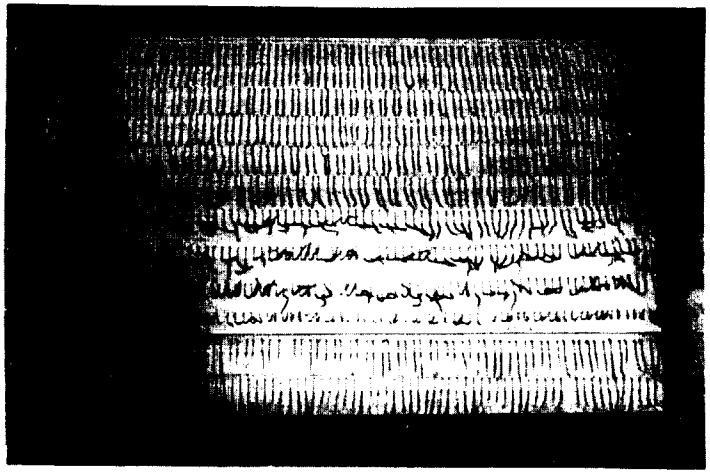

29% c Flap, α = 10°

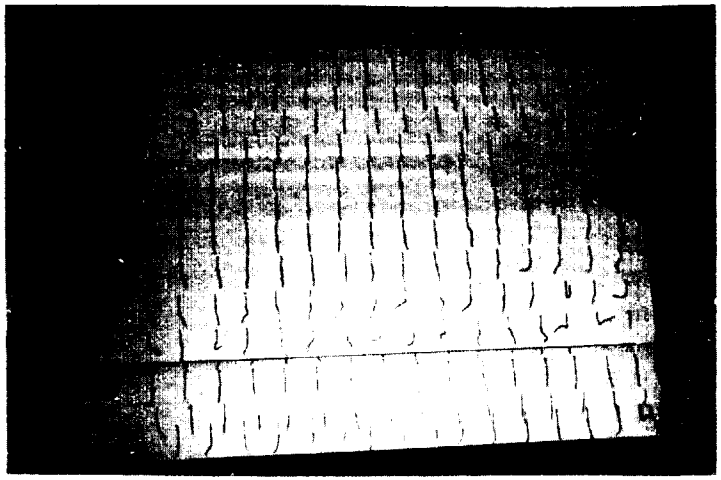

30% c Flap, α = 10°

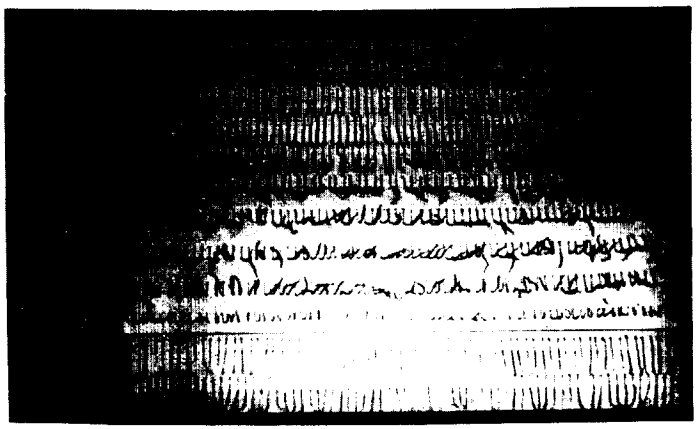

29% c Flap, α = 12.5°

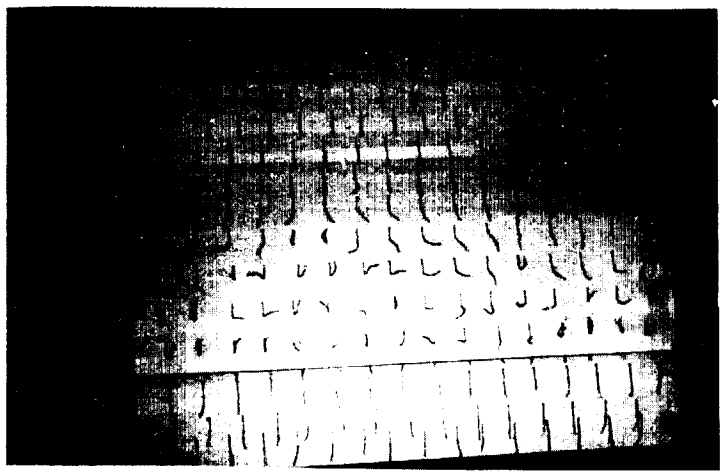

30% c Flap, α = 12.5°

Figure 56 - (Concluded) (c) α = 10° and 12.5°

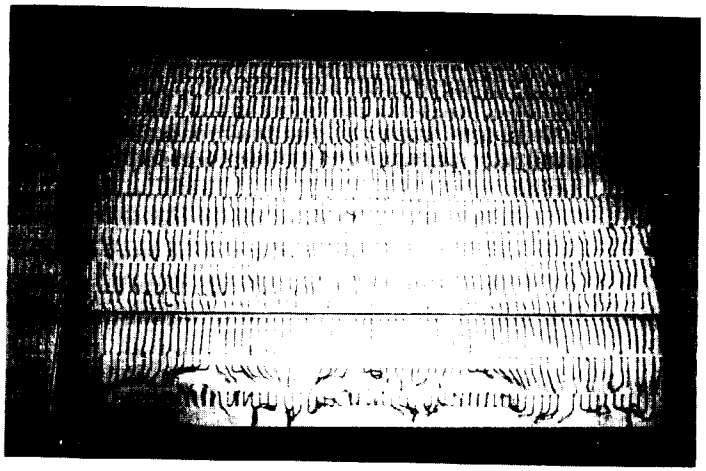

29% c Flap, α = 0°

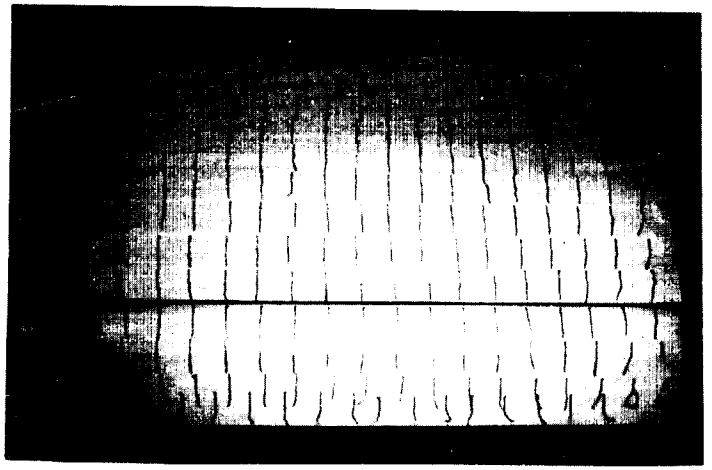

30% c Flap, α = 0°

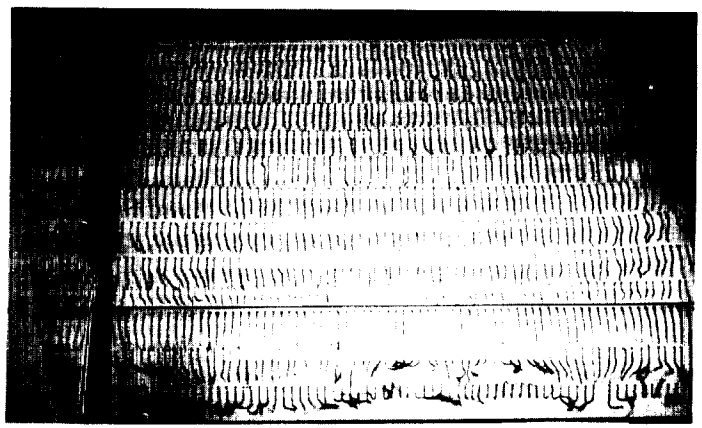

29% c Flap, α = 2.5°

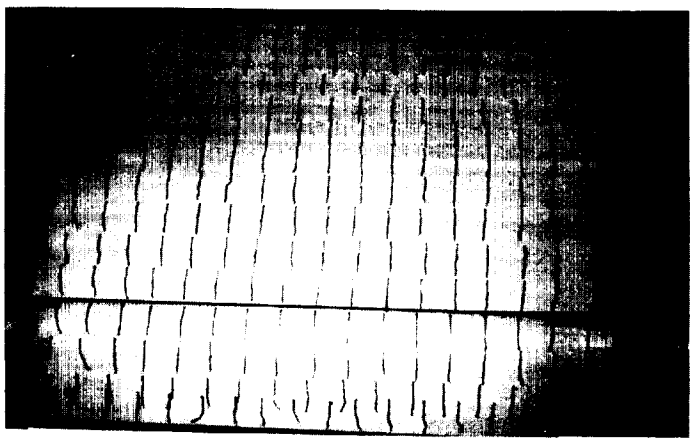

30% c Flap, α = 2.5°

Figure 57 - Flow Visualization, 35° Flap (a) α = 0° and 2.5°

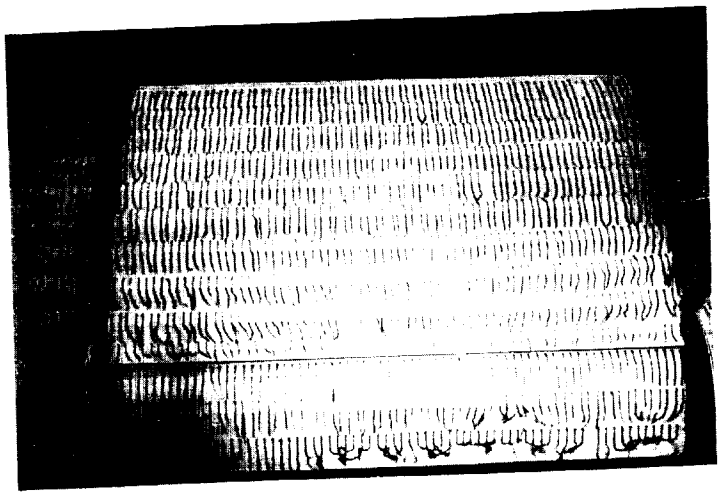

29% c Flap, $\alpha = 5°$

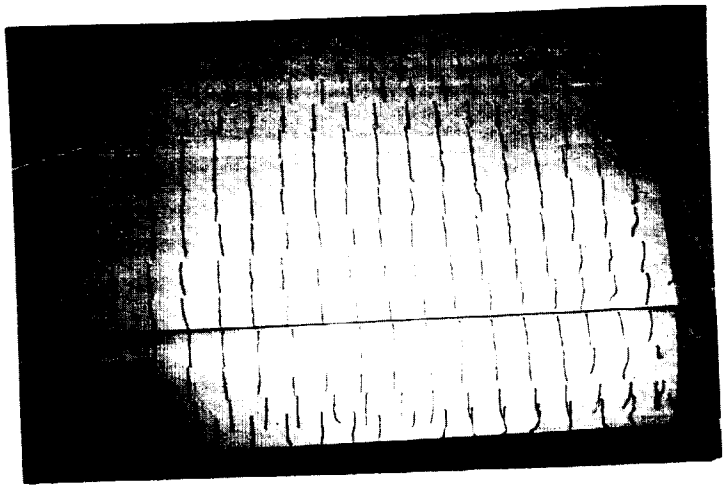

30% c Flap, $\alpha = 5°$

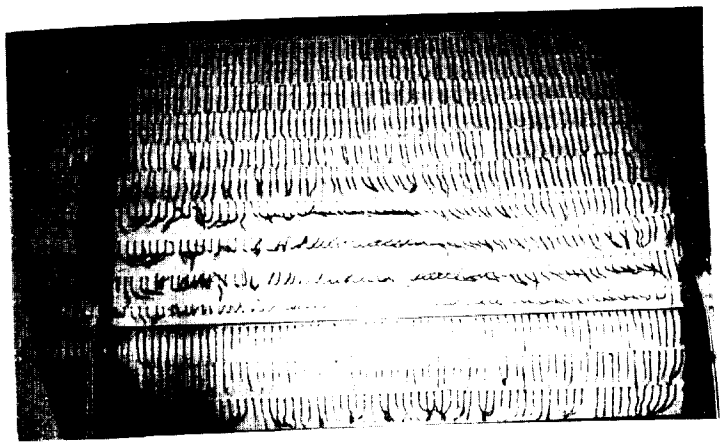

29% c Flap, $\alpha = 7.5°$

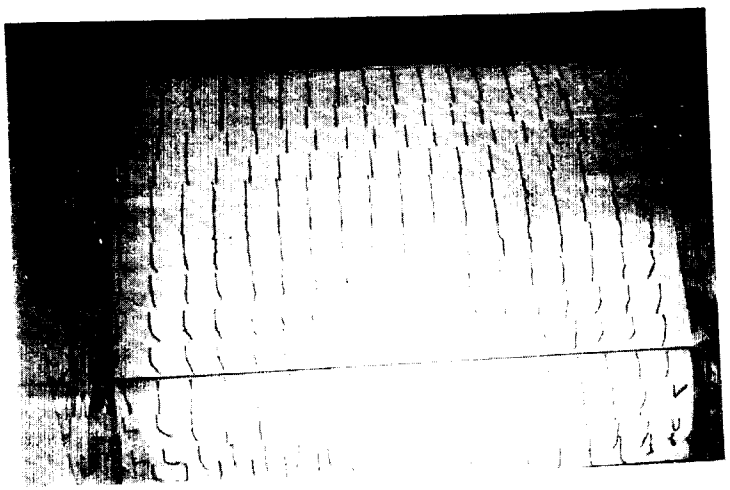

30% c Flap, $\alpha = 7.5°$

Figure 57 - (Continued) (b) $\alpha = 5°$ and $7.5°$

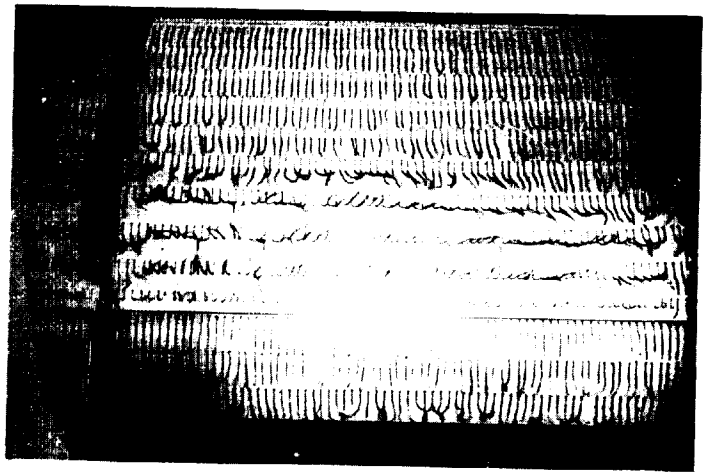

29% c Flap, α = 10°

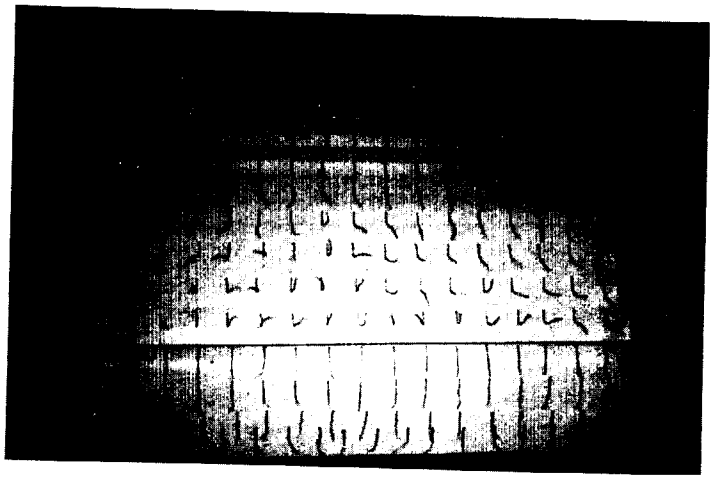

30% c Flap, α = 10°

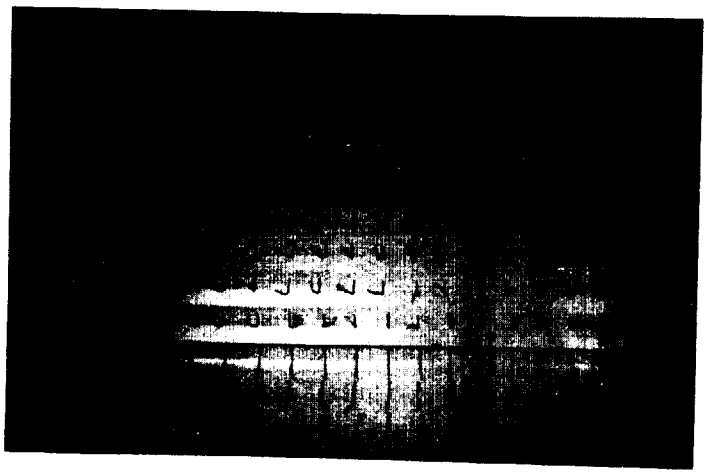

30% c Flap, α = 12.5°

Figure 57 - (Concluded) (c) α = 10° and 12.5°

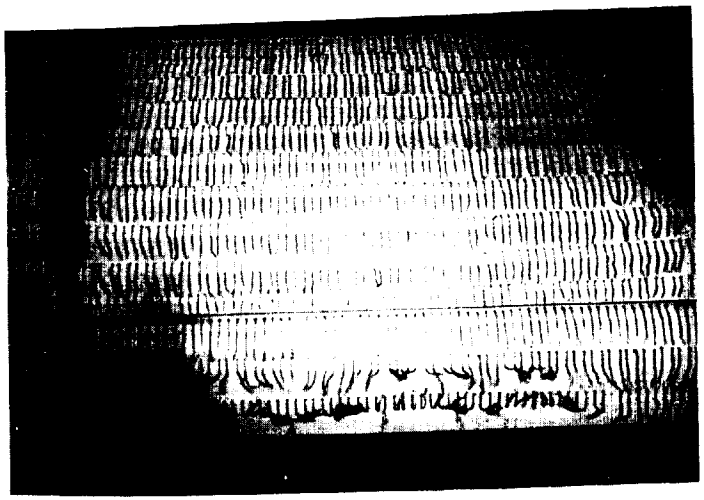

29% c Flap, Computer Settings

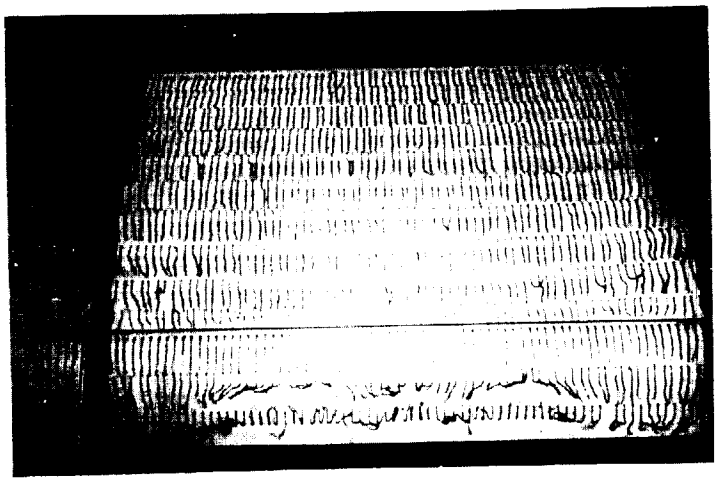

29% c Flap, Wind Tunnel Settings

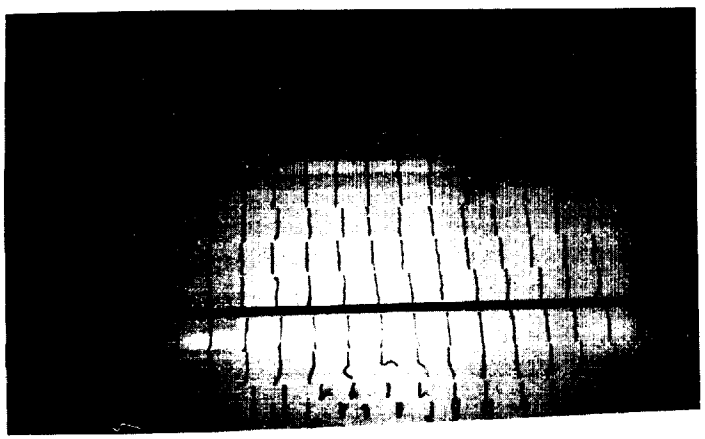

30% c Flap, Wind Tunnel Settings

Figure 58 - Flow Visualization, 40° Flap (a) $\alpha = 0°$

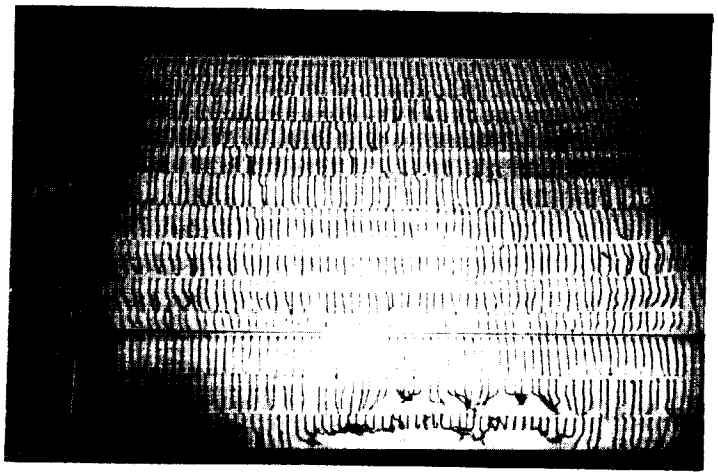

29% c Flap, Computer Settings

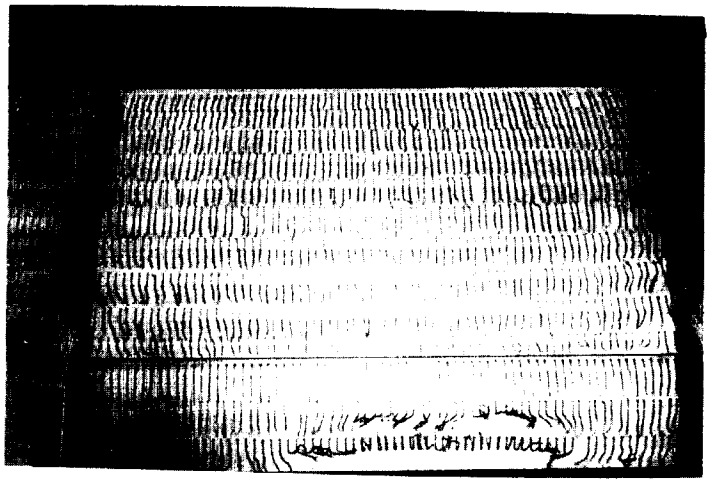

29% c Flap, Wind Tunnel Settings

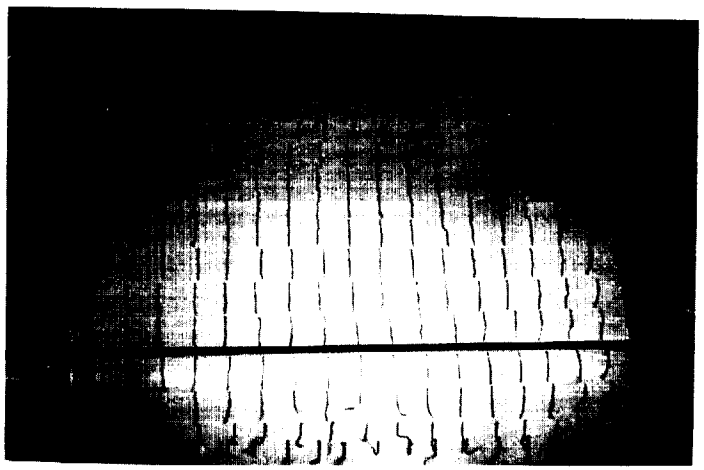

30% c Flap, Wind Tunnel Settings

Figure 58 - (Continued) (b) $\alpha = 2.5°$

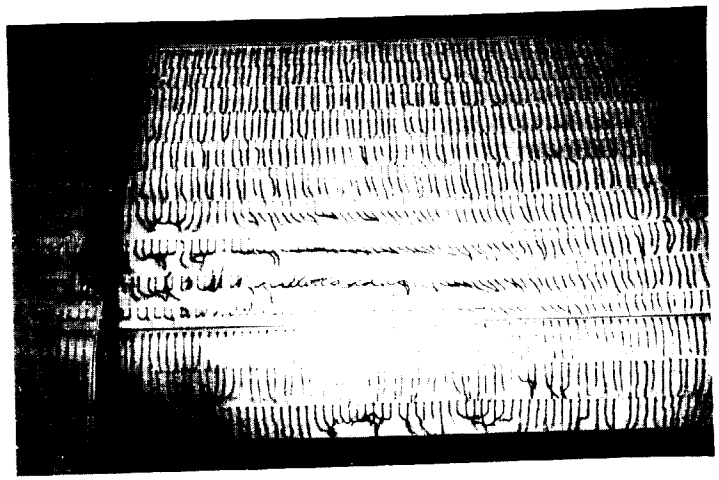

29% c Flap, Computer Settings

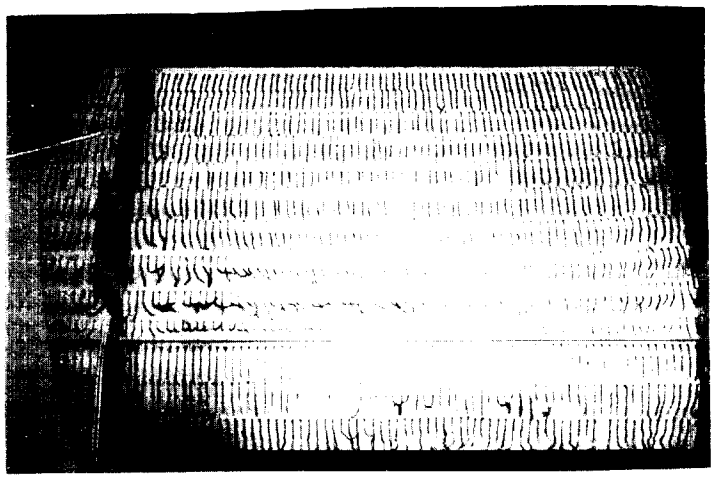

29% c Flap, Wind Tunnel Settings

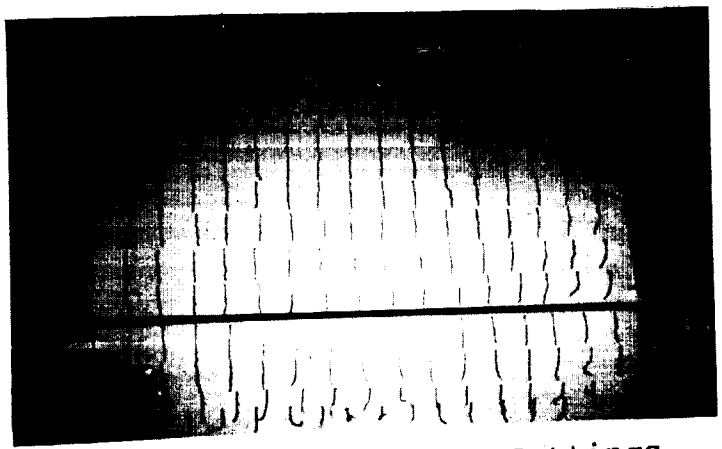

30% c Flap, Wind Tunnel Settings

Figure 58 - (Continued) (c) $\alpha = 5°$

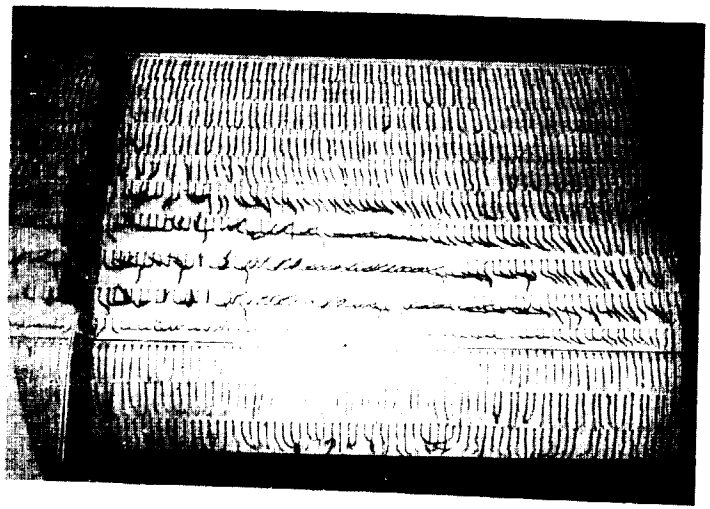

29% c Flap, Computer Settings

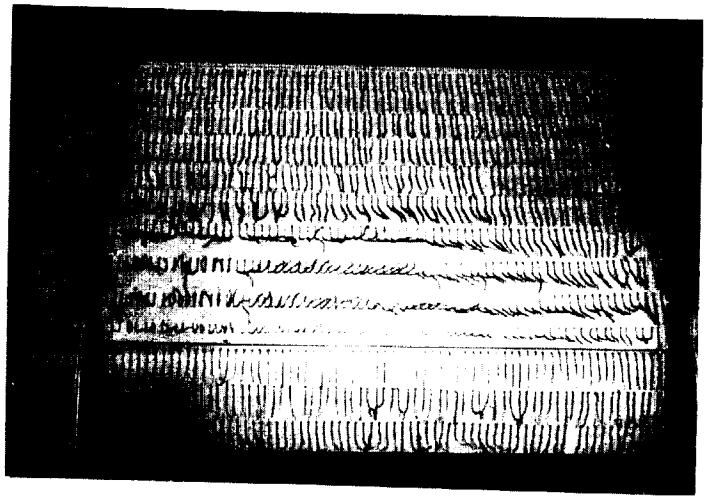

29% c Flap, Wind Tunnel Settings

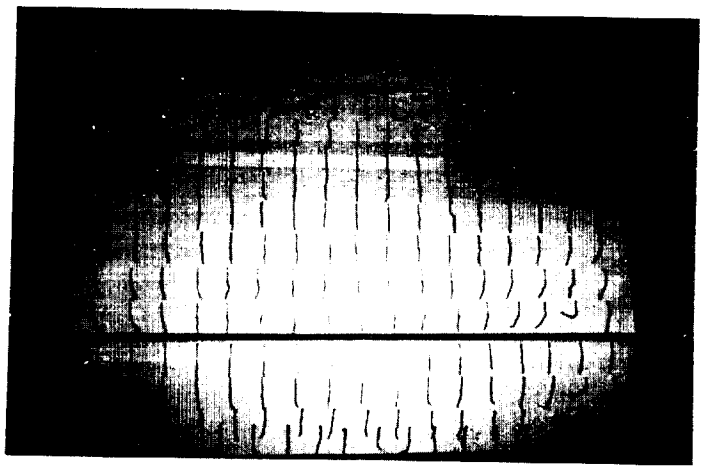

30% c Flap, Wind Tunnel Settings

Figure 58 - (Continued) (d) $\alpha = 7.5°$

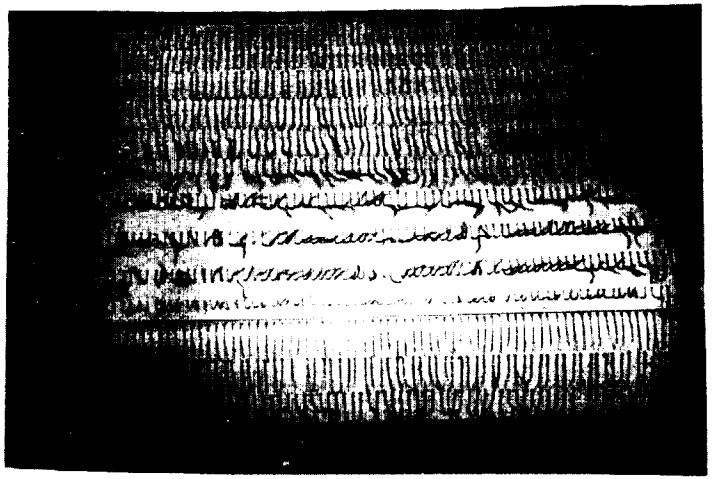

29% c Flap, Computer Settings

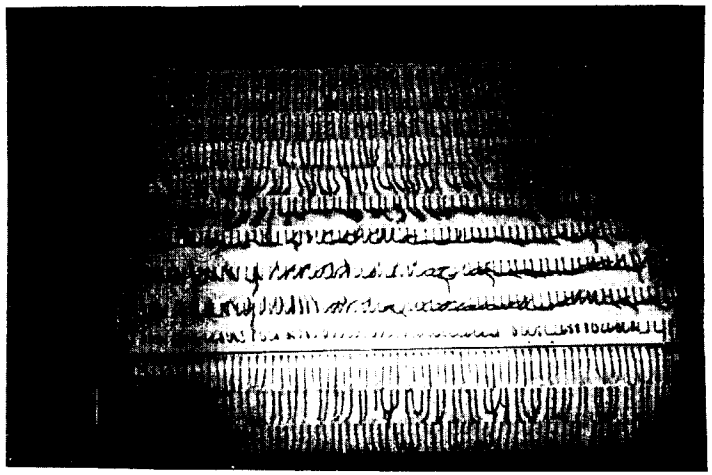

29% c Flap, Wind Tunnel Settings

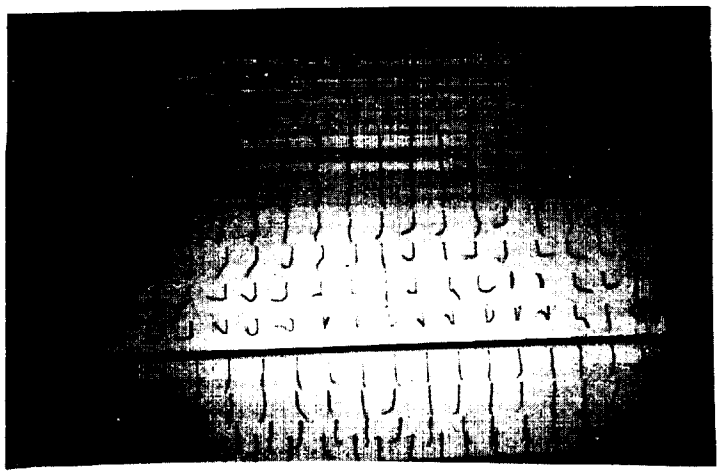

30% c Flap, Wind Tunnel Settings

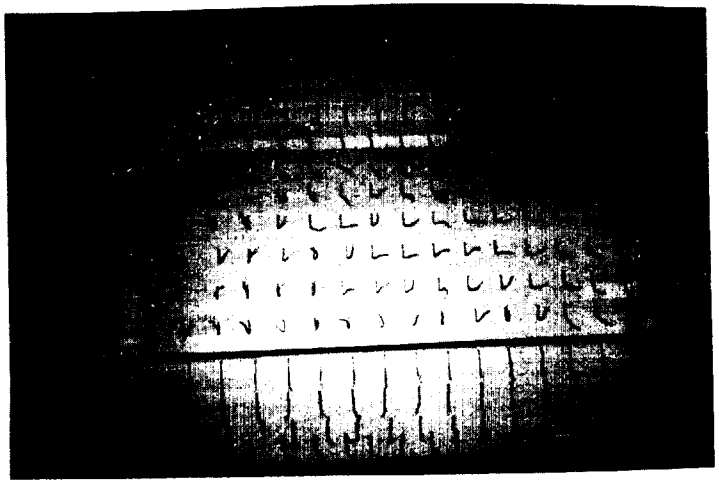

30% c Flap, Wind Tunnel Settings

Figure 58 - (Concluded) (e) α = 10° and 12.5°

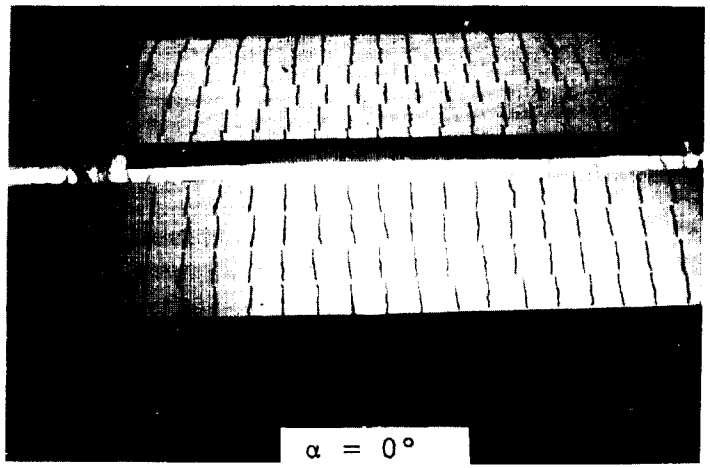

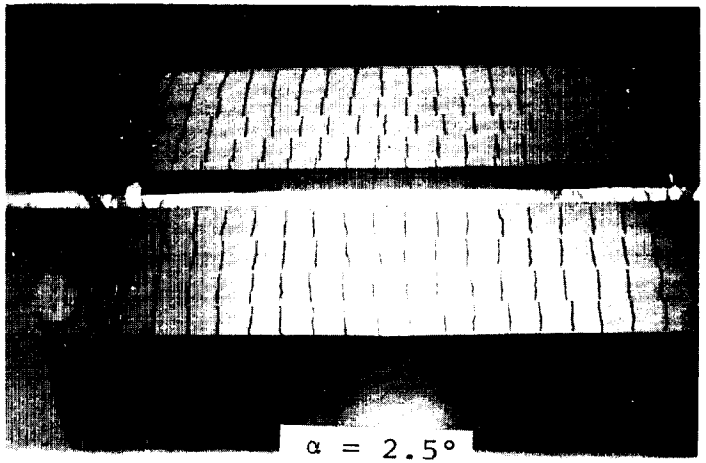

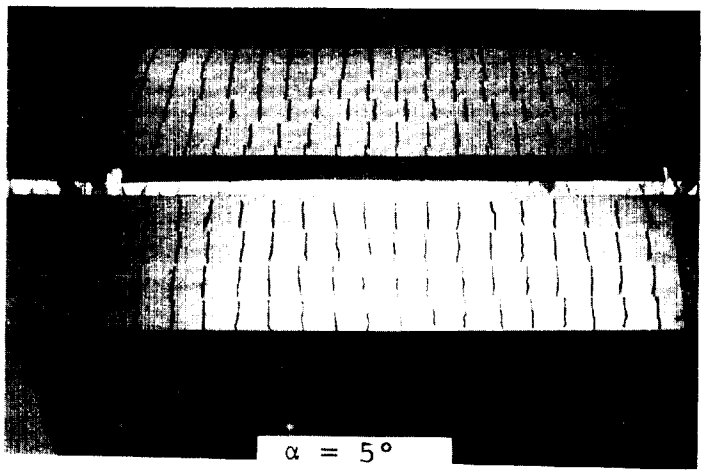

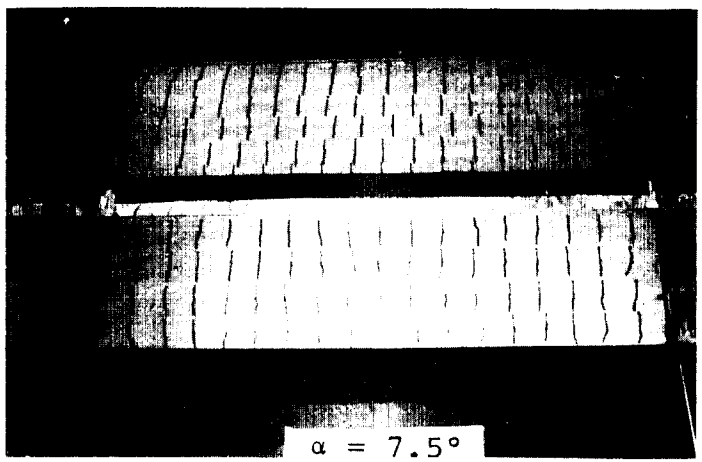

Figure 59 - Flow Visualization, Effects of Vortex Generators, Flap Nested (a) α = 0 to 7.5°

Figure 59 - (Concluded) (b) α = 10° and 12.5°

☆ U.S. GOVERNMENT PRINTING OFFICE: 1974—635-046 · 45